2017

Nitrosative stress sensing in Porphyromonas gingivalis: structure and function of the heme binding transcriptional regulator HcpR

Benjamin R. Belvin
Virginia Commonwealth University

Nitrosative stress sensing in *Porphyromonas gingivalis*: structure and function of the heme binding transcriptional regulator HcpR

A dissertation submitted in partial fulfillment of the requirements for the degree of Doctor of Philosophy in Biochemistry at Virginia Commonwealth University.

By:

Benjamin Ross Belvin

Bachelor of Science (Biochemistry), Virginia Tech, Blacksburg, Virginia, 2012

Masters of Science (Biochemistry), Virginia Commonwealth University, Richmond, Virginia, 2014

Director: **Janina P. Lewis, Ph.D.**

Professor

The Philips Institute for Oral Health Research

School of Dentistry, Virginia Commonwealth University

Virginia Commonwealth University

Richmond, Virginia

November, 13th, 2017

Acknowledgements

Getting a Ph.D. is a long road and there have been many people that have been critical to my success and have helped me immensely along the way.

First and foremost I would like to thank my Ph.D. advisor, Dr. Janina P. Lewis for this opportunity. None of this would have been remotely possible without her and it has been a privilege working in her laboratory. She has been an outstanding mentor and has given me the opportunity to grow as a researcher and individual as well as giving me the freedom to pursue my scientific interests and ideas no matter how off base they may have been. For this, I will always be grateful to her.

I would like to thank all the members of my committee: Dr. Todd Kitten, Dr. Phillip Hylemon, Dr. Darrell Peterson and Dr. Carlos Escalante. The insights they have shared and the guidance they have provided with regards to this work has been extremely helpful. Specifically I would like to thank Dr. Escalante for co-sponsoring my F31 award and both Dr. Kitten and Dr. Escalante (and members of their lab) for access to their lab and resources from time to time.

I would also like to acknowledge Dr. Faik Musayev and Dr. James Terner for their help. The crystal structures reported here would not have been possible without Dr. Musayev. He has also taught me much about X-ray crystallography and structural biology. Dr. Terner provided his time and lab for the resonance Raman experiments and helped teach a curious graduate student much about heme proteins and Raman spectroscopy.

I would be amiss if I did not thank the members of the Lewis lab, both past and present: our lab manager Nicai (and occasional PhD student therapist), Qin (our lab scientist), my fellow PhD student Kat, Dr. Justin Hutcherson, and other fellow students Chirs P, Steve, Chris W, Jacob and the many that came before them. These people have provided many hours of entertainment and made being in the lab a lot more enjoyable.

A special thanks to all of my colleagues in the Philips Institute. A good working atmosphere is imperative for being productive and enjoying what you do and many members of the institute have made working here that much more enjoyable.

Last, but definitely not least, I would like to thank my parents, David and Jackie, and sister, Emma for their endless love and support. I am indebted to my family for all they have done for me. They have kept me grounded and continued to support me despite the extended time it takes to complete a Ph.D. Without them none of this would have been possible.

Table of Contents

List of Figures

List of Tables

Abstract

NITROSATIVE STRESS SENSING IN *PORPHYROMONAS GINGIVALIS*: A STRUCTURE AND FUNCTION OF THE HEME BINDING TRANSCRIPTIONAL REGULATOR HCPR

By: Benjamin Ross Belvin, M.S.

A dissertation submitted in partial fulfillment of the requirements for the degree of Doctor of Philosophy in Biochemistry at Virginia Commonwealth University.

Virginia Commonwealth University, 2017

Major Director: Janina P. Lewis Ph.D.

Professor

The Philips Institute for Oral Health Research

School of Dentistry, Virginia Commonwealth University

Porphyromonas gingivalis, a Gram negative anaerobe implicated in the progression of periodontal disease, is capable of surviving and causing infection despite high levels of reactive nitrogen species found in the oral cavity due to its efficient nitrosative stress response. HcpR is an important sensor-regulator that plays a vital step in the initiation of the nitrosative stress response in many Gram negative anaerobic bacteria. We employ a combination of X-ray crystallography, SAXS, resonance Raman spectroscopy, UV-Vis spectroscopy, and molecular biology techniques to better understand this key regulator. Knockout of the *hcpR* gene in W83 *P. gingivalis* results in the inability of the bacteria to grow in physiological concentrations of nitrite and complementation of *hcpR* using the novel plasmid Pg108 rescues this phenotype. HcpR causes a drastic, dose dependent upregulation of *PG0893*, a gene coding for a putative NO reductase, when exposed to

nitrite or nitric oxide. Full transcriptome sequencing reveals that *hcp* is the only significantly upregulated gene when *P. gingivalis* is exposed to nitrite and knockout of *hcp* resulted in a phenotype that is similar to that of the *hcpR* deficient strain. HcpR directly regulates the expression of *hcp* via direct binding to an inverted repeat sequence in the promoter region of the *hcp* gene. We present a 2.6 Å crystal structure of the N-terminal sensing domain of HcpR and show that it is FNR-CRP regulator. A putative hydrophobic heme binding pocket was identified in the junction between the N-terminal domain and the dimerization helix. Mutation of two methionine residues (Met68 and Met145) in this pocket abrogates activation of HcpR thus verifying the binding site. Heme bound to HcpR exhibits heme iron as a hexa-coordinate system in the absence of nitric oxide (NO) and upon nitrosylation transitions to a penta-coordinated system. Finally, Small Angle X-ray Scattering experiments of the full length HcpR reveal that the C-terminal DNA binding domain of HcpR has a high degree of interdomain flexibility.

I.   Introduction

1.1 The Oral Microbiome in Health and Disease

The human oral cavity is home to a very diverse and active microbiome and is composed of viruses, protozoa, fungi, archaea and bacteria. Specifically, the bacterial community of the oral cavity is very complex with an estimated 1000 species present and accounts for the majority of the oral microbiome (1). The mouth provides a variety of surfaces for bacterial colonization: most are freely exposed however, there are a number of protected "pockets" on the occlusal surfaces of teeth, gaps between teeth, and on the gingival margin. Like a lock and key, the bacteria that call the oral cavity home have evolved and adapted to the various niches of the mouth where they reside. Within a day after birth *Streptococcus mitis* and *Streptococcus salivarius* begin to colonize the dental mucosa and saliva. As teeth erupt, bacteria associated with the dental enamel such as *Streptococcus sanguinis* begin to aggregate and colonize the mouth. As children grow into adulthood, the microbiome continues to expand until it forms a mature microbiome and the second most complex microbiome in the body behind the colon (2). It is estimated that 50% of the bacteria present in the mouth have not been cultured or are unable to be isolated thus making studying the microbiome difficult. Recent advancements in metagenomics and transcriptomics techniques have helped to reveal this enormous complexity and revolutionized what we know about the communities that call our bodies' home (3). Beyond the complexity of composition, recent studies have also elucidated the intricacy of the biogeography of the oral microbiome in the form of dental plaque, adding another layer of complexity to the picture painted by the oral microbiome (4).

The host-associated microbiome becomes intimately intertwined with the host at both the micron scale and the host scale. The oral microbiome is capable of critically influencing the promotion of health or disease thus it is very important to study the composition, biogeography, and physiology of the microbiome. A notable amount of study has gone into understanding the role of the healthy microbiome and how it is capable of promoting oral and systemic health. The presence of commensal species in the oral cavity plays a vital role in inhibiting the colonization of pathogens through colonization resistance. Virtually every surface of the oral cavity is colonized by a commensal, leaving few sites available for pathogens. Some bacteria have antagonistic relationships with potential oral pathogens. One example is the competitive relationship between *Streptococcus mutans* (a significant contributor to dental carries) and the commensal bacteria *Streptococcus sanguinis* and *Streptococcus gordonii* (5).

One of the most interesting properties of the commensal oral microbiome is the role it plays in nitrate metabolism. During and after a meal rich in nitrates, the commensal oral bacteria will convert nitrate to the more reactive nitrite anion using their nitrate reductase systems for respiration. Diet-derived nitrite is absorbed by the intestinal tract into the blood where it will be recycled back to salivary ducts and accumulate in the mouth. Roughly a quarter of the ingested nitrate/nitrite is returned to the oral cavity via this entero-salivary circuit (6). This diet derived nitrite also has a significant effect on blood pressure: nitrite that is taken up into the bloodstream is converted to nitric oxide via blood heme-globins, and can act as an important regulator of vasodilation and blood pressure (7). This effect is confirmed by the observation that use of an anti-microbial mouth-rinse partially

abolishes the increase in plasma nitrite following nitrate ingestions resulting in changes in blood pressure (8).

Nitrate also has an effect on the composition of the oral microbiome. A prolonged nitrate rich diet selects for certain species of bacteria that can utilize nitrate as a nutrient and species that thrive in the nitrate/nitrite rich environment. This includes *Neisseria flavescens, Rothia mucilaginosa,* and related species (9). These are also health-associated microbes in the oral cavity. In a study of the biofilm community comparing healthy mouths and those that are predisposed to caries, *Neisseria* species were heavily associated with a caries-free status and even provided a protective effect against the caries (10). Thus a nitrate rich diet and the microbes that utilize nitrate and nitrite not only promotes cardiovascular health but oral health also.

Conversely, a significant amount of research has gone into understanding oral diseases and the role the oral microbiome plays in the promotion of disease. Dental caries, endodontic infections, gingivitis, and periodontitis are bacterial infections of the oral cavity which have a significant impact on public health. It is estimated that from 1990-2010, oral conditions affected 3.9 billion people worldwide and untreated carries of adult permanent teeth was the most prevalent condition in the entire world. These numbers imply an estimated loss of 224 years per 100,000 population of dis-ability adjusted life years (11). Periodontal disease in particular is one of the most important oral diseases (with dental caries) contributing to the global burden of chronic diseases and is prevalent worldwide (12). In the United States, it is estimated the 46% of adults aged 30 and older have some form of periodontal disease, including an estimated 64.7 million suffering from periodontitis (13). This case is further complicated by the link between oral diseases and

other systemic diseases. As expected, a long-lasting but persistent periodontal infection and the chronic inflammation it generates can have a large impact on long term health, such as increasing the risk for cardiovascular diseases, chronic respiratory diseases, and diabetes (14).

Periodontitis is an oral inflammatory infectious disease that affects the soft tissue and bone that surround and support the teeth. It is defined by the presence of gingival inflammation at sites where there has been a pathological detachment of collagen fibers from the cementum and loss of the junctional epithelium. Put simply, it is an inflammatory disease that affects the tissues that surround and support the teeth. It is characterized by the loss of alveolar bone around the teeth which can lead to loosening and eventual loss of teeth if left untreated (15). If the bacteria of the mouth are left uncontested, they begin to aggregate into biofilms in the form of plaque and tartar. Bacterial plaque occupies the periodontium and attaches to the tooth and root surfaces. Coupled with the production of enzymes and toxins, bacteria penetrate the epithelium which leads to initiation and sustainment of the inflammatory response (16). It is this sustained inflammation which results in the bleeding and tissue loss which characterize periodontal disease. Periodontitis is diagnosed via clinical examination of the tissue surrounding the teeth and and radiographic examination to evaluate the bone loss surrounding the teeth (15).

1.2 *Porphyromonas gingivalis* and Dysbiosis

Under normal homeostatic conditions, there is a balance between the host immune response and the normal oral flora. This equilibrium is not indiscriminate but a highly evolved process: the dental bacteria have adapted to living and growing in the selective conditions of the mouth and the host immune response limits growth via a combination of

4

innate and adaptive immune responses. When the balance between the oral flora and the host response is upset the oral homeostasis is disrupted; the loss of this homeostatic interaction leads to the development of periodontal diseases (17). The primary driver behind this loss of homeostasis is the development of dysbiotic individual members of the microbiota relative to their abundance in health. Current research implies that this altered microbiota leads to changes in the host-microbe cross talk which is capable of disrupting homeostasis and initiating a chronic inflammatory disease (18). Keystone pathogens, such as *Porphyromonas gingivalis, Tannerella forsythia,* and *Prevotella intermedia* promote community virulence despite their low abundance as members of the microbiota (19). This suggests that periodontal disease is a polymicrobial disease and is not dependent on a monoculture or single bacteria but rather a community of organisms.

P. gingivalis is a rod-shaped, non-motile, Gram-negative anaerobic, pathogenic bacterium that forms black colonies on blood agar plates and is found almost exclusively in the oral cavity. It is an asaccharolytic bacterium that does not use sugars as a source of energy, instead it must acquire nutrients from host-derived substrates and metabolizes peptides and other nitrogenous compounds as a source of energy making it dependent on its proteolytic properties for energy. The proteases secreted by *P. gingivalis*, specifically the lysine and arginine specific cysteine proteases (known as gingipains or Rgp and Kgp) also play an important role in its pathogenic potential by directly degrading structural proteins of the periodontal tissues, disrupting host signaling, and promoting subversion of complement (20-22). Beyond its proteolytic potential, *P. gingivalis* employs a number of virulence factors that are capable of interaction with and invasion of host

cells (fimbriae), manipulation of neutrophils, and disruption of macrophage responses (23-25).

If the bacteria of the mouth are left uncontested, they begin to aggregate in biofilms in the form of plaque and tartar. Under normal conditions, the host inflammatory-immune response is capable of controlling overgrowth and overt pathogenicity. It is in these biofilms that *P. gingivalis* inserts itself where, despite its low abundance, it helps to orchestrate the dysbiosis between the host and its flora and elevate the pathogenicity of the entire community using its abundance of virulence factors. Recent studies have shown that *P. gingivalis* has evolved methods to evade components of the host immune system and instead of acting directly as the sole pro-inflammatory bacterium, *P. gingivalis* impairs innate immunity in ways that alter the growth of the entire oral biofilm. These actions by the bacterium change the normally homeostatic host-biofilm cross talk, promoting a destructive, inflammatory shift in the host-biofilm interaction eventually leading to periodontal diseases. *P. gingivalis* alone is not sufficient to cause periodontal disease, implying that the dysbiosis caused by *P. gingivalis* is the cause for the disease (26). This suggests that removal or targeting of the keystone pathogen, while leaving the commensal species intact, is a potential approach to restoring the normal host-biofilm equilibrium and reducing inflammation, thereby treating periodontitis.

1.3 Oral N-oxides and Sources of Nitrosative Stress

The primary N-oxides in the oral cavity are nitrate (NO_3^-), nitrite (NO_2^-), and nitric oxide (NO). The source of these inorganic molecules is dietary derived and the host immune system. As previously mentioned, the commensal oral microbiome has the potential of reducing the nitrate derived from our diet to nitrite, which can have profound

effects on human physiology (Fig. 1). One side effect of this entero-salivary circuit of N-oxides is an increase in concentrations of nitrite in the oral cavity that can exceed 2mM after a nitrate rich meal, resulting in a high level of reactive nitrogen species in the oral cavity. This increases the burden on the bacteria in the mouth making it necessary for them to employ an efficient nitrosative stress response to survive.
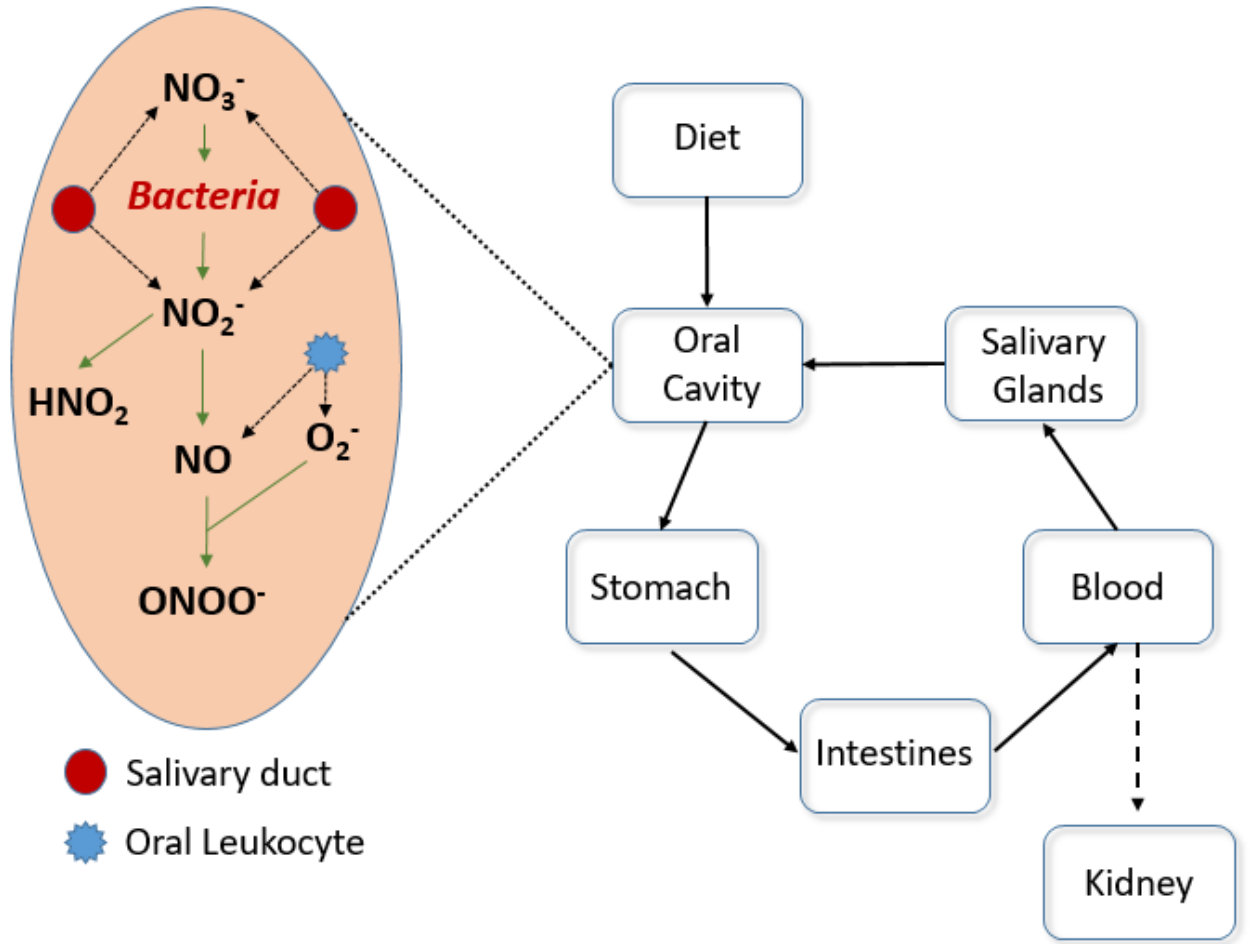
Figure 1 – Enterosalivary circuit and reactive oxygen species in the oral cavity

Nitric Oxide (NO) is a signaling and defense molecule in eukaryotic organisms. It is most notable for its role in the regulation of vasodilation in the cardiovascular system (1998 Nobel Prize in Physiology and Medicine) and its secretion by the immune system as a means to combat bacterial infection. NO is a free radical and can stabilize its unpaired electron two ways: reaction with species containing other unpaired electrons and interaction with the d-orbitals of transition metals, such as iron. In its reaction with iron, NO can form a rapid, stable, high-affinity coordination bond with a ferrous iron in a heme group. NO is uncharged and highly soluble in hydrophobic environments – a characteristic that allows it to freely diffuse through biological membranes. This not only makes it an excellent signaling molecule but a potent antimicrobial agent (27).

Despite being a radical, NO is quite stable in biological environments depending on the components of the solvent and the concentration of oxygen (despite the common misconception that all free radicals are unstable and highly reactive); however, NO is still quite capable of causing damage to biological systems (28). Sulphonic acids, disulfides and S-nitrosothiols are some of the most abundant products arising from nitrosative modifications of thiol groups and can modify and disrupt protein activity. Nitric oxide also has a negative effect on iron-sulfur centers. Attack of NO on the [4Fe4S] centers of redox enzymes and electron transport chains is well noted and can cause these iron centers to break down resulting in loss of activity (29). As many bacteria rely heavily on iron based metabolism, NO can act as a potent antimicrobial. Reactive nitrogen species act in conjunction with reactive oxygen species to damage cells. NO will react very quickly with other free radicals and most reactive oxygen species, forming highly reactive products (Fig. 2). The reaction between superoxide and NO forms peroxynitrite, a very reactive,

powerful oxidant that can damage proteins, lipids and DNA. It has been reported that the

rate constant for the reaction of NO and O_2^- approaches the diffusion limit (30). Ultimately,

peroxynitrite is capable of degrading to the very reactive and highly toxic hydroxyl radical

(Fig. 2). NO will also react with O_2 to form nitrite, nitrate, and nitrous anhydride. The

interconversion of these compounds can also be catalyzed by bacterial sources, of which

NO is an obligate step. When we eat a meal, bacteria in our mouth and gut can produce

nitrogen species as metabolic byproducts. Although not as reactive as peroxynitrite, high

concentrations of these products can be a source of nitrosative stress to hosts and

bacteria. NO is capable of reacting with ammonia to stimulate the creation of

hydroxylamine. Hydroxylamine is common mutagenic species that is capable of causing

base-pair point mutation, and must be cleared.
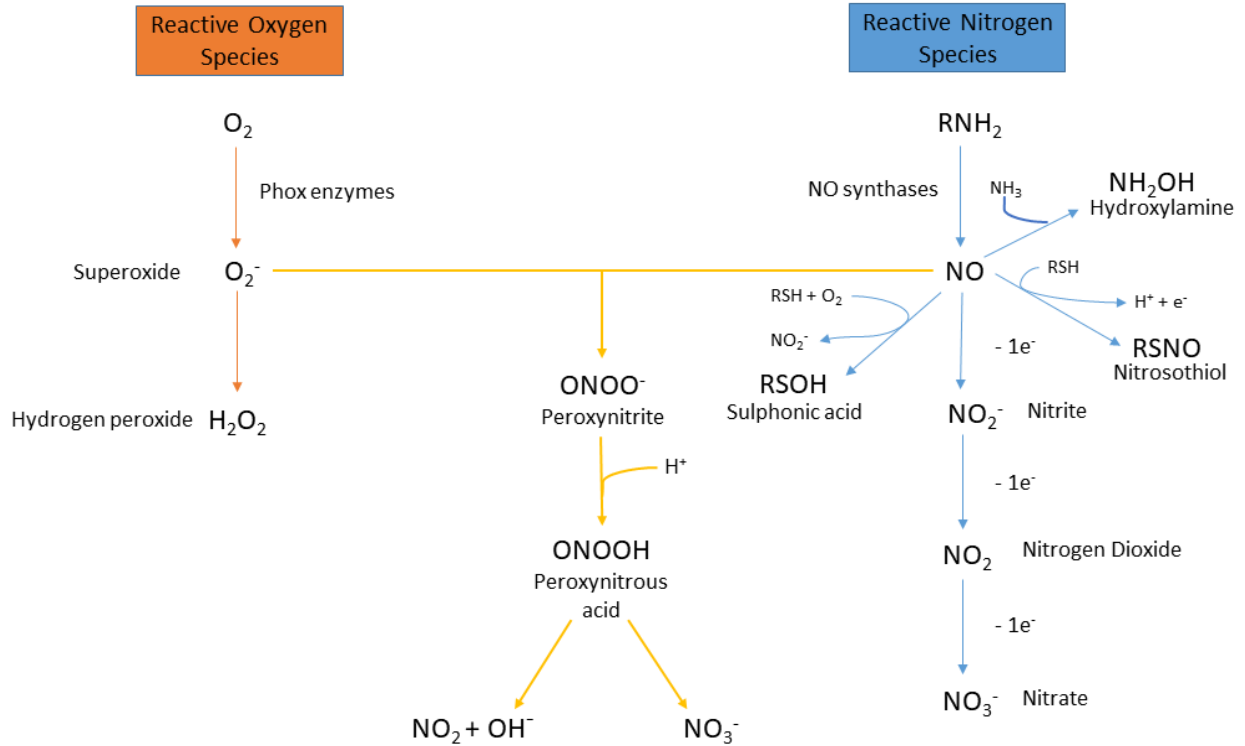
Figure 2- **Reactive oxygen species and reactive nitrogen species in biology.**
Reactive oxygen species and reactive nitrogen species are generated by the host
immune system as an antimicrobial strategy and as a by-product of microbial metabolism.
These species are capable of reacting with each other and forming reactive species such
as peroxynitrite and the hydroxyl radical.

One important aspect of nitrite is the capability of hemoglobin and other heme binding "globins" to reduce it to nitric oxide (31). As oxygen tension decreases, nitrite reactions with deoxygenated hemoglobin may generate NO through the following reaction:

(1) $\qquad NO_2^- + HbFe^{2+} + H^+ \rightarrow NO + HbFe^{3+} + OH^-$

(2) $\qquad NO + HbFe^{2+} \rightarrow HbFe^{2+}\text{-}NO$
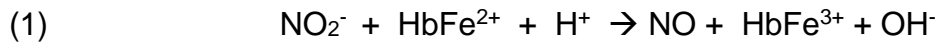
creating 1 mole of methemoglobin and 1 mole of NO. In the context of the periodontal pockets, which are beset by a large amount of inflammation and bleeding (a hemoglobin source), a largely anoxic environment at its base, and potential for high nitrite concentrations, this chemical reaction is another potential source of NO and nitrosative stress. Furthermore, the gingipains (Kgp and Rgp) play an important role in the binding and degrading of erythrocytes in the acquisition of heme from hemoglobin, further contributing to the hemoglobin levels present in the environment and periodontal pockets (32).

NO is also synthesized intra-cellularly by eukaryotic cells through the action of NO synthases or NOS enzyme. NOS enzymes catalyze the NADPH and O_2 dependent oxidation of arginine to citrulline and NO. The enzymatic synthesis of NO by the enzymes is complex and is dependent on many prosthetic groups and cofactors (33). Two types of NOS are relevant to bacterial infection:

(1) – eNOS (NOS3) – generates low levels of NO and is found in endothelial and epithelial cells among other cells types (such as cardiac myocytes and neurons) (34).

(2) – iNOS (NOS2) – inducible, generates the highest level of NO and is found in cells of the immune system that stimulate the inflammatory response (35).

Inducible Nitric Oxide synthase (iNOS) has been shown to play an important albeit complicated role in periodontal diseases. Many of the etiological factors of periodontitis such as inflammatory cytokines and the periodontal pathogens are responsible for enhanced iNOS-derived NO production, however this increased NO burden can also lead to tissue damage. Under normal homeostatic conditions iNOS is required for normal development of the alveolar bone; however, it has also been shown to be vital for *P. gingivalis* induced alveolar bone loss (36). Furthermore, it was demonstrated in a rat ligature-induced periodontitis model, that iNOS inhibition prevents alveolar bone loss implicating NO in the pathology of periodontitis, probably by stimulating osteoclast differentiation and activity (37). Conversely, iNOS and NO production are important elements of the host innate immune defense against *P. gingivalis* and play an important role in the modulation and signaling of leukocyte function. Mice lacking iNOS show an impaired killing of *P. gingivalis* in an abscess model, with abscess fluids from iNOS$^{-/-}$ mice possessing significantly more bacteria and an increase in the percentage of dead leukocytes (38). Thus iNOS is partially responsible for the pathology of periodontal disease, however it also an important component of the hosts defense against the bacteria implicated in periodontitis.

1.4 Transcription factors

Gene regulation and proper regulation of transcription is a central process in all organisms. An increase in gene complexity requires the development of mechanisms for gene regulation at the transcript level. Furthermore, for a single cell organism, these mechanisms must be highly responsive due to how quickly the environment can change. Transcription factors are regulatory proteins that bind to a specific sequence of DNA,

thereby controlling the expression of a gene at the transcriptional level. Transcription factors can promote, repress, or actively recruit RNA polymerase to an operon depending on the state of the cell (39). A characteristic feature of transcription factors is the presence of a DNA binding domain that is specific for a sequence of DNA. This domain allows them to augment the flow of gene expression by binding directly to DNA of the genome (40). The activities of many transcription factors are directly regulated by binding of a signal cytoplasmically or indirectly regulated by binding of extracellular proteins and peptides to cell-surface receptors. Structural analysis of many prokaryotic transcription factors has revealed that most are homo-dimers that bind to palindromic DNA sites (41). Transcription factors regulate cell development, growth, differentiation, and coordinate stress responses. There are many transcription factors that are divided into families according to their DNA binding motif (helix-turn-helix, zinc finger), cofactor binding, and role (42). In addition, transcription factors may contain partner domains which are involved in protein-protein interaction, ligand binding, or cofactor binding (43). In most cases certain classes of partner domains are associated with certain types of DNA binding domains (43). These domains are important in the activation and regulation of the transcription factors and can enhance the diversity of regulatory functions that these proteins are responsible for.

Fumarate-nitrate regulator/cyclic-AMP receptor protein (FNR-CRP) regulators are a class of bacterial transcriptional regulators that play essential roles in metabolism, stress response, and virulence (44). Named after the first two characterized members of the family, these regulators exist throughout the bacterial kingdom with the paradigm *E. coli* cyclic AMP receptor (CAP or CRP) having attained text book status. In all cases, these proteins are capable of sensing intra- or extra-cellular stimuli and inducing

transcription of the appropriate response. Despite the diversity of stimuli and function in bacteria, all members of the FNR-CRP family have a similar structural orientation: (i) β-barrel fold in the N-terminal sensing domain, (ii) form homo-dimers through the use of a long helical domain, and (iii) are capable of binding to DNA using a C-terminal helix-turn-helix domain (45-47). In general, binding of stimuli leads to a conformational change in the protein that results in an increase in affinity to their promoter DNA sites. Beyond these shared attributes, there are significant differences in sequence identity between members, indicating potential differences in the allosteric mechanisms of activation. Most variation between members of the family occurs in the N-terminal sensing domain, where changes in sequence will accommodate different stimuli or the binding of cofactors.

1.5 Nitrosative Stress Response and *P. gingivalis*

Bacterial cells must develop methods to protect cellular components from damage by reactive nitrogen species and pathogenic bacteria must withstand host environments and responses during infection that incorporate release of reactive nitrogen species. An efficient nitrosative stress response will not only allow a pathogenic bacterium, such as *P. gingivalis*, to withstand stressful conditions but also express virulence associated genes in an appropriate manner. Thus the stress response is an important aspect of the virulence of bacteria and its capability to cause an infection (48).

Nitrosative stress responses detect increased concentrations of reactive nitrogen species and modulate the expression of necessary genes to clear the toxic species, usually through enzymatic means or the use of globins to consume NO (49). Several enzymes have been implicated in the detoxification of RNS in microbial species: microbial

heme proteins, nitric oxide reductases, hydroxylamine reductases, and peroxynitrite reductases (50-52). Many bacteria upregulate globins, such as the flavin-hemoglobin Hmp in *E. coli* and *Salmonella* species in response to NO stress. These proteins will scavenge and capture NO using a heme cofactor and convert it to nitrate (53). Furthermore, in some species these antioxidant methods are required for pathogenicity and necessary for resistance to the host immune response and survival inside host cells (52, 54, 55).

Despite the high levels of reactive nitrogen species in the oral cavity and importance of NO in periodontal diseases, the mechanisms of denitrification in *P. gingivalis* (and other oral pathogenic anaerobes) is not fully understood. Studies have shown that a putative redox enzyme, hybrid cluster protein (Hcp) (Pg0893), plays an important role in the response of *P. gingivalis* to NO (52). Hcp is found in other anaerobic bacteria (*Desulfovibrio*) and facultative anaerobic bacteria (*Escherichia coli, Pseudomonas aeruginosa, Salmonella enterica*) where it is induced by nitrate, nitrite or nitric oxide indicating that it plays a role in nitrogen metabolism as a putative nitric oxide reductase. However, in many of the facultative anaerobes, Hcp expression has been shown to be regulated by OxyR (*E. coli*) or FNR as part of larger shift in metabolism (56). In *P. gingivalis*, Hcp is upregulated in response to NO and nitrite and this upregulation is dependent on the transcriptional regulator HcpR. A *P. gingivalis* strain deficient in the *hcpR* gene (PG1053) does not grow in the presence of physiological concentrations of nitrite (1-2mM) and nitrite and NO dependent upregulation of Hcp is abolished. Furthermore, the knockout strain shows a decrease in the survival with host cells indicating that the nitrosative stress response plays an important role in virulence. Finally,

binding of recombinant HcpR to DNA of the Hcp promoter is heme dependent indicating that heme potentially plays an important role in the nitrosative stress response (54).

It should be noted that HcpR has been implicated as necessary for the survival of *P. gingivalis in vivo.* Using a transposon insertion library, an HcpR mutant was identified as having reduced ability to colonize host cells as well as survive in mice thus indicating that the regulator plays an important role in virulence of the bacterium and survival in the host (57). Of the transcriptional regulators observed in the study, HcpR was one of the most important genes and the loss of HcpR had the most dramatic effect on the competitive index of the bacteria to survive in the mouse model.

1.6 Heme Proteins and Mechanisms of Heme Based Gas Sensors

The heme iron complex is one of the most important cofactors in biological systems. Its primary function is to serve as a binding site for the diatomic gas molecules most relevant to biology: carbon monoxide (CO), nitric oxide (NO), and diatomic oxygen (O_2). These gaseous molecules can have significant impact on many biological processes and can also act as toxic molecules. Heme is most well-known for its role as the site of O_2 binding in hemoglobin, allowing the protein to carry out a function (the binding and transport of O_2) that it would not be able to carry out with the use of the cofactor. An important and novel role of the heme iron complex is its function as gas-sensing site and heme-based gas sensor proteins. These sensor proteins allow for physiological responses to the presence of these gases in the environment on a cellular level.

Most heme based gas sensors utilize an N –terminal heme bound sensing domain and a C-terminal functional domain. This sensing domain must not only recognize a target

ligand but also discriminate against the other heme ligands (58). To achieve this goal the sensing domains of these proteins utilize a combination of binding and allosteric factors to discriminate between O_2, CO, and NO. Natively the affinity for each gas to heme is different (NO << CO << O_2). This creates a "sliding scale rule" where the affinity of one of the gases can be predicted if the affinity for one of the other ligands is known (59). One way the heme proteins distinguish between the gases is through the regulation of binding affinity depending on the target gas. The environment of the heme binding pocket and the residues that surround the pocket can enhance the binding affinity of one gas over the other (i.e. O_2 likes to make electrostatic interactions, CO and NO are repulsed by them) (60). In addition, heme proteins can achieve greater selectivity through allostery that is specific to one gas. Heme proteins can distinguish between the different gases through their binding geometries to heme and the contacts they make with vital residues in the pocket (i.e. sGC selects for a 5-coordinate heme geometry that is produced by NO when bound, not the 6-coordinate geometry that is produced by CO or O_2 binding) (58, 60). These properties of heme binding proteins allow them to robustly respond to a stimulus in a specific manner.

In heme-based sensor proteins, the ability to change the coordination state of the heme-iron is utilized for signaling and allosteric activation. The innate affinity of NO for heme is much higher than that of CO or O_2 due in large part to its strong backbonding with the iron. This increased affinity causes NO to exert a strong trans effect on Fe(II), resulting in a long and weak bond to an axial ligand (61, 62). This unique property of the NO-Fe(II) bond is used to the advantage of other heme based NO sensors. The primary molecular event correlated with sGC activation is the dissociation of the heme-proximal

histidine bond upon NO binding to the distal face of the heme. This event (loss of proximal His coordination) triggers the structural allosteric changes within sGC that activate it (63, 64). CO and O_2 do not apply a strong enough trans effect on the iron to break the His-iron bond. This allows for the NO selective activation in both of these sensors. This effect can also be seen in the binding of hemoglobin to O_2 and NO (Fig. 3). In the α-subunit of Oxy-hemoglobin His87 acts as an important axial ligand helping to stabilize the O_2-Fe bond. However, due to the higher affinity of NO for the heme iron, this axial bond is dissociated from the iron complex. This is an important distinction that is utilized by heme based NO sensors.

In general, all heme based gas sensors resemble bi-stable switch proteins with an active and inactive state that is influenced by the binding or dissociation of a gas molecule to the heme iron (65) (Fig. 4). This event induces a perturbation of the heme and the surrounding residues that form the binding pocket in the sensor domain. This perturbation extends through the protein to the functional domain, where functions such as catalysis or DNA binding activity are modified. Typically, important residues act as axial ligands by coordinating to the heme iron complex. Interaction of the gas with the heme iron influences these residues causing changes in the heme iron coordination and mediating allosteric activation of the protein (58). Thus, understanding the heme binding properties, the residues involved in heme iron coordination, and the effects gaseous ligand has on the coordination state is necessary for determination of the mechanism of action.

A.

B.
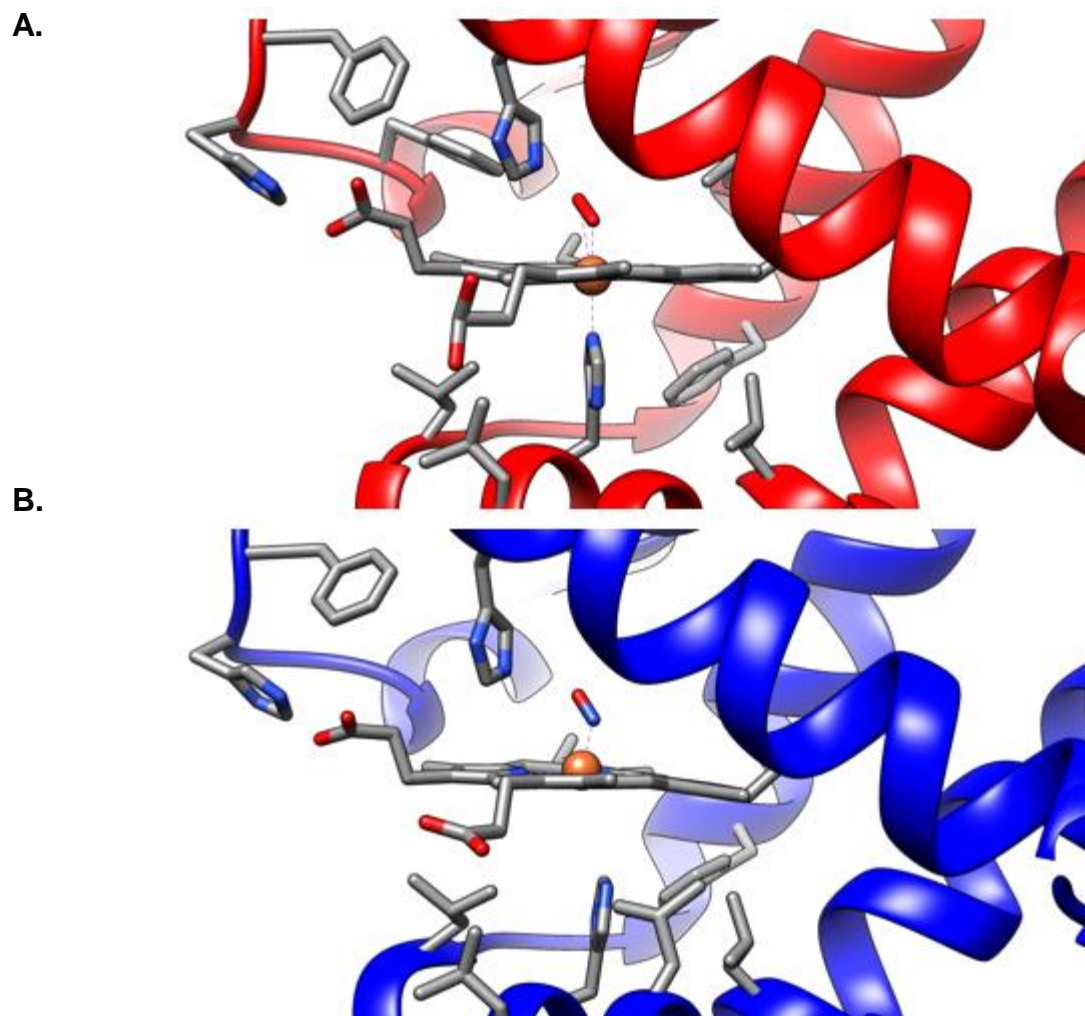
Figure 3 – Binding of NO to heme creates a strong trans-effect on the heme iron.
A. Binding of oxygen to the alpha subunit of hemoglobin (PDB ID 2DN1). **B.** Binding of
NO to the alpha subunit of hemoglobin (PDB ID 4N8T).
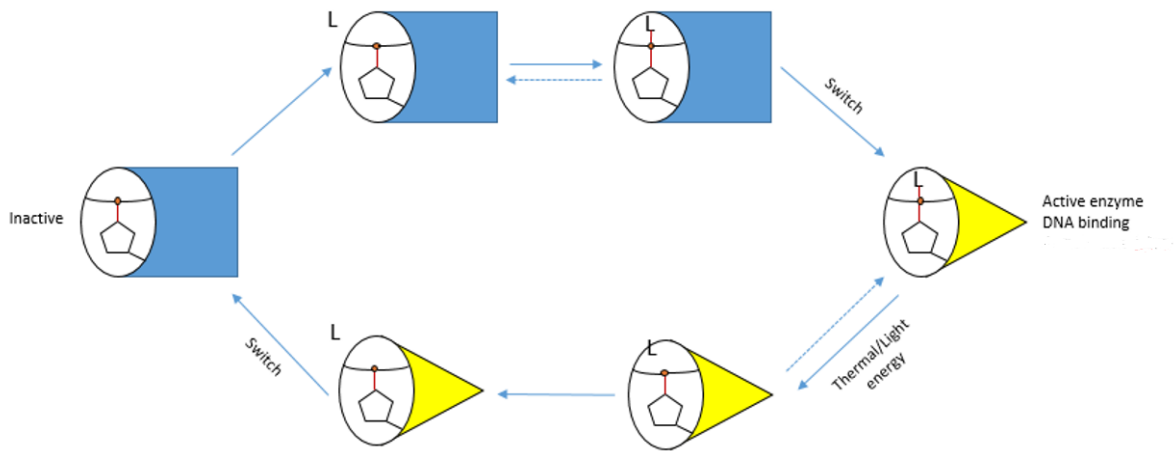
Figure 4 – General scheme of inter-protein signal transition of a heme sensor. Heme based gas sensors act as bi-stable switch molecules with an on and off state that is dependent on gas association/dissociation from the protein bound heme cofactor.

The gas sensing members of the FNR-CRP family sense changes in the environment through their cofactors, either iron-sulfur clusters (FNR) or heme (CooA/DNR) (44, 66). In heme based gas sensors, the heme iron complex functions as the binding site for gaseous molecules such as NO, CO, and O_2. Although not all HcpRs utilize heme as a cofactor, a growing subset are being characterized as heme binding proteins (67). The hypothesis that HcpR may use the heme co-factor is supported by studies done with other sensor regulators and homologues of HcpR: DNR (NO sensing in *P. aeruginosa*), and CooA (CO sensing in *Rhodospirillum rubrum*). CooA utilizes the heme cofactor to bind to CO and induce transcription at operons coding for genes necessary for the oxidation of CO to CO_2 (68). Although it is a CO sensor, CooA has been shown to bind to NO under saturating conditions (69). DNR is a heme binding transcriptional regulator that senses and binds NO, controlling expression of denitrification gene clusters (70, 71). The full-length and sensing domain structures of both CooA and DNR in the apo form and the heme bound form of CooA has been determined by X-ray crystallography. Both proteins form a hexacoordinate heme system, utilizing two axial bonds from the protein (70, 72). However, of the known structures of bacterial heme binding sensor proteins (CooA, DNR), there are significant differences in sequence: the residues involved in coordination of the heme iron are not conserved. Furthermore, these proteins are derived from facultative anaerobic organisms; HcpR is found in obligate anaerobes that grow under low oxygenated conditions. This creates a very different oxidative environment and could play a significant role in the mechanism of protein detection and activation.

Aims and Goals of this study

In this study we aim to shed light on the molecular mechanisms by which *P. gingivalis* HcpR is capable of sensing changes in the levels of reactive nitrogen species in the environment, and how this mechanism differs or agrees with the known heme sensor proteins. Furthermore, we aim to establish HcpR as the master regulator of the nitrosative stress response in *P*. gingivalis and to further explore the role of the regulator. To achieve these goals, the structure of the N-terminal sensing domain of HcpR has been solved and the heme and NO binding properties of the protein have been characterized. The function of HcpR *in vivo* has was also explored to better understand its role in the nitrosative stress response and how it acts as a transcriptional regulator. As HcpR plays an important regulatory step in the nitrosative stress response in many Gram negative anaerobes these findings shed light on understanding of the mechanism not only in the periodontal pathogen, *P. gingivalis,* but also in other anaerobic bacteria. Furthermore, this work contributes to our knowledge of the mechanism of action of the growing family of FNR-CRP heme-based regulators present in a variety of organisms.

II.   Materials and Methods

Growth of Bacterial Strains

Bacterial strains grown in this study are listed in table 3. All strains of *P. gingivalis* are derived from the W83 strain type. The bacteria were grown anaerobically in an atmosphere consisting of 85% N_2 10% CO_2 and 5% H_2 at 37 ºC in an anaerobic chamber (Coy Manufacturing). All *P. gingivalis* strains were maintained on TSA sheep's blood agar plates with appropriate antibiotic when needed. Liquid cultures of *P. gingivalis* were grown in BHI broth supplemented with hemin (5.0 µg/mL) and vitamin K_3 (1 µg/mL). Tetracycline or clindamycin (both 0.5 µg/mL) were used to select for transformants.

Growth Studies

Overnight cultures of *P. gingivalis* grown in BHI broth were started from TSA blood agar plates and allowed to grow to confluency. This overnight culture served to inoculate growth studies carried out in mycoplasma broth supplemented with vitamin K_3 (1 µg/mL). All growth studies were started at an OD_{660} of 0.15 and time points were taken ever 3, 6, and 24 hours or 2, 4, 6, and 24 hours. For growth studies and exposure studies in nitrogen species, cultures were prepared in mycoplasma broth with the appropriate concentration of nitrite, *S*-Nitrosoglutathione (GSNO), or Diethylamine (DEA) NONOate.

Generation of *hcp* Mutant Strain

A fragment of the *P. gingivalis* W83 genomic DNA coding for the Hcp protein (PG0893) was PCR amplified using Pg0893F and Pg0893R primers. The PCR fragment containing the *hcp* gene was digested and cloned into the m-pET21d vector using the *Bam*HI and *Xho*I restriction sites following a standard T4-ligase cloning procedure.

Recombinant plasmids were transformed and screened in *Escherichia coli* DH5-α and positive clones were subsequently sequenced to confirm and transformed into *E. coli* BL21 (DE3) cells (Bioline) for protein expression. The *ermF* cassette was amplified using the primers *hcp-ermF*-F and *hcp-ermF*-R; these primers were engineered to contain 15 base pair overlaps at the center of the *hcp* gene. The hcp-pET21 vector was amplified using the primers p21hcpKO-F and p21hcpKO-R; these primers amplify the plasmid starting at base-pair 825 of *hcp* and extending out and around the plasmid. The two PCR fragments were then joined using the NEB HiFi-assembly master mix (New England Biolabs). The recombinant plasmid was then transformed and screened in *E. coli* DH5- α and positive clones were subsequently sequenced to confirm the insertion of the ermF gene into the center of the *hcp* gene creating the *hcp*-KO construct. The construct was amplified using PCR and concentrated to approximately 1μg/μL. Ten μL of the concentrated PCR product was then added to 50 μL of washed wild type *P. gingivalis* cells and placed into an electroporation cuvette. The samples were electroporated using a Gene Pulser II electroporation system (BioRad). Immediately after electroporation, 500 μL of warm BHI broth was added to the cuvette and immediately placed in the anaerobic chamber where the 550 μL of sample was added to 2mL of anaerobic BHI broth. After growing overnight, the samples were then plated on TSA-Blood agar plates with 0.5 μg/mL of clindamycin for selection. Colonies appeared after approximately 1 week and were re-plated. To screen, PCR was performed on the sample using primers specific for the *hcp* gene. Strains positive for the insertion mutation were stored.

Cloning and generation of mutant HcpR strains

The Pg108 vector is a shuttle vector derived from the pYHBA1 plasmid and confers tetracycline resistance in *P. gingivalis* and an erythromycin resistance in *E. coli* (73). A synthesized construct containing a wild-type copy of the *hcpR* gene down-stream of the *ermF* promoter was PCR amplified and cloned into the Pg108 vector utilizing the *Bam*HI and *Sph*I restriction sites creating the Pg108-*hcpR* construct. The entire synthesized construct is available in the appendix. The QuikChange II Site-Directed Mutagenesis Kit (Agilent Technologies) was utilized to create the M68A, M145A, and H149A mutations on the Pg108-*hcpR* construct following the manufacturers protocol. Subsequent PCR generated plasmids were screened and sequenced.

Table 1 – Primers used in this study

Primers for Cloning

pET21-*hcpR*-Forward	CTTCCAGGGATCCCCAGAATTCGATCTTC
pET21-*hcpR*-Reverse	GCGCACTCGAGTTACTCCAGCCTCGACA
pFC20K-*hcpR*-Forward	TTGTGTTTAAACCTCCAGCCTCGACAA
pFC20K-*hcpR*-Reverse	GCCGGCGATCGCCATGGATCCCGAAT
Pg108-*hcp*-Forward	CGATGGATCCTGATTTTTCTCTGAATCCATACAAGTA
Pg108-*hcp*-Reverse	GATCCTGCAGTTATGCGATCAGCGTCC
Pg108-*HcpR*-Forward	CTGAAGGCATGCTTGCTCATCTGCAACTTTTTTTTCTTTGG
Pg108-*HcpR*-Reverse	GATCAAGCTGCAGTTACTCCAGCCTCCACAATCG

Primers for Mutagenesis

L156*-Forward	ATCTTGCCCTGCTAACTTCGCAAGCTGAG
L156*-Reverse	CAGCTCAGCTTGCGAAGTTAGCAGGGCA
H149A-Forward	CGCAAGCTGAGCTGAGCGATTTTCTTCAT
H149A-Reverse	GTGCTTTCCTGATGAAGAAAATCGCTCAG
C33A-Forward	GCCCTGCTTGAGAGTGCTTCATACAGA
C33A-Reverse	CCACTCTGTATGAAGCACTCTCAAGCA
H124A-Forward	GAAGAGTTCAAAGGGATGATGGCTAAGT
H124A-Reverse	CCATCAGAGTAGGATACTTAGCCATCATC
M68A-Forward	CCGGAAGGCCCCACCGCCTCAGCACGAATCTC
M68A-Reverse	GAGATTCGTGCTGAGGCGGTGGGGCCTTCCGG
M145A-Forward	TGAGCTGATGGATTTTCTTCGCCAGGAAAGCACTGATATCGG
M145A-Reverse	CCGATATCAGTGCTTTCCTGGCGAAGAAAATCCATCAGCTCA
149HcpR_M145A-Forward	GAGCTGAGCGATTTTCTTCGCCAGGAAAGCACTGATATCG
149HcpR_M145A-Reverse	CGATATCAGTGCTTTCCTGGCGAAGAAAATCGCTCAGCTC
Hcp-prom-del-Forward	CAAGAGTACCCGGATAGTTTCAGGCAGATAGCAG
Hcp-prom-del-Reverse	CTGCTATCTGCCTGAAACTATCCGGGTACTCTTG

Primers for qPCR

hcp-Forward	AAAGCTGTCATCGTCCTGCT
hcp-Reverse	CGATCAGCGTCCGAATATCT
HcpR-Forward	GCCCTGCTTGAGAGTTGTTC
HcpR-Reverse	GCAAACAGGGTAACGGGTAA
*P.g.*16s-Forward	AGGCAGCTTGCCATACTGGC
P.g.16s-Reverse	ACTGTTAGCAACTACCGATGT
hcp-prom-Forward	CCATACAAGTAAATAGAGAGTCGGACTCTTTCTTC
hcp-prom-Reverse	GATGACACAAAAGTAGAAGCTGCTATCTGCCTG

27

Table 2 – Plasmids used in this study

Pg108	*P.gingivalis* shuttle plasmid, derived from pYHBA1
Pg108-*hcpR*	Wildtype *hcpR* gene in Pg108, expressed via *ermF* promoter
Pg108-hcpR-C33A	Pg108-*hcpR* with the C33A mutation
Pg108-*hcpR*-H124A	Pg108-*hcpR* with the H124A mutation
Pg108-*hcpR*-H149A	Pg108-*hcpR* with the H149A mutation
Pg108-*hcpR*-L156*	Pg108-*hcpR* with the L156* mutation – expressed truncated protein
Pg108-*hcpR*-M68A	Pg108-*hcpR* with the M68A mutation
Pg108-*hcpR*-M145A	Pg108-*hcpR* with the M145A mutation
Pg108-*hcpR*-M145A/H149A	Pg108-*hcpR* with the M145A/H149A double mutation
Pg108-*hcpR*-M68A/M145A	Pg108-*hcpR* with the M68A/M145A double mutation
Pg108-*hcpR*-Flag	Pg108-*hcpR*, has 3x FLAG tag on N-terminal
Pg108-*hcpR*-Flag_L156*	Pg108-*hcpR*-FLAG L156* - truncated HcpR with 3x FLAG tag
Pg108-*hcp*	Wildtype *hcp* gene in Pg108, expressed via native promoter
Pg108-*hcp*-prom-mut	Pg108-*hcp*-prom-mut – mutation at HcpR binding site
m-pET21-*hcpR*	Expression of HcpR with 6x His tag in *E. coli* BL21
m-pET21-hcpR-L156*	Expression of HcpR-SD with 6x His tag in *E. coli* Bl21
pFC20K-*hcpR*	Expression of HcpR with HALO tag in *E. coli* BL21

Table 3 – Strains used in this study

P. gingivalis strains

V2802	*P. gingivalis* W83 wildtype strain
V2807	*P. gingivalis hcpR* (PG1053) insertional mutant strain (Δ*hcpR*) derived from V2802
V3226	V2807 complemented with Pg108-*hcpR*-C33A
V3227	V2807 complemented with Pg108-*hcpR*-H124A
V3228	V2807 complemented with Pg108-*hcpR*-H149A
V3237	V2807 complemented with Pg108-*hcpR*-L156*
V3211	V2807 complemented with Pg108-*hcpR* – wild type HcpR
V3263	V2807 complemented with Pg108-*hcpR*-M68A
V3265	V2807 complemented with Pg108-*hcpR*-M68A/M145A
V3268	V2807 complemented with Pg108-*hcpR*-M145A/H149A
V3269	V2807 complemented with Pg108-*hcpR*-M145A
V3243	V2807 complemented with Pg108-*hcpR*-FLAG
V3237	V2807 complemented with Pg108-*hcpR*-FLAG L156*
V3239	*P. gingivalis* W83 *hcp* (PG0893) insertional mutant strain (Δ*hcp*) derived from V2802
V3242	V3239 complemented with Pg108-*hcp*
V3246	V3239 complemented with Pg108-*hcp*-prom-mut

E. coli strains

V3116	BL21 (DE3) m-pET21-*hcpR* for expression and purification via 6x His Tag
V3164	BL21 (DE3) m-pet21-*hcpR* L156 for expression and purification of the HcpR-SD
V3250	BL21 (DE3) pFC20K-*hcpR* for expression and purification via halo tag

Transformation of Plasmids into *P. gingivalis*

The *hcpR* deficient mutant strain of *P. gingivalis* W83 (Δ*hcpR*) was generated as previously described (54). The plasmids for transformation into *P. gingivalis* were purified from *E. coli* and concentrated to approximately 500 ng/ μL. Ten μL of the concentrated plasmid was then added to 50 μL of washed wild type *P. gingivalis* cells and placed into an electroporation cuvette. The samples were electroporated using a Gene Pulser II electroporation system (BioRad). Immediately after electroporation, 500 μL of warm BHI broth was added to the cuvette and immediately placed in the anaerobic chamber where the 550 μL of sample was added to 2mL of anaerobic BHI broth. After growing overnight, the samples were then plated on TSA-Blood agar plates with 0.5 μg/mL of tetracycline for selection. Colonies appeared after approximately 1 week and were re-plated. To screen, PCR was performed on the sample using primers specific for the genes on the plasmid. Strains positive for transformation were stored.

RNA Isolation and cDNA Generation for qPCR analysis

For RNA isolation all strains were grown to an early logarithmic phase (OD$_{660}$ 0.4-0.6) in mycoplasma media supplemented with 0.25 μg/mL of tetracycline. Samples were then treated with NaNO$_2$ for 15 minutes then harvested via centrifugation at 7000 x g RCF at 4 °C. RNA was isolated from cell pellets using an RNeasy mini-kit (Qiagen) following the manufacturer's protocol. Residual DNA was removed using the DNA-free DNase kit (Ambion) following manufacturer's protocol.

qRT-PCR analysis of gene expression

Real-time quantitative reverse transcriptase PCR (qRT-PCR) was performed using a Syber green based detection system on an Applied Biosystems 7500 fast real-time PCR system. Primers used in this study are listed in Table 1. The cDNA was generated using a sensifast cDNA synthesis kit (Bioline) as per manufacturer's protocol. The qPCR reaction was performed using a SYBR green qPCR mix (Applied Biosystems). The equivalent of 10ng of cDNA was added to each reaction and experimental samples were tested in triplicate. The samples were normalized to a probe specific for 16s rRNA.

RNA-seq Library Generation

Samples of wildtype and V2807 *hcpR* mutant *P. gingivalis* were grown in an overnight culture of BHI media. The overnight cultures were used to inoculate cultures of mycoplasma media starting at an OD_{660} of approximately 0.15. Cultures were grown to mid-log phase and then exposed to 200 µM nitrite for 1 hour before being centrifuged and harvested. RNA isolation was carried out using the RNeasy mini-kit (Qiagen) following manufacturers protocol. Residual DNA was removed using the DNA-free DNase kit (Ambion) following manufacturers protocol. For RNA-seq library generation, the Ovation complete Prokaryotic RNA-Seq DR multiplex kit (Nugen) was used. The library was generated following the manufacturers protocol and subsequently sequenced by VCU nucleic acid sequencing core.

HcpR *in vivo* activity assay

Growth studies utilizing the plasmid-complemented strains of V2807 were performed in mycoplasma media in 0.25 µg/mL tetracycline plus/minus 2mM $NaNO_2$

(Sigma-Aldrich) with a starting OD_{660} of 0.15. The OD_{660} of each culture taken at the 3, 6, and 24 hour mark. Simultaneously, 5 mL of culture was harvested at the mid-log phase (OD_{660} 0.4 – 0.7) for RNA isolation and qRT-PCR studies.

HcpR *in vivo* ChIP

An HcpR construct that places a 3x FLAG tag on the N-terminus of HcpR downstream of the ermF promoter was synthesized and cloned into the Pg108 vector at the *Sph*I and *BamH*I sites to create the Pg108-*hcpR*-FLAG plasmid. The entire sequence of the synthesized construct is located in the appendix. This plasmid was mutated using the L156*-Forward and L156*-Reverse primers using the Quik-Change site directed mutagenesis kit (Agilent Technologies) to create the plasmid Pg108-L156*-*hcpR*-FLAG. This plasmid expresses a truncated FLAG-tagged HcpR lacking the DNA binding domain that was used as a negative control. Both of these plasmids were electroporated into the Δ*hcpR* knockout mutant strain (V2807) to create the strains V3243 (Pg108-*hcpR*-FLAG) and V3237 (Pg108-*hcpR*-FLAG L156*).

Strains V3234 and V3237 were grown on blood plates with appropriate antibiotics and used to inoculate an overnight culture of BHI media. The overnight culture was used to inoculate a culture of 5mL mycoplasma media with 0.25 µg/mL tetracycline at OD_{660} of 0.15. At mid-log phase the cultures were exposed to 2mM nitrite for 2mM. After nitrite treatment formaldehyde was added to a final concentration of 1% to cross link and incubated at room temp for 20 minutes. After incubation cross-linking was quenched via the addition of glycine to a final concertation of 0.5 M. Cells were harvested via centrifugation and washed with ice cold PBS. Washed cells were suspended in 1mL of lysis buffer (50mM Tris HCl, pH 7.5, 150 mM NaCl 1mM EDTA, 1%-Triton X-100, plus

protease inhibitor cocktail). Lysozyme was added to a final concentration of 1 mg/mL along with Cell Lytic B (Sigma) to lyse cells. Cells were lysed at room-temp for 15 minutes.

After incubation, the lysis mixture was sheared on ice in a bath sonicator. After sonication, insoluble material was removed via centrifugation at 13,000xg for 10 minutes. The cleared lysates were added to ANTI-FLAG M2 magnetic beads. The samples were incubated for 2 hours at room temp with gentle shaking. Resin was washed 5 times at room temp with 20x packed gel volumes of TBS on a magnetic separator. Samples were eluted from the resin using 5 packed gel volumes of 3x FLAG peptide elution buffer (TBS containing 20 µg/mL of FLAG peptide). Samples were incubated with elution buffer for 30 minutes. After incubation the supernatant was removed and stored at -20°C. The samples were de-crosslinked via treatment with 20 µg protease K at 65ºC for 15 minutes and boiled for 15 minutes.

Cloning and Expression of Recombinant Proteins

The *hcpR* gene (PG1053) was cloned into a modified pET21d vector (a TEV cleavage site was added downstream of the N-terminal 6x His-tag for removal via TEV protease digestion) using gene specific primers that added *Bam*HI and *Xho*I sites to the 5' and 3' end of the gene respectively. The PCR fragment containing the *hcpR* gene was digested and cloned into the m-pET21d vector using these restriction sites following a standard T4-ligase cloning procedure. As an alternative purification route the *hcpR* gene was also cloned into the pFC20K vector (Promega) using the *Sgf*1 and *Eco*ICRI restriction sites to add a C-terminal Halo tag. Recombinant plasmids were transformed and screened in *Escherichia coli* DH5-α and positive clones were subsequently sequenced to confirm and transformed into *E. coli* BL21 (DE3) cells (Bioline) for protein expression.

The N-terminal sensing domain of HcpR (referred to as HcpR-SD) was made using QuikChange II Site-Directed Mutagenesis Kit (Agilent Technologies). Primers were designed to change Leucine 156 to a stop codon on the HcpR-pET21 plasmid. Subsequent PCR generated plasmids were screened and sequenced. Plasmids positive for stop codon insertion were transformed into BL21 (DE3) *E. coli* for protein expression.

Cells for expression of HcpR (full-length and SD) were grown overnight with antibiotic in auto-induction media or in LB broth to an OD_{660} of 0.5-0.7 and induced using 1mM of IPTG. Cells that expressed HcpR from the m-pET21d plasmid were lysed via 10x Cell Lytic B detergent mix. Benzonase nuclease (250 units) was used to degrade genomic DNA. Samples were centrifuged at 25000xg to clear cell lysates. HcpR was purified using Ni-NTA agarose (Qiagen) following manufacturer's protocols and eluted in 50 mM $NaPO_4$, 300 mM NaCl, 250 mM Imidazole pH 8.0 buffer.

Cells that expressed HcpR from the pFC20K plasmid were frozen and lysed using lysozyme (1 mg/mL) at room temp. Benzonase nuclease (250 units) was used to degrade genomic DNA. Samples were centrifuged at 25000xg to clear cell lysates. HcpR was purified using Halo Affinity agarose (Promega) and removed from the agarose via acTEV (Thermo Fisher Scientific) protease digestion as per manufacturer's protocol in 25 mM HEPES, 150 mM NaCl, 1mM TCEP buffer. Recombinant HcpR from the m-pET21d vector and purified from the Ni-NTA column was digested with TEV protease to remove the 6x His-tag from HcpR; after digestion the sample was passed through a Ni-NTA column to remove free tag, uncut protein, and TEV protease.

Reconstitution of HcpR with Heme

To reconstitute with heme, a ~2.5 molar excess of heme was added to the purified and digested HcpR. The sample was then dialyzed overnight in 1 L of a 20mM $NaPO_4$ (pH 7.5), 150mM NaCl, 1mM TCEP, and 5% glycerol buffer to remove excess heme.

Crystallization and Structure Determination

His-tagged purified HcpR-SD protein was dialyzed against 25mM Tris-HCl, pH 7.0, 0.1M NaCl, 1mM TCEP after TEV digestion and concentrated to 15 mg/ml. Crystallization experiments were carried out using Crystal Gryphon robot (Art Robbins Instruments) at 20°C. A wide range of commercially available crystallization conditions were screened; 58 µl reservoir solution and 400nL crystallization drops were dispensed on 96 well INTELLI-PLATES by Gryphon Dispenser. Small crystals were obtained in one week with a number of different precipitants, and further refinement of conditions resulted in diffracting crystals from ammonium sulfate as precipitant. Attempts to improve the quality and size of crystals using sitting drop vapor diffusion method was performed up to microliter range in 24 well VDX crystallization plates (Hampton Research). Two crystal forms were obtained using 1.2-1.4 M ammonium sulfate, 0.2M NaCl, and 0.1M Na Acetate, pH 4.5 as a reservoir solution. However, both crystal forms diffracted to 4-5 Å resolution. Crystal dehydration was applied to improve diffraction quality of crystals (74). Prior to data collection, the crystals were first washed in 2.5 µl cryoprotectant solution containing 0.1M Na Acetate, pH 4.5, 1.3 M ammonium sulfate, 0.2M NaCl and then transferred stepwise to similar solutions containing 5, 10, 12.5, 15, 17.5, and 20% glycerol. All steps were exposed to air and soaking time for each step was about 3-4 minutes. Also 2 additional annealing steps in cryopropectant solution (25% glycerol)

improved diffraction quality of crystals. X-ray data sets of the tetragonal crystal form were obtained at 100K on an R-axis IV++ image plate detector using CuKa X-ray (λ = 1.5418) from Rigaku Micro-MaxTM -007 X-ray source equipped with Varimax confocal optics operating at 40 kV and 20 mA (Rigaku, The Woodlands, TX). Crystals diffracted to 3.15 Å resolution and belonged to space group $P4_122$ with typical cell constant of 145.30, 145.30, 77.93 Å with 2 monomer per asymmetric unit. Intensity data were integrated, scaled and merged using d*trek and converted to amplitudes with TRUNCATE in the CCP4 suite (75). Heavy atom derivatives of HcpR was prepared by soaking of tetragonal crystal for 2 hours in 0.1 M Na Acetate, pH 4.5, 1.3M ammonium sulfate, 0.2M NaCl solution containing 0.5 mM Potassium tetrachloro palatinate (II) (K_2PtCl_4). The second crystal form of HcpR belonged to the space group C2221 with unit cell dimensions 133.47, 138.85, and 44.55 Å and diffracted to 2.24 Å resolution . Diffraction data set was collected at the Stanford Synchrotron Radiation Light Source (SSRL). The data was processed with the program imosfilm (CCP4 suite). Diffraction data statistics for all three data sets are shown in appendix.

Phasing, Model Building and Refinement

Phases were calculated to 3.5 Å based on isomorphous and anomalous differences for Pt derivative. Heavy atom sites were determined and phasing was done by SOLVE following the density modification in RESOLVE (76). The optimal solution had a BAYES-CC 35.1, FOM 0.39, map skew 0.12 with 2 Pt sites identified for derivative K_2PtCl_4. Auto Model building resulted in an initial model of 238 amino acids residues build with R_{work} 0.41 and R_{free} 0.47. Phases were transferred to the isomorphous native data and extended to 3.15 Å resolution. The model was refined by using phenix to a final R-

work of 19.60 and R-free of 23.90. Crystal structure of orthorhombic form was determined by molecular replacement method using tetragonal structure as a starting model and refinement was accomplished in phenix followed manual rebuilding into 2mFodFc maps in COOT (77). The structure was refined to 2.6 Å resolution with final Rwork/Rfree 23.50/30.47. The final model consists of two monomers, while the biological dimer is formed with other symmetry related molecules.

Small Angle X-ray Scattering (SAXS) experiments

Recombinant HcpR was purified and sent to the SIBYLS beamline at the Lawrence Berkeley National Laboratory. A concentration gradient of 0.5 mg/ml, 1.0 mg/ml, and 2 mg/ml of Apo-HcpR was exchanged in 25 mM Tris, 100 mM NaCl, and 2 mM TCEP at pH 7.5 buffer. Each form of the protein was dialyzed against 2 L of the buffer overnight before being sent off. The matching buffer was sent with it. All SAXS data was collected at the Advanced Light Source (ALS), a national user facility operated by Lawrence Berkeley National Laboratory on behalf of the Department of Energy, Office of Basic Energy Sciences, through the Integrated Diffraction Analysis Technologies (IDAT) program, supported by DOE Office of Biological and Environmental Research. The ATSAS software pack was used to analyze the scattering profiles and create the graphs (78). DAMMIN was used to create the ab initio models (79). Rigid body modeling of the homodimer chimeric model was performed using SASREF (80). The chimeric model was superimposed on the *ab initio* model using SUPCOMB (81). EOM was use to evaluate the conformational flexibility of full length HcpR (82).

Sedimentation Velocity Experiments

Recombinant halo-purified HcpR was dialyzed into a 50 mM HEPES, 150 mM NaCl, and 1mM DTT buffer and diluted to 0.2 mg/mL, 0.5 mg/mL, and 1.0 mg/mL. A Beckman Optima XL-1 analytical ultracentrifuge was used to analyze the samples. The sedimentation velocity experiment was run at 4000, 5000, and 7000 RPM in a four position AN-60Ti rotor at 20 °C in aluminum double sector cells. Concentration profiles were recorded using UV absorption (280nm).

Luminol Assay

HcpR-SD was reconstituted with heme and dialyzed into a 10mM Phosphate, 100mM NaCl, 1mM TCEP, pH 7.5 buffer. Approximately 10 μg was added to a native 4-16% polyacrylamide gel and the protein was resolved under native conditions. *P. gingivalis* OxyR reconstituted with heme was used as a negative control for the heme binding study. The heme binding proteins were detected by soaking the gel in luminol (Perkin-Elmer) for 5-10 minutes and then activating the heme with hydrogen peroxide (3%). The luminescence signal marking the presence of heme was detected using film.

UV-Vis Spectrum Experiments

Spectrum of heme reconstituted HcpR or HcpR-SD was recorded on a Biomate 3S UV-Vis spectrophotometer (Thermo-Fisher Scientific) in a gas tight 1 cm quartz cuvette in a 25 mM Tris 100 mM NaCl, 1mM TCEP pH 7.5 buffer or a 10mM Phosphate, 100mM NaCl, 1mM TCEP, pH 7.5 buffer. The ferrous form of heme was obtained by adding an excess of sodium dithionite (1mM). An excess of S-Nitrosoglutathione (GSNO) or NONOate (Sigma) was used to attain the nitrosylated forms of the protein.

Resonance Raman Spectroscopy

Recombinant HcpR was dialyzed into a 25 mM Tris, 100 mM NaCl, and 1mM TCEP buffer at pH 7 and concentrated to 20 mg/mL. An equimolar amount of heme was added to the sample with 5 mM of dithionite to achieve ferrous heme. The sample was then desalted through a PD-10 desalting column in an anaerobic chamber to remove excess unbound heme and diluted to 10 mg/mL. The nitrosylated form of HcpR was obtained by the addition of 100 μM of NONOate. The anaerobic samples were added to glass melting point capillaries and sealed. The resonance Raman spectra was obtained with a krypton ion laser at 406.7 nm (Spectra-Physics, model 171-01; Mountain View, CA). The detection system used was a liquid N_2 cooled 400 x 1340 CCD detector (Princeton Instruments, Roper Scientific, Trenton NJ) and a 0.5 m spectrograph (Spex model 1870; Horiba/Jobin-Yvon, Edison NJ). GRAMS/AI version 7.0 was used to perform spectral baseline leveling by a fifth order polynomial routine. The mathematical peak fitting module of Origin Pro version 7.5 was used to deconvolute band shapes and generate the spectral graph.

Bioinformatics

All figures of structures were generated using UCSF Chimera or PyMOL (83). InterproScan5 was used to match the sequence of HcpR against a number of databases to predict conserved domains of HcpR (84). The buried solvent excluded calculations and comparison overlays of homologues were calculated using UCSF Chimera. The volume of the hydrophobic pocket was calculated using the CASTp server (85). The alignments were made using Clustal omega (86). MODELLER was used to create the chimeric HcpR model (87). The C-terminal domain was modelled using the DNA binding domain of the

crystal structure of the full length DNR as a template (PDB ID 3DKW) (88). The Basic Local Alignment Search Tool (BLAST) was used to find proteins similar to that of HcpR. The structure of HcpR was compared to that of other heme binding FNR-like regulators: the crystal structure of DNR from *Pseudomonas aeruginosa* is known (PDB 3DKW) and the Crystal structure of CooA from *Rhodospiridium rubrum* is also known (PDB 4K8F). Using the crystal structure of HcpR, the Backphyre program, part of the Phyre II protein folding server, was utilized to find structures related to HcpR (89). Using DNR as a template and the one-to-one threading method of Phyre protein folding server, a 3-Dimensional homology model of HcpR was constructed.

III. Results

Part 1: HcpR is necessary for the survival and response of *P. gingivalis* to reactive nitrogen species

Previously it was reported that HcpR regulates the expression of *hcp* in response nitrite and nitric oxide and was necessary for survival of *P. gingivalis* (54). To confirm this the wild-type *P. gingivalis and* the Δ*hcpR* mutant strain (V2807) were grown in varying concentrations of nitrite and the growth was monitored over time using OD_{660} (Fig. 1.1). The wildtype strain is capable of growing in concentrations of nitrite of 4mM and exhibits no significant loss of growth at 1mM concentrations of nitrite. It is not until the concentration of nitrite reaches 8mM that the bacterium is incapable of growing. This is in contrast to the V2807 knockout strain which shows a great decrease in the ability to survive in nitrite. At 200 µM nitrite the bacterium is almost incapable of growing and at 1mM there is no growth at all. HcpR is not needed for growth in media if there is no reactive nitrogen species present as there is no difference between growth of the wildtype strain and the Δ*hcpR* knockout strain (V2807) at 0mM nitrite. It should be noted that the levels of nitrite in the oral cavity can exceed 2mM, especially after a meal rich in nitrates (9). Thus HcpR is necessary for survival of *P. gingivalis* at physiological concentrations of nitrite.

A.
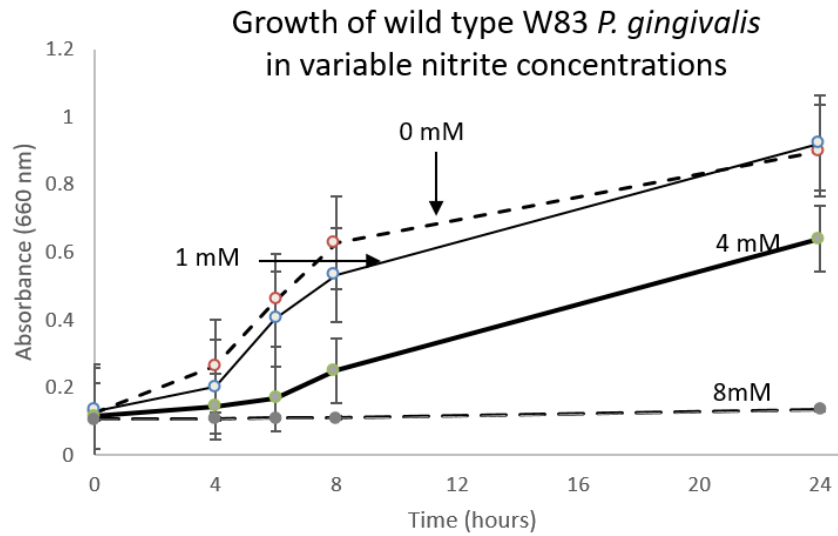
B.
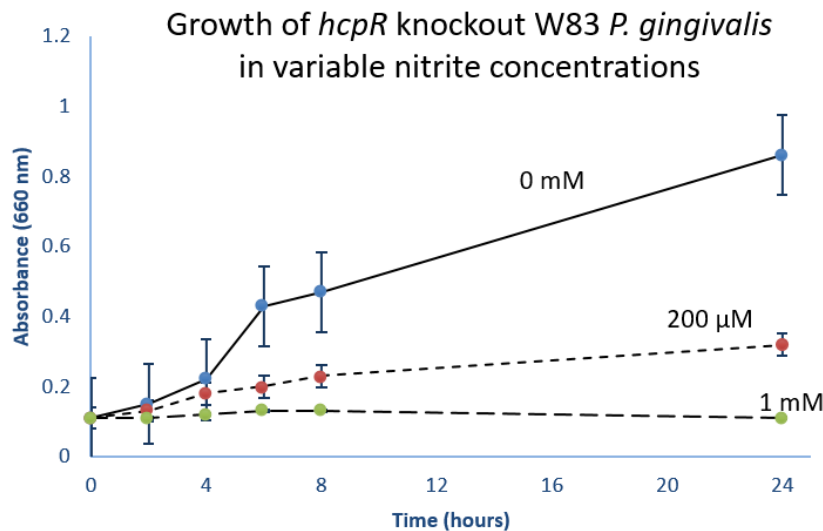
Figure 1.1 - Growth of wildtype *P. gingivalis* and *hcpR* knockout strain in variable concentrations of nitrite. **A**. Growth curve of the *P. gingivalis* wild type strain plus/minus nitrite in mycoplasma media. **B.** Growth curve of the *P. gingivalis hcpR* knockout strain (V2807). Without *hcpR*, the strain is not capable of growing in physiological concentrations of nitrite.

The exposure of *P. gingivalis* to reactive nitrogen species leads to the upregulation of *hcp* at the transcript level. This response is elicited by both nitrite and nitric oxide and can be observed through qPCR (Table 4). Exposing the wild type strain to 200 µM nitrite results in an approximately 250 fold upregulation of *hcp* transcript. This upregulation is not seen in the V2807 knockout strain and the levels of *hcp* stay at unstimulated levels. HcpR is much more sensitive to nitric oxide stimulation as nM concentrations of NO are capable of stimulating *hcp* expression. GSNO and DEA-NONOate are nitric oxide generating species that both release the NO radical. As with nitrite, the V2807 knockout strain is not able to upregulate *hcp* in response to the presence of these reactive nitrogen species. GSNO releases NO at a 1:1 molar ratio and DEA-NONOate release NO at a 1:2 molar ratio (for every 1 mole of NONOate 2 moles of NO are released). Indeed, there is a 2x increase in the *hcp* induction when comparing GSNO to NONOate.

It should be noted that previous studies have implicated Hcp as a putative hydroxylamine reductase (52, 90). Hydroxylamine is a common intermediate in biological denitrification cycles that is can also act as a mutagen so it is necessary for bacteria to avoid hydroxylamine buildup (91). However, in our studies we do not see *hcp* overexpression in response to hydroxylamine; there is no change in *hcp* transcript levels in either the wildtype or Δ*hcpR* strains (V2807) when exposed to hydroxylamine. This is in line with recent studies that suggest Hcp acts as a high affinity NO reductase in anaerobic environments rather than a scavenger of hydroxylamine (92).

Table 4 - HcpR is necessary for the expression of *hcp* (PG0893) in response to nitrite.

Differential Expression of PG0893 (*hcp)* + / - nitrosative stress		
	W83	V2807
200 µM Hydroxylamine	0.66 ± 0.1	0.93 ± 0.2
200 µM Nitrite	250.5 ± 24.9	1.6 ± 0.0
100 nM GSNO	150 ± 20.2	0.97 ± 0.1
100 nM DEA-NONOate	304.4 ± 25.2	1.07 ± 0.1
100 nM S-glutathione	0.71	1.14

*Standard deviations calculated for each value.

GSNO exhibits a dose-response relationship with *hcp* upregulation. Exposure of *P. gingivalis* to an increasing amount NO results in a dose-dependent increase in the *hcp* expression when measured by qPCR (Fig. 1.2). HcpR is capable of detecting low nM

amounts of NO in the environment. For a 15 minute exposure time there is an approximately 40 fold increase at 50nM GSNO. This attests to the sensitivity of HcpR to detect these species and upregulate the expression of *hcp* quickly.

GSNO dependent increase in PG0893 expression
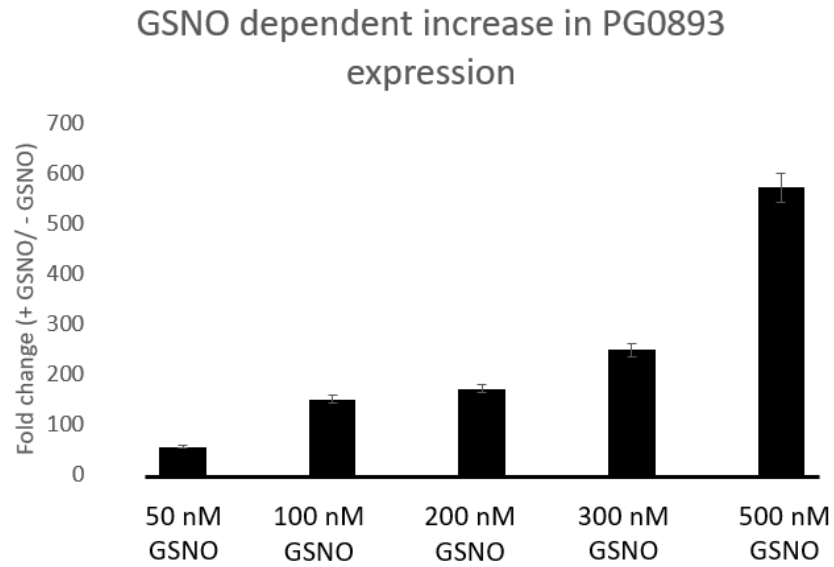
Figure 1.2 – Dose dependent response of HcpR to nitric oxide. Increasing amounts of the nitric oxide generating species results in an increase in the *hcp* transcript level in response.

The V2807 knockout strain was complemented using the Pg108-*hcpR* plasmid via electroporation. When the wild type, V2807, and complemented strain are grown in 0 mM nitrite there is no significant difference in the growth (Fig. 1.3A). This also indicates that the plasmid is not exerting an effect on the growth rate. When the 3 strains are grown in 2mM nitrite, the plasmid is capable of complementing the loss of *hcpR* in the V2807 strain (Fig. 1.3B). The wildtype and complemented strain grow at comparable rates and there is no significant difference in the growth.

The cDNA of the wildtype, V2807, and complemented strain was purified and the expression of *hcpR* was observed utilizing end-point PCR (Fig. 1.4A). The Pg108-*hcpR* plasmid is capable of producing a stable *hcpR* transcript in the complemented strain. This creates a functional HcpR protein *in vivo* that is capable of resuscitating upregulation of *hcp* in response to nitrite (Fig. 1.4B). There is no significant difference in this upregulation between the wildtype and complemented strains.

A.

Growth in 0mM Nitrite

B.

Growth in 2mM Nitrite
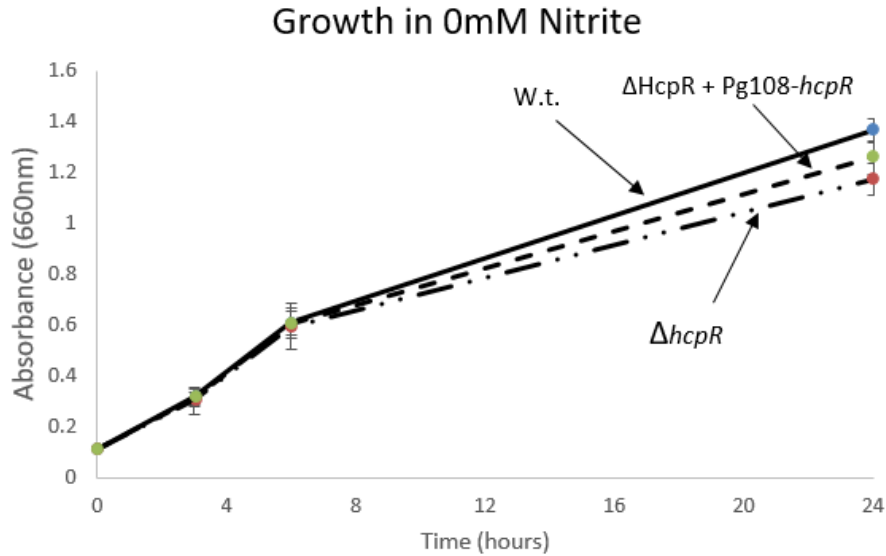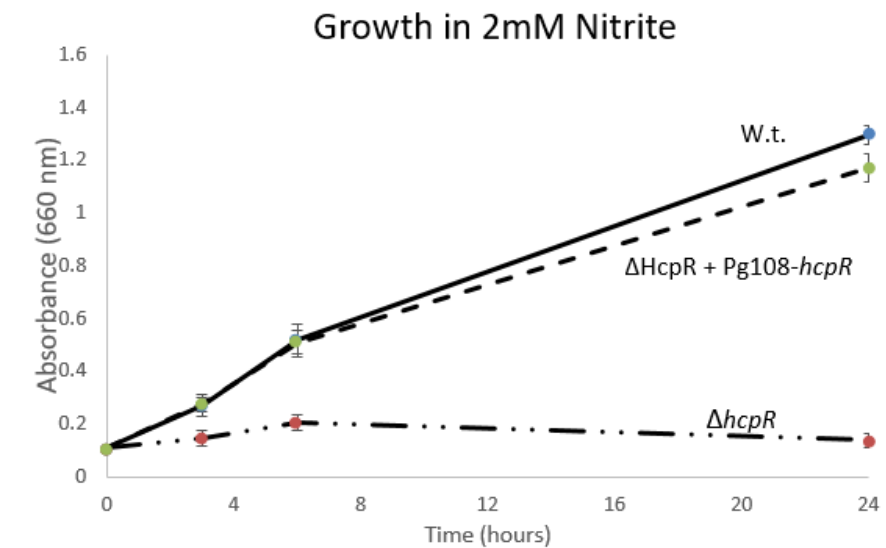
Figure 1.3 - Complementation of the *hcpR* knockout mutant strain utilizing the Pg108 vector. A. The wildtype, Δ*hcpR* knockout (V2807), and complemented strains grown in mycoplasma media show no difference in growth rate. **B.** The wildtype and complemented strains are capable of growing in 2mM nitrite, while the *hcpR* knockout strain (V2807) is not capable.

A.
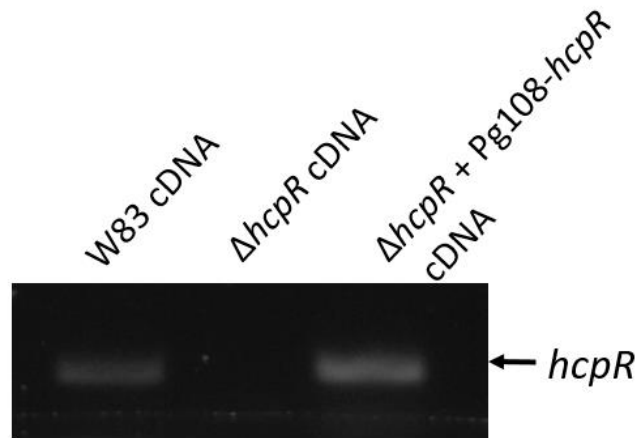
B.
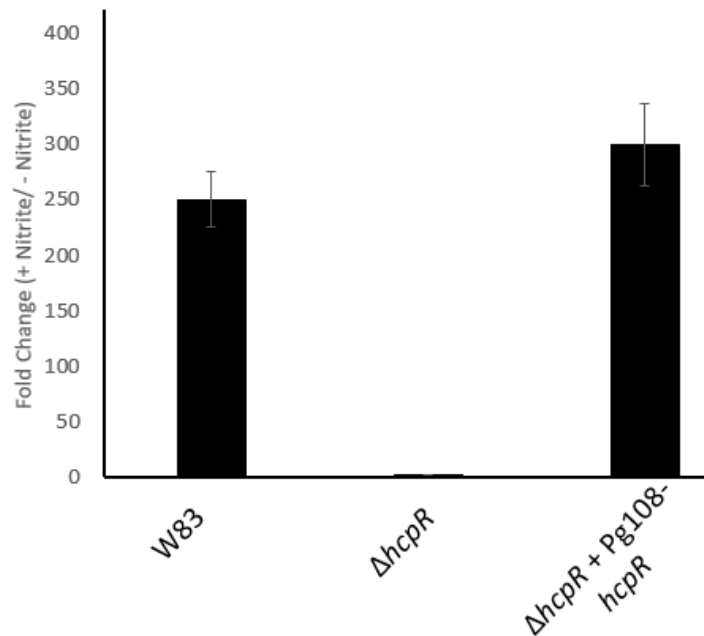
Figure 1.4 - Complementation of the *hcpR* knockout strain using the Pg108 vector restores the ability of the strain to respond to nitrite. A. Expression of *hcpR* transcript from the wild type strain, Δ*hcpR* knockout (V2807), and from the Pg108-*hcpR* vector in the complemented V2807 strain. **B.** Expression of *hcp* via qPCR in the wildtype, V2807 knockout strain, and the complemented strain.

To better understand the role HcpR may play in the nitrosative stress response and to identify other genes that could play a role in the nitrosative stress response a whole transcriptome sequencing approach was taken. Libraries of the wildtype and *hcpR* knockout mutant strains with and without exposure to 200 µM nitrite were generated and then sequenced. The sequencing results were then compared and the top 20 most upregulated and downregulated genes of each comparison are listed in tables 4-7. For the comparison between samples, any gene with less than 10 reads was not analyzed and genes that were differentially regulated ~2.5 fold were focused on.

First, the transcriptome of the wildtype with and without nitrite was compared (Table 4). The most upregulated gene, by a large margin, is *hcp* (PG0893) at 144.15 fold higher in the nitrite treated sample which agrees with previous qRT-PCR studies. However, there is a significant drop off in genes upregulated. The second most up-regulated gene is just upstream of *hcp,* PG0890 and is increased only 2.91 fold. This gene codes for a putative radC protein, involved in DNA repair and is believed to be required for repair of strand breaks and after recombination (93). However, the increase of PG0890 may be artificial, due to its proximity to the very highly upregulated PG0893 (*hcp*). The next most up-regulated gene is PG1979 and is increased 2.59 fold. This gene codes for a small hypothetical protein with unknown function that is found only in *P. gingivalis*. After these 3 genes, there are no other genes that are up-regulated more than 2 fold. The presence of nitrite does not exert any change in the expression of HcpR at the transcript level. This is in contrast to *Desulfovibrio desulfuricans*, where recent studies have shown that one of its *hcpR* proteins *(hcpR1)* binds to its own promoter and regulates itself in response to NO and nitrite (67).

Of the downregulated genes, no major gene stands out significantly. PG1534 is the gene that is most down regulated in W83 when exposed to nitrite, however it is only regulated 1.67 fold. Nitrite does not have much of an effect on the down regulation of genes via transcription.

Next we compared the genes most up-regulated and down-regulated in the response to nitrite in the V2807 knockout mutant strain (Table 5). Two of the genes most upregulated are both subunits of the cytochrome d ubiquinol oxidase, *cydA* and *cydB*. These genes are up regulated comparably at 3.61 and 3.23 fold respectively. Both the *cydA* and *cydB* genes are regulated and expressed as a transcriptional unit and this is reflected in their similar fold changes. The other significantly down-regulated gene, PG1222, codes for a hypothetical protein of unknown function that is well conserved among *P. gingivalis* strains.

The 4 most significantly downregulated genes are PG2104, PG1167, PG0337, and PG1840. When compared to the profile of the wildtype strain plus/minus nitrite, more genes are down regulated in the profile of the V2807 strain plus/minus nitrite. However, this could be because nitrite is arresting growth, thereby slowing metabolism and leading a broad decrease in transcription. The most down regulated gene in the V2807 strain in response to nitrite is PG2104 at -7.15 fold. This region of the genome codes for a small hypothetical protein. This protein does resemble a partial domain of a hemoglobin found in *Pagothenia bernacchii*. Thus although its function is unknown, it may play a role as a heme binding protein. The next most significantly down regulated genes in the nitrite treated samples are PG1167 at 6.39 and PG0337 at 4.85. Both genes code for hypothetical proteins of unknown function that are well conserved across many *P.*

gingivalis strains. PG1840 is down regulated 4.27 fold and codes for a well conserve

gene that bears resemblance to a zinc metalloprotease family.

Table 5 – Genes most upregulated (left) and downregulated (right) when the wildtype *P. gingivalis* is exposed to nitrite (+ Nitrite / - Nitrite).

W83 + Nitrite vs. W83					
Upregulated by nitrite			Downregulated by nitrite		
Gene	Fld[2]	P[1]	Gene	Fld	P
hcp	144.1513	0.000591	PG1476	-1.41792	0.542104
PG0890	2.91208	0.013652	PG1457	-1.42356	0.503132
PG1979	2.591288	0.060828	PG1492	-1.43092	0.335521
groEL	1.604616	0.018719	PG2019	-1.44276	0.153225
htpG	1.509264	0.008476	PG0242	-1.4446	0.100372
dnaJ	1.483316	0.171433	PG0572	-1.45465	0.203872
groES	1.423766	0.078255	PG1487	-1.4576	0.45643
PG1811	1.418838	0.086747	PG1515	-1.48328	0.210173
PG2043	1.384237	0.392613	PG1556	-1.48837	0.505656
grpE	1.374339	0.095567	PG2046	-1.48902	0.415697
DnaK	1.374317	0.042703	*radC*	-1.48906	0.407503
PyrH	1.350379	0.409306	PG0628	-1.49153	0.223338
PG0659	1.333261	0.083265	PG1827	-1.49197	0.120438
clpB	1.306898	0.510695	PG0901	-1.49899	0.014109
PG1778	1.297413	0.025267	*tpr*	-1.51157	0.699076
PG1618	1.294029	0.345995	PG1514	-1.51415	0.291326
PG1649	1.278902	0.327177	PG2082	-1.56086	0.335778
PG0975	1.271526	0.344402	PG1570	-1.58889	0.464792
PG0747	1.269849	0.434224	PG0556	-1.59319	0.079292
aroA	1.257298	0.450317	PG1534	-1.67076	0.308358

[1]P value calculated via t-test using 4 biological replicates

[2]Fld- fold change of transcript between conditions

Table 6 - Genes most upregulated (left) and downregulated (right) when the V2807 *hcpR* knockout strain of *P. gingivalis* is exposed to nitrite (+ Nitrite / - Nitrite)

V2807 + nitrite vs V2807					
Upregulated by nitrite			Downregulated by nitrite		
Gene	Fld[2]	P[1]	Gene	Fld	P
cydA	3.610688	0.006042	*rplS*	-1.98204	0.199748
PG1222	3.37876	0.115489	PG1484	-1.99588	0.030074
cydB	3.228729	0.001138	*pruA*	-2.00158	0.08307
PG1869	1.896938	0.014896	PG0555	-2.02056	0.140401
htpG	1.894053	0.084675	PG1904	-2.03365	0.003426
groEL	1.824173	0.013915	*rplO*	-2.05698	0.1466
PG0429	1.739138	0.134498	*rpsP*	-2.07932	0.226307
sodB	1.734448	0.090886	PG1271	-2.08023	0.087042
hprA	1.714129	0.11633	PG0265	-2.1393	0.24387
PG1512	1.670446	0.165155	PG2046	-2.16475	0.082784
PG0778	1.633451	0.161092	*rplI*	-2.17355	0.175355
etfB-1	1.632825	0.010516	PG2213	-2.17481	0.03522
clpB	1.631526	0.307977	*rpmA*	-2.1749	0.35156
PG0901	1.629436	0.387775	PG0662	-2.18413	0.058576
clpC	1.585894	0.135537	PG1270	-2.19347	0.116656
4hbD	1.573836	0.089949	*rpmG*	-2.22311	0.27426
dnaK	1.569741	0.079833	PG0505	-2.34496	0.01291
PG0433	1.533124	0.143825	PG0985	-2.35585	0.305981
PG0850	1.510975	0.226498	PG1421	-2.38897	0.176481
PG1868	1.505946	0.289821	*rpmH*	-2.59136	0.171304

[1]P value calculated via t-test using 4 biological replicates
[2]Fld- fold change of transcript between conditions

When comparing the number of the expression profiles of the wild type and V2807 strains, there is no significant difference that stands out. The most differentially regulated genes are PG1555, PG0283, and PG1570 which are higher in the wildtype and PG1979 which is higher in the mutant. All 4 of these genes code for hypothetical proteins of unknown function.

Finally, we compared the transcriptome of the wildtype and V2807 knockout mutant strains when exposed to nitrite. The overall levels of transcription are higher in the wildtype strain than they are in the V2807 strain. As with comparing the V2807 strain plus/minus nitrite, the presence of nitrite is arresting the growth of the mutant strain, thereby causing an overall decrease in the level of transcription. There appears to be 20 genes that are highly differentially regulated when comparing the wildtype to the mutant strain. As expected, the *hcp* gene (PG0893) is 250 fold higher in the wildtype strain than in the V2807 strain. This gene is by far the most drastically differentially regulated. The 2nd most differentially regulated gene PG1556 is 5.43 fold higher in the wildtype than in the mutant. This gene is a hypothetical protein that is conserved in *P. gingivalis* and contains a very well conserved domain of unknown function. PG0524 is 4.39 fold higher in the wildtype strain and codes for a conserved hypothetical protein found in *P. gingivalis* with no known function. Beyond the 3 most upregulated genes, there appears to be a higher overall level of transcription in the wild-type strain when compared to the mutant strain as a number of hypothetical genes appear to be slightly upregulated in the wild type strain.

Table 7 – Genes most differentially regulated in the wildtype W83 strains and V2807 Δ*hcpR* knockout strain (Wild Type / V2807).

	W83 vs. V2807				
Genes highly expressed in WT			Genes highly expressed in Mut		
Gene	Fld[1]	P[1]	Gene	Fld	P
PG1555	3.314837	0.321361	*acpP*	-1.40072	0.040995
PG1570	2.72173	0.340616	*pyrH*	-1.41012	0.196704
PG0283	2.617069	0.451883	PG2202	-1.41098	0.238494
PG1489	2.427553	0.427274	*rpsT*	-1.42066	0.362186
PG0285	2.424748	0.48499	PG0482	-1.45354	0.084735
thiE	2.395568	0.465477	*rho*	-1.46635	0.082446
PG0915	2.381308	0.456723	*htpG*	-1.46937	0.299362
PG0524	2.363152	0.521246	*rpsL*	-1.4932	0.138316
cas2-1	2.335153	0.149822	PG0723	-1.53632	0.018638
PG1179	2.279655	0.476292	PG2076	-1.54004	0.338469
PG0870	2.274541	0.476803	*dnaJ*	-1.54131	0.130512
PG0682	2.259556	0.461247	*grpE*	-1.56599	0.215825
thiG	2.235858	0.430072	*rpmJ*	-1.5662	0.109376
PG1554	2.234359	0.344358	*dnaK*	-1.56844	0.3907
PG0280	2.161234	0.452099	*groEL*	-1.63244	0.113613
PG1975	2.154308	0.338492	*clpC*	-1.69512	0.376672
PG1904	2.149993	0.496139	*groES*	-1.81687	0.059147
PG1180	2.147853	0.501924	*clpB*	-1.92152	0.506215
PG1984	2.105787	0.170539	PG1979	-3.50914	0.071445
PG1655	2.078442	0.431367	PG1053	-5.25083	0.021826

[1]P value calculated via t-test using 4 biological replicates
[2]Fld- fold change of transcript between mutant and wild type

Table 8 – Genes most differentially regulated in the wildtype W83 strains and V2807 Δ*hcpR* knockout strain when both strains are exposed to nitrite (Wild Type / V2807).

W83 + Nitrite vs V2807 + Nitrite					
Genes highly expressed in WT			Genes highly expressed in Mut		
Gene	Fld[2]	P[1]	Gene	Fld	P
hcp	250.636	0.000555	PG1015	-1.63675	0.038743
PG1556	5.432605	0.011271	PG1779	-1.65241	0.088599
PG0524	4.397573	0.00173	PG0723	-1.6554	0.134593
PG0915	3.490749	0.097521	PG0778	-1.66213	0.190018
PG1799	3.393247	0.094796	PG1317	-1.70054	0.063632
PG0890	3.347394	0.113834	*groES*	-1.74311	0.206198
PG0732	3.346344	0.065161	*dnaK*	-1.79146	0.138055
PG1489	3.330302	0.13541	PG0429	-1.80543	0.097497
PG1270	3.271221	0.114499	*etfB-1*	-1.81317	0.00571
PG0080	3.215698	0.141283	*htpG*	-1.84398	0.190629
PG1630	3.166724	0.054824	*groEL*	-1.85581	0.067195
PG1904	3.165124	0.063185	*acpP*	-1.90602	0.027631
PG1461	3.16408	0.120871	*sodB*	-1.94088	0.022038
PG2115	2.914874	0.16131	*clpC*	-2.18764	0.112206
PG1480	2.904793	0.125562	PG1869	-2.23512	0.008077
topB-2	2.858075	0.040376	*cydB*	-2.32466	0.000578
PG1655	2.784859	0.201573	*clpB*	-2.39881	0.190658
PG0283	2.772278	0.154333	*cydA*	-2.68268	0.003504
PG1861	2.764586	0.209749	PG1222	-2.7982	0.128974
PG0662	2.724927	0.159596	PG1053	-5.43299	0.017924

[1]P value calculated via t-test using 4 biological replicates
[2]Fld- fold change of transcript between mutant and wildtype

Since by far the most regulated gene in *P. gingivalis* is PG0893 (*hcp*), and no other gene is close, we decided to create a knockout mutant of *hcp* and determine whether the mutant has a similar phenotype to the *hcpR* knockout strain. Previously it was reported that the hcp was important in the resistance of *P. gingivalis* to nitric oxide stress where it played a role as a hydroxylamine reductase (52). We have shown that HcpR is important for the survival of *P. gingivalis* in response to nitrite and nitric oxide and regulates *hcp* in response to these chemicals but is not activated in response hydroxylamine. We created an isogenic knockout using the V2802 strain and exposed it to nitrite. Indeed, the *hcp* knockout strain V3242 is not capable of growing in physiological concentrations of nitrite (2mM) (Fig. 1.5).

Previously it was shown that HcpR binds to the *hcp* promoter using an electro-mobility shift assay (EMSA) (54). We confirmed the binding of HcpR to the *hcp* promoter *in vivo* using a ChIP based approach (Fig. 1.6). The *hcpR* mutant strain V2807 was complemented with the Pg108-*hcpR*-FLAG construct that produces a 3x FLAG tagged HcpR in *P. gingivalis*. The FLAG tagged HcpR is active *in vivo* and is capable of rescuing the nitrite sensitive phenotype of the knockout mutant. For a negative control, a truncated FLAG tagged HcpR missing the DNA binding domain was utilized. PCR using primers specific for the *hcp* promoter was performed utilizing the ChIP elutions. In the lanes using the full length HcpR ChIP, a band indicating the presence of the *hcp* promoter was found. This band is absent in the negative control lane. This result further confirms the binding of HcpR to the *hcp* promoter *in vivo* and that this binding is specific.
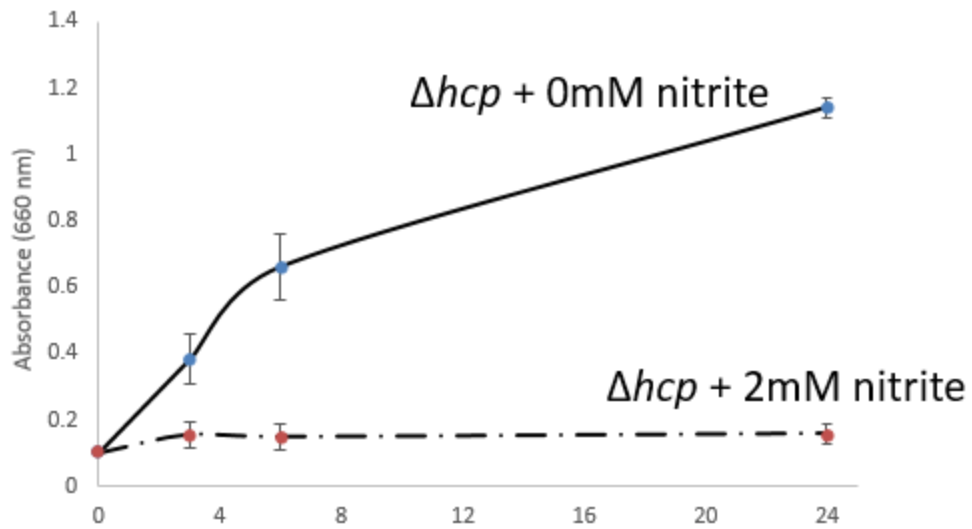
Figure 1.5 – Growth of *Δhcp* knockout strain in nitrite. The *Δhcp* knockout strain

(V3242) was grown plus/minus 2mM nitrite. As with the *hcpR* knockout strain, the *Δhcp*

knockout strain is not capable of growing in the presence of physiological

concentrations of nitrite.
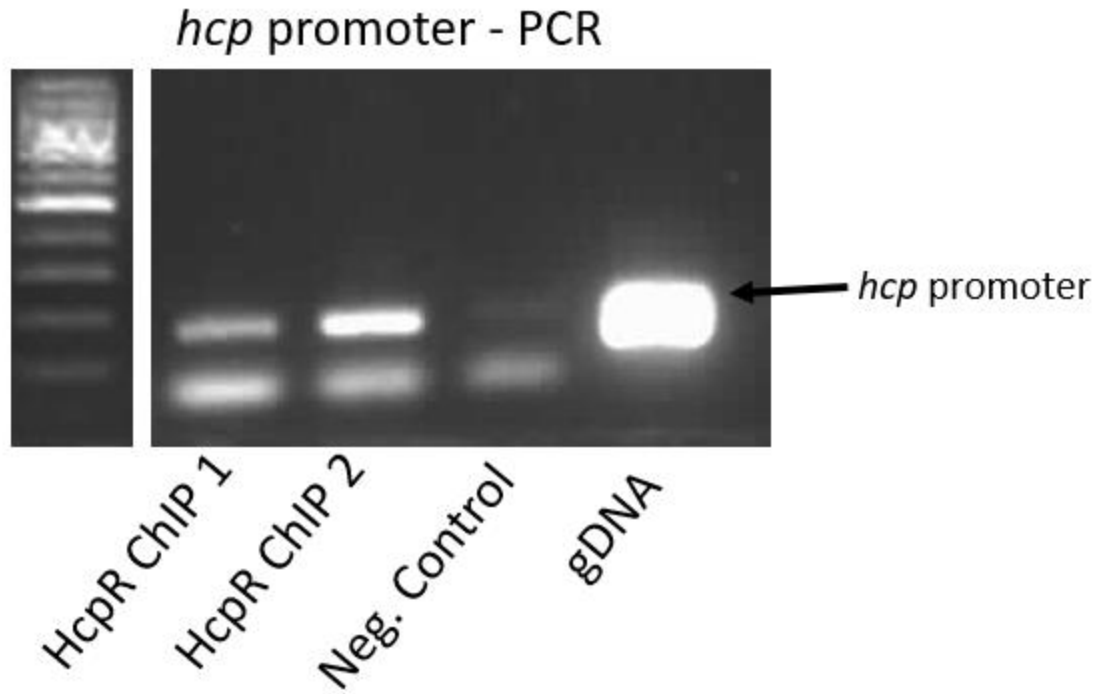
Figure 1.6 – PCR detection of the *hcp* promoter from HcpR ChIP. ChIP samples were eluted from FLAG antibody magnetic beads using FLAG peptide. Samples were digested with proteinase K and the samples were purified using Qiagen PCR purification kit. PCR was performed using the hcp promoter specific primers.

This and previous work have shown that HcpR regulates *hcp* through direct binding to its promoter however, it is not confirmed where the exact binding site of the promoter is located. *In silico* analysis of HcpR implicates it as a member of the FNR-CRP protein family. Typically, these proteins will bind to inverted repeats upstream of the transcription and translation start sites and the promoter region of *hcp* has one such site (Fig. 1.7A). To confirm that this is the location that HcpR binds to, we utilized our *hcp* knockout strain. We complemented this strain by simply cloning the *hcp* gene, including its promoter, into the PG108 vector (creating the Pg108-*hcp* vector). The inverted repeat sequence of the Pg108-*hcp* vector was deleted via site-directed mutagenesis to create the Pg108-*hcp*-prommutation vector. Both vectors were transformed into the *Δhcp* knockout mutant strain. Complementation with a wild-type copy of the promoter is capable of rescuing the nitrite sensitive phenotype of the mutant strain (Fig. 1.7B). However, the plasmid missing the inverted repeat sequence is not capable of rescuing the growth the *Δhcp* mutant (Fig. 1.7B).

A.

B.
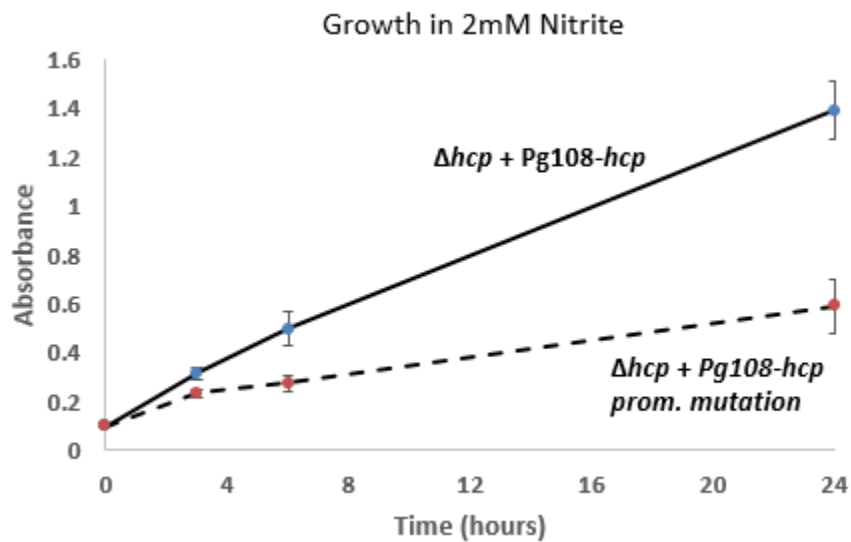
Figure 1.7 Binding of HcpR to the *hcp* promoter occurs at an inverted repeat upstream of the transcription start site of the gene. A. Overview of the *hcp* gene and location of the inverted repeat that is the HcpR binding site. B. The Pg108-*hcp* vector is capable of complementing the *hcp* knockout strain. When the inverted repeat is deleted from the promoter of this Pg108-*hcp* vector, the complement is not capable of growing in 2mM nitrite.

Conclusion – Part 1

HcpR is an integral part of the nitrosative stress response in *P. gingivalis*. An Δ*hcpR* knockout mutant strain cannot survive in physiological concentrations of nitrite and loss of HcpR abolishes the up-regulation of *hcp* (PG0893). Complementation of Δ*hcpR* strain using the Pg108-*hcpR* rescues the nitrite sensitive phenotype and restores the capability to up-regulate *hcp* in response to nitrite. Whole transcriptome sequencing reveals that *hcp* is by far the most differentially upregulated gene in *P. gingivalis* in response to nitrite. The *Δhcp* knockout mutant strain is not capable of growing in physiological concentrations of nitrite and has a similar nitrite sensitive phenotype. HcpR directly binds to the *hcp* promoter at an inverted repeat to control gene expression of *hcp.*

Part 2: Heme and Nitric Oxide binding properties of HcpR

Previously it was shown that *P. gingivalis* HcpR requires heme to bind to DNA of the *hcp* promoter *in vitro*, implicating heme as a potential cofactor (54). However, it is not known if heme directly binds to HcpR and what the properties of the heme binding were. To determine the heme binding properties of HcpR a number of different biochemical techniques were employed. Furthermore, having a solid understanding of the heme binding properties is necessary for understanding the gas sensing properties of heme based gas sensors.

FNR-CRP family regulators utilize an N-terminal sensing domain to bind ligands and small molecules. Binding of a ligand to this domain will cause allosteric activation of the protein. The variability of this N-terminal domain allows these family members to bind to different stimuli and incorporate different cofactors such as heme. To determine the heme binding ability of HcpR, an equimolar amount of heme was added to a purified sample of the HcpR Sensing domain (HcpR-SD). The binding of heme to the protein was detected by resolving the protein on a native gel and visualizing the peroxidase activity of heme through luminescence in a gel soaked in luminol and exposed to peroxide. Excess heme ran down the gel and heme bound to HcpR migrated with the protein and no heme binding was observed in the negative control sample (Fig. 2.1).
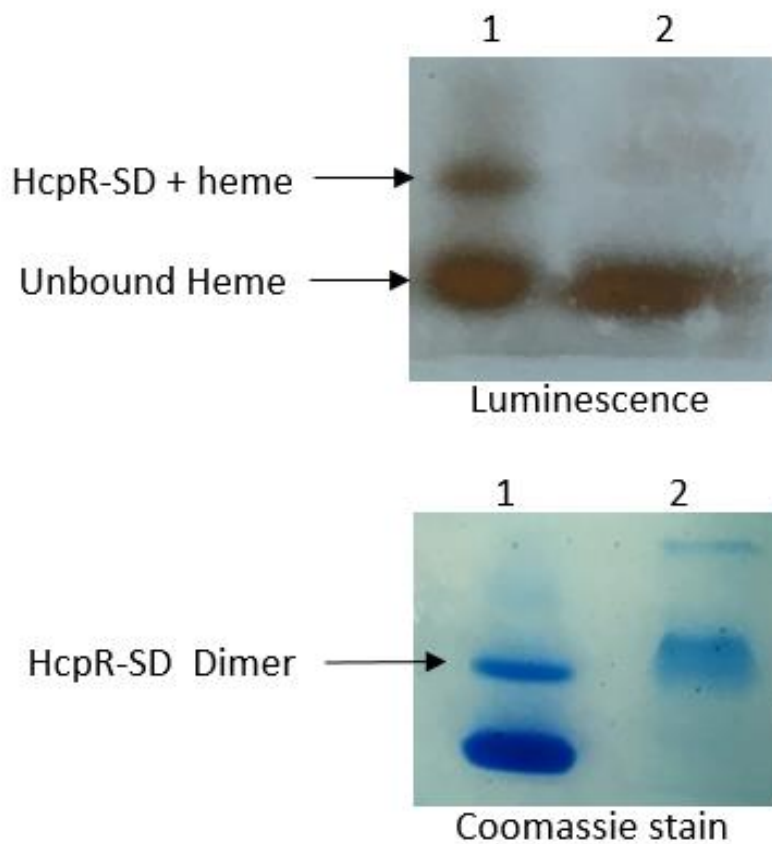
Figure 2.1 – Luminol heme binding assay of HcpR. All samples (Lane 1: HcpR-SD; Lane 2: Negative Control – *P.g.*OxyR) were reconstituted with heme and run on a native gel. Luminol was added to the gel and chemiluminescence indicates the presence of heme after the addition of 3% H_2O_2. Excess heme ran down the gel whereas bound heme migrated with the protein.

UV-Vis spectroscopy can be utilized to garner information about the properties of heme binding. The Soret peak is an intense peak in the 400 nm region of the visible spectrum. This region is sensitive to the π to π* transitions of the electron cloud typically found in porphyrin compounds such as heme (Fe bound protoporphyrin IX). The Soret peak is sensitive to changes in binding to heme iron and studies of the wavelength shift of this absorption band can give indications of the molecular mechanisms utilized by heme based gas sensors. Furthermore, porphyrins also exhibit a region of weaker, but still intense, Q bands that have absorption at the 500-750nm range of the spectrum. The α and β absorption bands that are characteristic of heme appear in this region. These bands can give information on the coordination and spin state of the heme iron.

The heme binding of HcpR was verified using UV-Vis spectroscopy under anaerobic conditions (Fig. 2.2). The reduced derivative was obtained by adding excess of sodium dithionite to the sample. Both the heme-bound form of the full length HcpR and HcpR-SD were compared. Both forms of the protein give a large Soret peak at 425 nm. This is consistent with 6 coordinate heme bound form in the non-gas bound state. In the upper regions of the spectrum the α and β bands appear at 558nm and 535nm respectively (Fig. 2.2 Inset). This is consistent with a low spin heme iron that has 6 coordinating bonds.
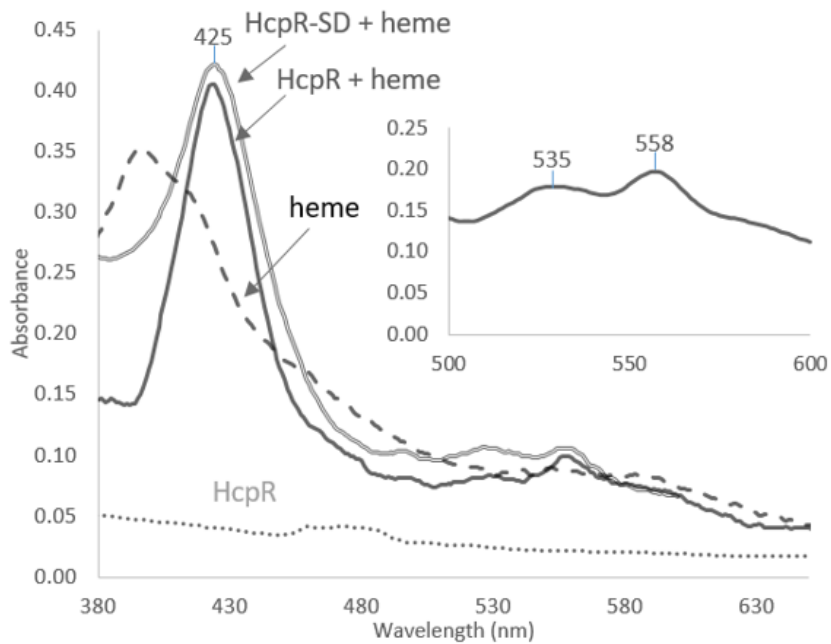
Figure 2.2 – UV-Vis spectrum of heme binding. Spectral properties of reconstituted heme bound HcpR (1 mg/mL) under reduced, anaerobic conditions. Bound heme reveals a Soret peak at 425 nm which is indicative of a ferrous 6-cooridnate heme. Inset: α and β region of the heme bound HcpR.

Binding of a gas to the heme iron will also cause changes in the UV-Vis spectrum. To learn about the gas binding dynamics the heme bound protein was nitrosylated using NONOate in both the Fe(II) (ferrous reduced form) and Fe(III) (ferric oxidized form) of heme. The addition of NO to the reduced protein produces a spectrum with a peak at 401 nm and a broad band in the visible region (~530 nm). This result suggests a 5-coordiante, NO bound system, indicating that heme coordination in HcpR goes from a 6-coordinate non-gas bound state, to a 5-Coordinate ligand bound system when nitric oxide is added (Fig. 2.3A). This is similar to other characterized NO sensors (94). Ferric heme added to HcpR under anaerobic conditions reveals a Soret band at 413 nm which suggests a 6-coordinate, ferric heme system. Interestingly, NO is capable of converting the ferric form of the protein to what appears to be the ferrous form (Fig. 2.3B). This would suggest that NO is capable of reducing the heme found in HcpR under anaerobic conditions.
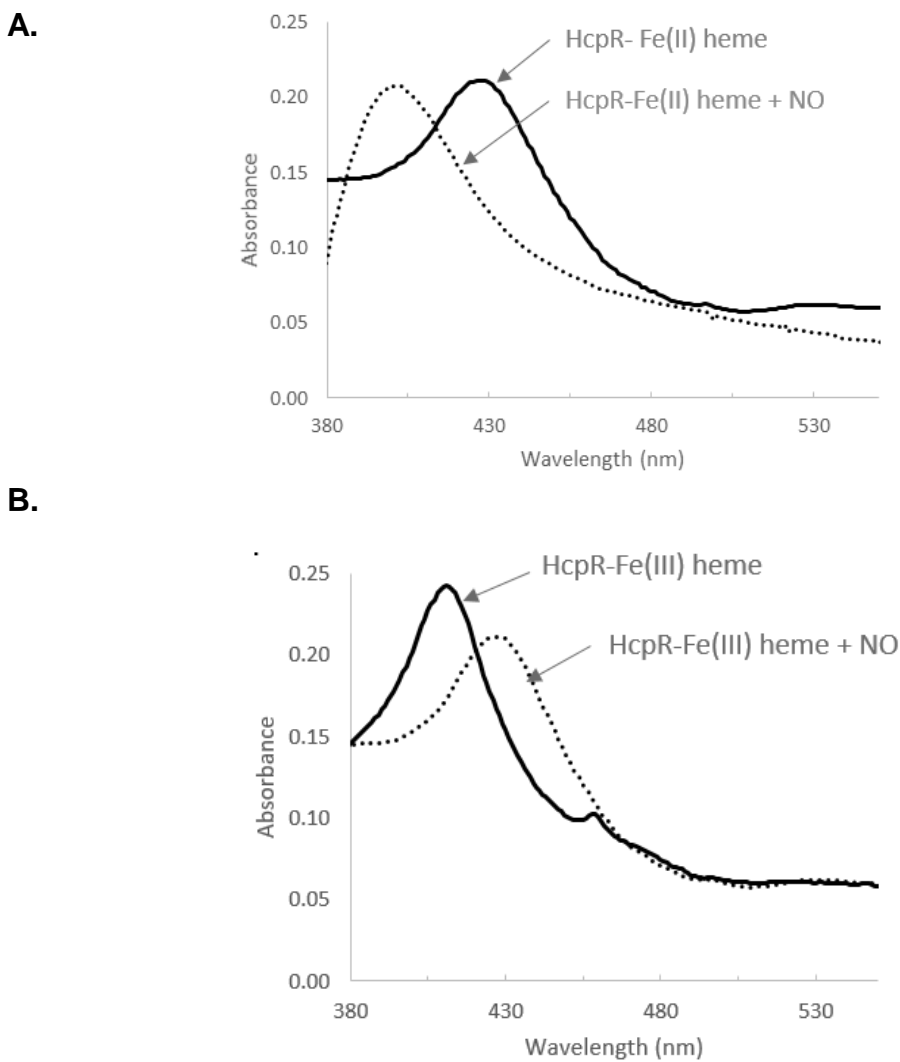
Figure 2.3 – Effects of NO binding on the UV-Vis spectrum of HcpR A. Spectrum of

reconstituted HcpR (10 µM) before (bold line) and after (dotted line) the addition of NO

under anaerobic conditions. After the addition of NONOate to the sample, Soret peak

shifts to 401 nm indicating the transition from a 6-coordinate to a 5-Coordinate state. **B.**

Spectrum of reconstituted HcpR (10 µM) with oxidized heme under anaerobic

conditions. Before the addition of NO, the Soret peak is positioned at 413nm indicating

a 6-Coordinate Ferric heme. After the addition of NO the Soret peak shifts to 425 nm

most likely due to the reduction of the Fe^{3+} to Fe^{2+} by NO.

Resonance Raman spectroscopy is a very important tool for the study of heme binding proteins, since the porphyrin ring is a chromophore with a high electronic absorbance at the ~400 nm band. This leads to large Raman enhancements for vibrational modes of the Raman spectrum of heme. This allows for the monitoring of heme structural changes which may be related to axial ligand coordination and gas binding. Therefore, to learn more about the nature of the heme environment of HcpR and the effects NO binding has on this environment we employed resonance Raman spectroscopy at an excitation of 406.7 nm.

A series of resonance Raman spectra of heme bound HcpR before and after the addition of NO is displayed in Figure 2.4 and the results are summarized in Table 9. In the reduced HcpR sample, the most prominent band of the high frequency region is the v4 band located at the 1362 cm^{-1} position of the ferrous sample which is characteristic of a hexa-coordinate ferrous heme. Other vibrational markers in the high frequency region appear: v3 at 1492 cm^{-1} 1, v2 at 1586 cm^{-1} and v10 at 1625 cm^{-1} which have been shown to be sensitive to gas binding and confirm the hexa-coordinate, low spin nature of the un-nitrosylated heme (Fig. 15A) (95, 96). When compared to the prototypical NO sensor soluble guanylate cyclase (sGC), there are marked differences in the vibrational spectrum (Table 9). In the un-nitrosylated state, sGC exists as a penta-coordinate, high spin system (94, 97). The Raman spectrum of HcpR in the un-nitrosylated state is more consistent with that of a hexa-coordinate system as seen in CooA (72). Although the large majority of the HcpR sample is in the hexa-coordinate state, a small percentage of the sample appears to be in the penta-coordinate state. The v3 region of the spectrum is sensitive to coordination state of the heme iron and the

1492 cm^{-1} peak (indicating a hexa-coordinate system) is strongest in this part of the spectrum, however a small portion of the sample appears to be in the penta-coordinate state indicated by the shoulder at 1471 cm^{-1}. This is further confirmed by observing the polarizing component of the Raman spectrum (Fig. 2.5). In the Raman spectrum the 1362 cm^{-1} (indicative of hexa-coordinate system) dominates the v4 frequency, however by observing the polarizing component of the spectrum it allows us to see the hidden 1376 cm^{-1} peak. This would imply that one of the axial side chain ligands responsible for the sixth bond to the heme iron is a weak or moderate donor, forming a weak, transient bond with the iron.

Upon NO binding, the heme skeletal markers exhibit a very similar spectrum to that of sGC and CooA producing a 5-coordinate NO bound system with a high spin factor. The v4 mode is shifted completely to 1376 cm^{-1} upon the addition of NO. Furthermore, v3 shifts to 1508 cm^{-1}, v2 shifts to 1584 cm^{-1}, and v10 shifts to 1646 cm^{-1} (Fig. 2.4). These changes in the spectrum are indicative of heme binding and expected range for a 5 coordinate, high spin Fe(II)NO heme, as opposed to a 6 coordinate Fe(II)NO heme. Furthermore, the v (Fe-NO) is found at 535 cm^{-1} which is consistent with 5-coordinate Fe-NO system.
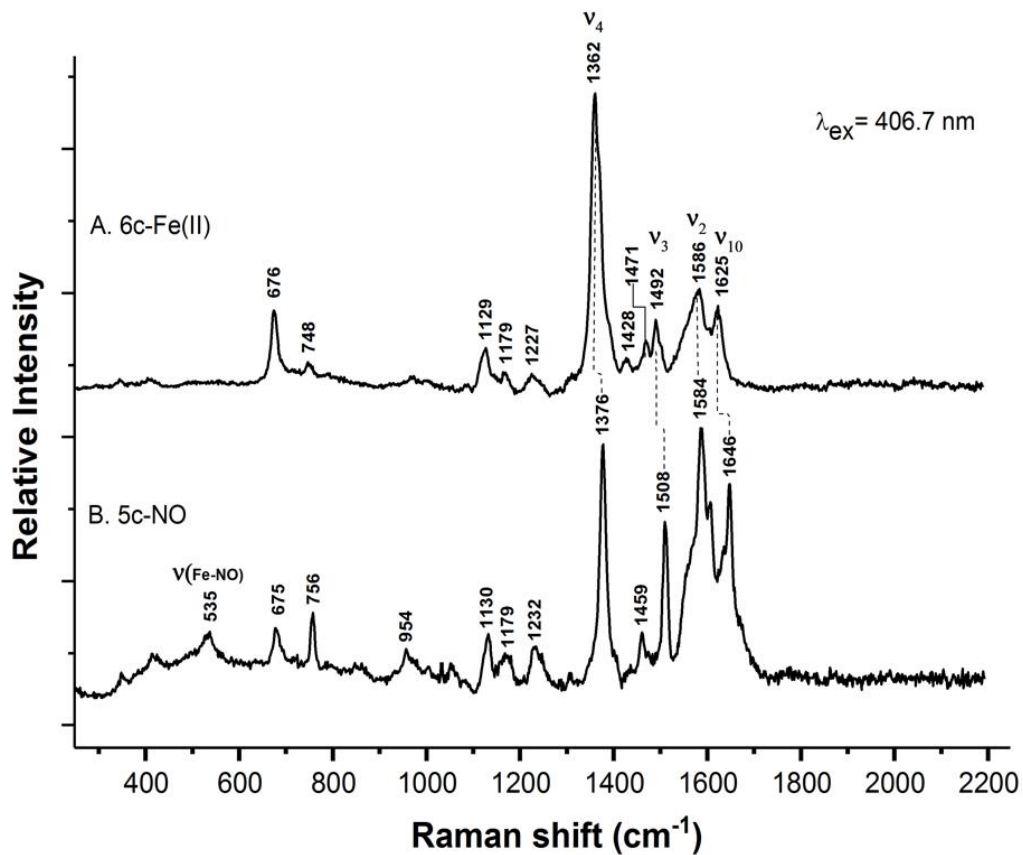
Figure 2.4- Resonance Raman Spectra of Reconstituted HcpR at 406.7nm

excitation. A. Reduced Heme bound HcpR (10 mg/mL) under anaerobic conditions

was excited at 406.7 nm at room temperature. The frequencies of the marker bands are

representative of a 6-coordinate system. **B.** Reduced heme bound HcpR (10 mg/mL)

plus NO under anaerobic conditions was excited at 406.7 at room temperature. The

frequencies of the marker bands are representative of a 5-coordiante NO bound

system. The ν(Fe-NO) frequency appears at 535 nm.

Table 9 - Heme vibrational markers and vibrational modes and Nitric Oxide

Binding

Protein	Coord.	Spin	v_2	v_3	v_4	v_{10}	v(Fe-NO)
Unligated							
HcpR	6	ls	1586	1492	1362	1625	
sGC	5	hs	1562	1471	1358	1606	
CooA	6	ls	1580	1492	1361	1616	
NO bound							
HcpR	5	hs	1584	1508	1376	1646	535
sGC	5	hs	1584	1509	1375	1646	525
CooA	5	hs	1582	1506	1376	1641	523

All values are given in cm^{-1}; ls = low spin; hs = high spin
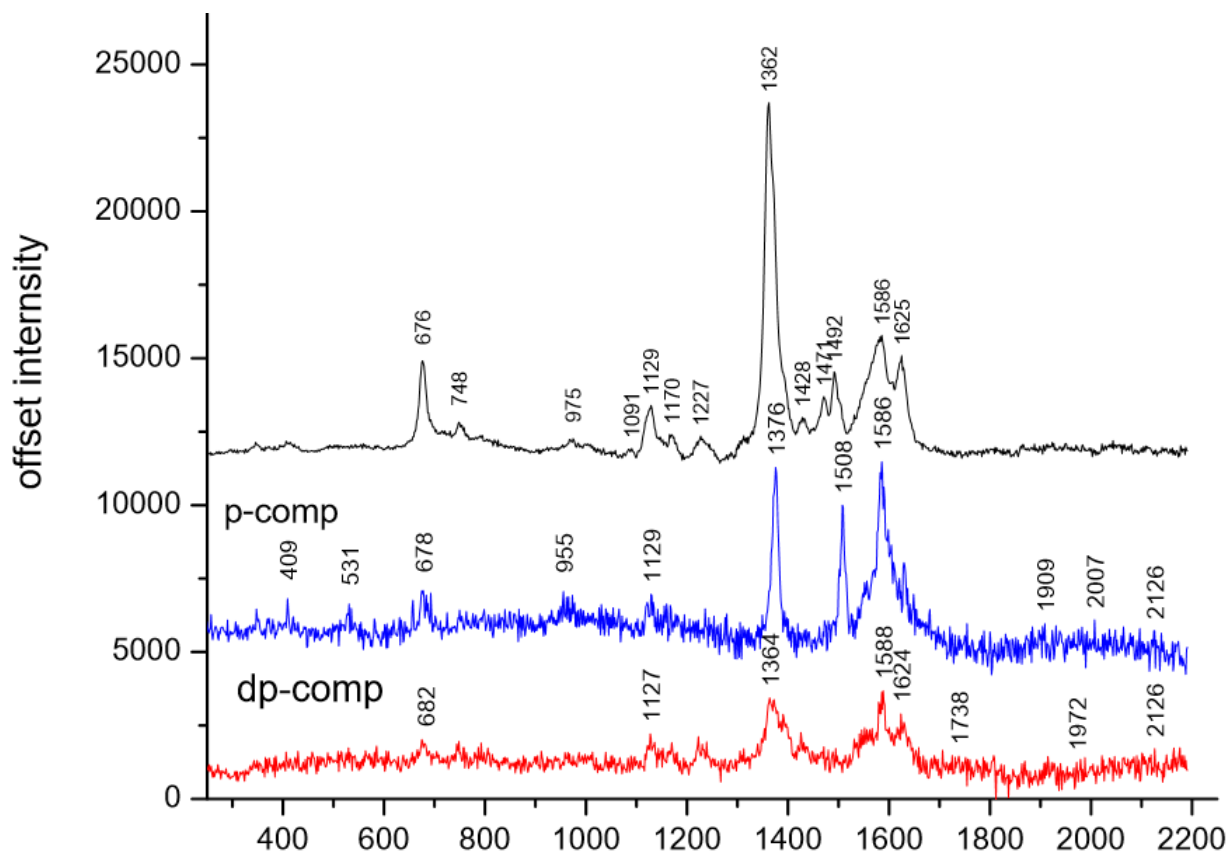
Figure 2.5 – Polarizing and Depolarizing components – Polarizing (blue) and depolarizing (red) complements of the resonance Raman spectrum (black) of the reduced heme bound form of HcpR.

Conclusion – Part 2

Using a combination of biochemical techniques, we show that the HcpR protein is capable of binding the heme cofactor. The luminol shows that heme binds to the HcpR sensing domain but not the negative control. Furthermore, the UV-Vis spectrum reveals that both the HcpR-SD and full length HcpR protein bind heme in a specific manner with a 6-coordinate, low spin heme. Binding of NO to the heme transitions the heme environment to a 5-coordinate, nitrosylated system. The nature of heme binding is confirmed through the use of resonance Raman spectroscopy, confirming that HcpR is consistent with other heme based NO sensors. The resonance Raman spectroscopy also reveals that the side chain responsible for the 6th axial ligand to the heme iron potentially forms a weak, transient bond with the heme iron.

**Part 3 – Structure of the HcpR sensing domain: HcpR is a member of the FNR-CRP family of regulators**

Previously, *in silico* analysis of HcpR and its possible regulatory pathways identified the protein as a potential member of the FNR (Fumarate-Nitrate reductase)/ CRP (cyclic AMP receptor protein) family of transcriptional regulators (98). The *hcpR* gene codes for a 228 amino acid protein that is approximately 24 kDa in size with two primary domains: an N-terminal sensing domain and a C-terminal helix-turn-helix binding domain and a long alpha helical region that spans between them. The N-terminal sensing domain spans residues 1 to 168 and contains most of the dimerization helix and the DNA binding domain spans residues 169 to 228 (Fig. 3.1). Sequence analysis of the N-terminal sensing domain reveals that it bears similarity to a cyclic AMP receptor domain. It is in this domain that the heme binding would hypothetically occur. Indeed, it was shown that the HcpR-SD (HcpR sensing domain) is capable of binding to the heme cofactor (Fig. 12-13) however the environment heme binding pocket and key residues involved in heme iron coordination are not known. To gain insight into the heme-coordination and NO binding by HcpR the N-terminal sensing domain was crystalized. The C-terminal DNA binding domain is highly dynamic, making the determination of the full-length structure through crystallization difficult.

Initial crystals belonging to the space group $P4_1 22$ diffracted to 3.5 Å. A structure was solved using Pt Single-wavelength Anomalous Diffraction (SAD) by soaking crystals in a solution of potassium tetrachloroplatinate. A model from the tetragonal crystal was refined to a final R_{work} of 19.6 and R_{free} of 23.9 (Fig. 3.2). This HcpR model was used for molecular replacement of a second crystal form that belongs to the space

group C222$_1$. This new model was refined to 2.6 Å (Fig. 3.3). There is no significant loss of electron density along the backbone of the tetragonal or orthorhombic crystal structures. The full table of data collection details and refinement statistics can be found in the appendix.

In the tetragonal crystal form there are two molecules in the asymmetric unit that represents the biological dimer (Fig. 3.2). However, in the orthorhombic crystal form, the biological dimer is formed between monomers of symmetry related molecules (Fig. 3.3). To create the biological dimer of the higher resolution model (orthorhombic), the orthorhombic crystal structure was overlaid using the tetragonal form as template. In both crystal structures, no electron density accounting for the cofactor was found, therefore we conclude that this is the apo-form of the protein.
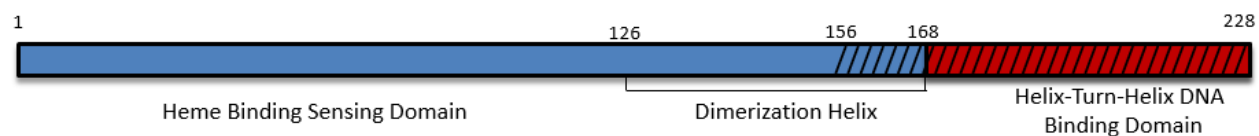
Figure 3.1 – **Overview of the HcpR-SD**. Schematic representation of the domain organization of the full length HcpR (region of the protein that was not crystalized is denoted by dash marks).
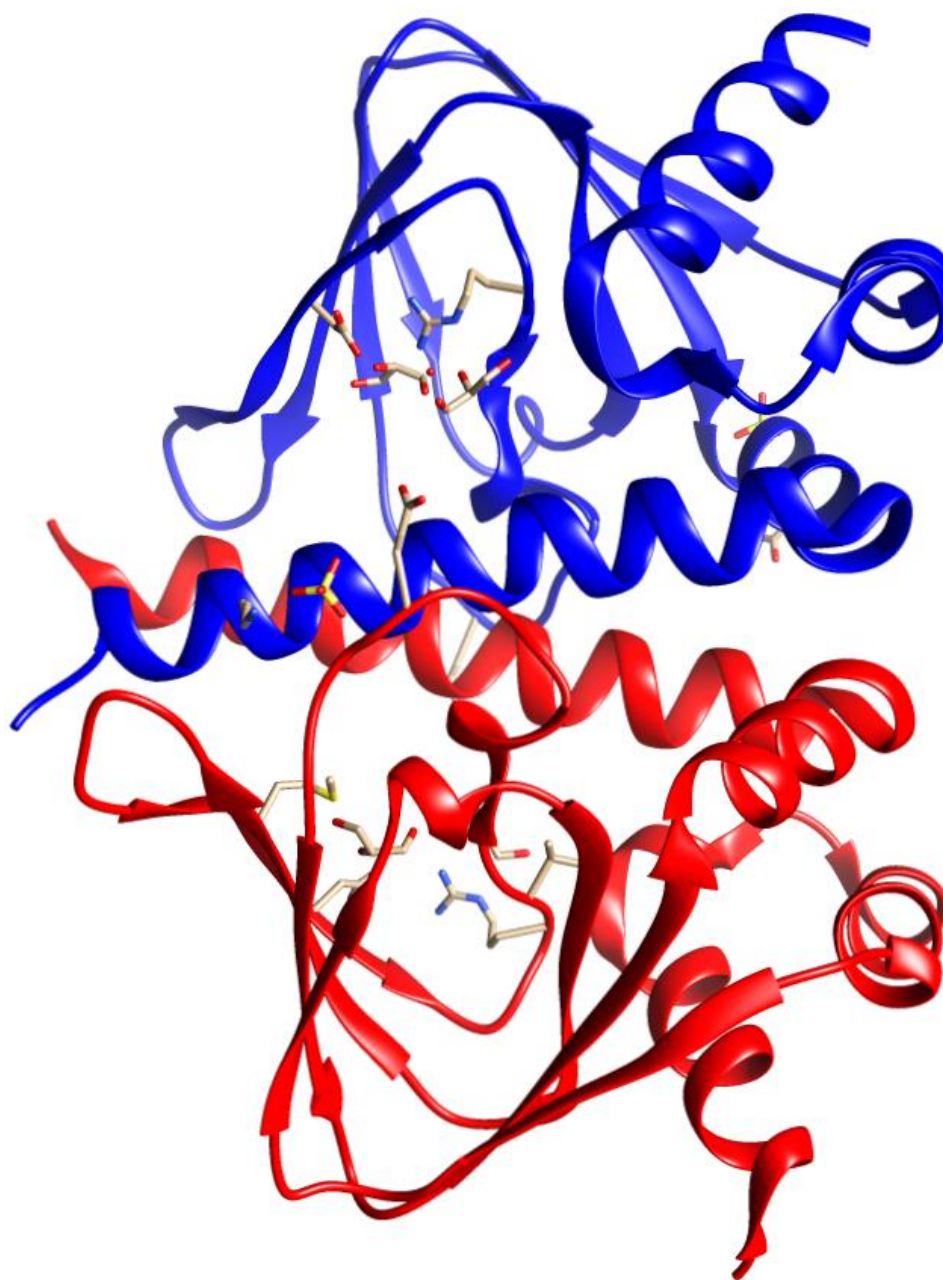
Figure 3.2 - Crystal structure of the P4$_1$222 form of HcpR-SD at 3.5 Å. Ribbon diagram of the HcpR-SD dimer with subunit A in blue and subunit B in red.

Figure 3.3 - Crystal structure of the C222$_1$ form of HcpR-SD at 2.6 Å. Ribbon diagram

of the HcpR-SD dimer with subunit A in blue and subunit B in red.

The ligand sensing domain of HcpR consists of 7 α-helices and 7 β-sheets. The 7 β-sheets form a beta-barrel like structure which is common in the sensing domain of other CRP-like regulators (Figure 3.5). A small subdomain composed of a helical bundle is located at the N-terminus. Additionally, the "flap", a region shown to be important in the allosteric activation of CRP and FNR-CRP proteins, is located between β-strands 5 and 6 (99). Located along residues 68-77 in HcpR, the flap is important for transmitting the allosteric activation of the protein upon binding of a ligand to the sensing domain and has been shown to play a role in both the interdomain and intersubunit interaction necessary for transmission of a binding signal. The 7th alpha helix (α-7) forms a dimerization interface that interacts with the corresponding helix of the opposing chain. The mainly hydrophobic residues across the dimerization helix make hydrophobic contacts with the opposing monomer (Fig. 3.6). The two dimerization helices interact over a buried solvent excluded area of 258.4 Å which acts to stabilize the dimer. A superposition of chains A and B results in a RMSD of 0.413 Å for the backbone atoms indicating no significant deviation between the two backbone chains of the homodimer.
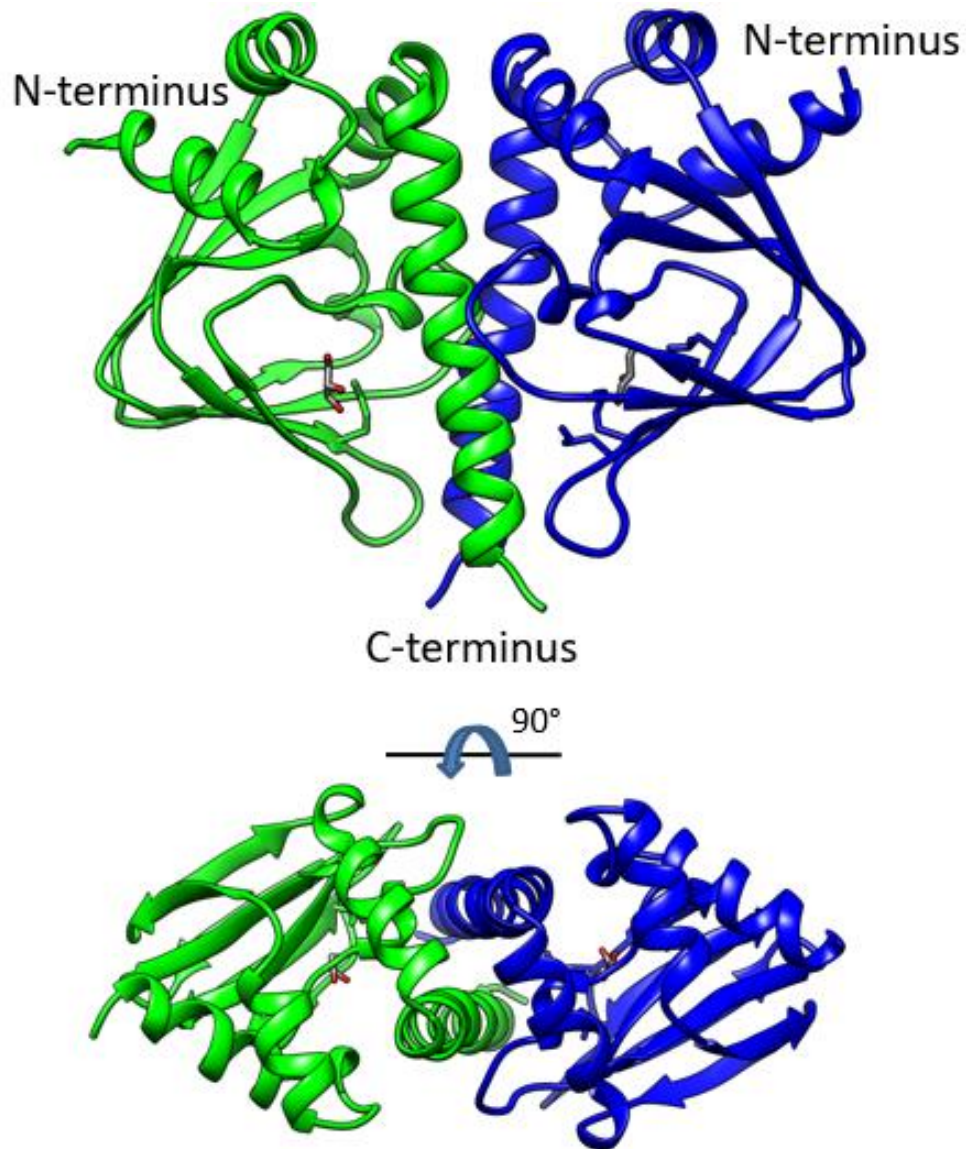
Figure 3.4 – Overview of the N-terminal sensing domain. Ribbon diagram of the N-terminal domain of HcpR side view (top) and bottom view (bottom) showing the tertiary and quaternary orientation of the structure. Chain A is colored green and Chain B is colored blue. The two chains form a homodimer through the interaction of the dimerization helix.
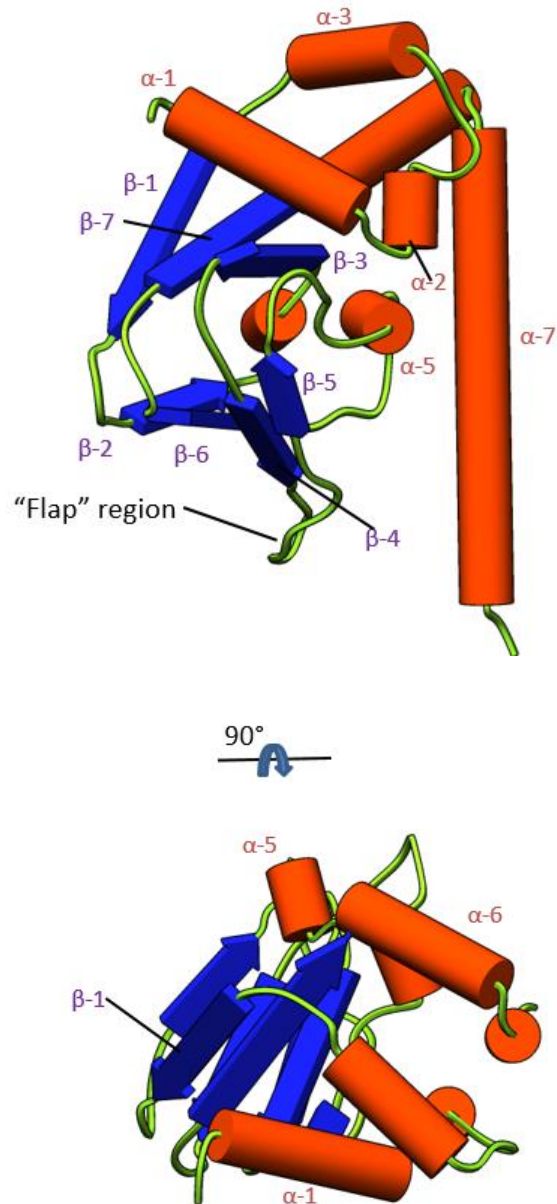
Figure 3.5 – Secondary structure orientation of HcpR-SD. HcpR contains 7 different alpha helical regions (α-1 through α-7) that are shown in red. The α-7 is the dimerization helix. There are 7 different beta sheet regions in HcpR (β-1 through β-7) that make up the B-barrel structure. The flap region is labeled and is located in the loop region between β-4 and β-5.
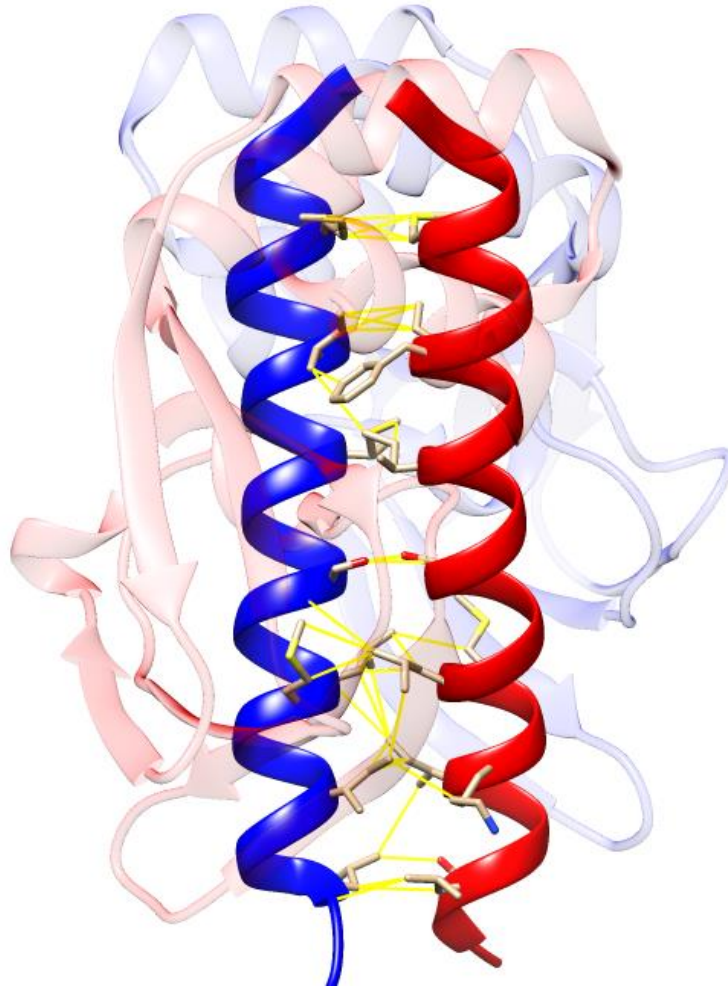
Figure 3.6 – Hydrophobic interaction between the dimerization helices. Potential contacts between the dimerization helices are highlighted by a yellow trace between them.

A CASTp search resulted in two well defined pockets that could incorporate a heme molecule. The pockets are located in the space between the β-barrel motif and the dimerization helix of the opposite chain. Thus the homodimer has two pockets on opposite faces of the protein (Fig. 3.7A). The core of the cavity is surrounded by hydrophobic residues derived from β-sheet 5, the helical region between β-5 and β-6, and the dimerization helices of both chains with the opening lined by a ring of hydrophilic residues derived from the lower part of the dimerization helix and Arg84 (Fig. 3.7B). Together these residues form a pocket that is approximately 520 Å^3 in volume. Heme (protoporphyrin IX) has a volume of approximately 510 Å^3, thus it is possible for the pocket to dock heme.

A.
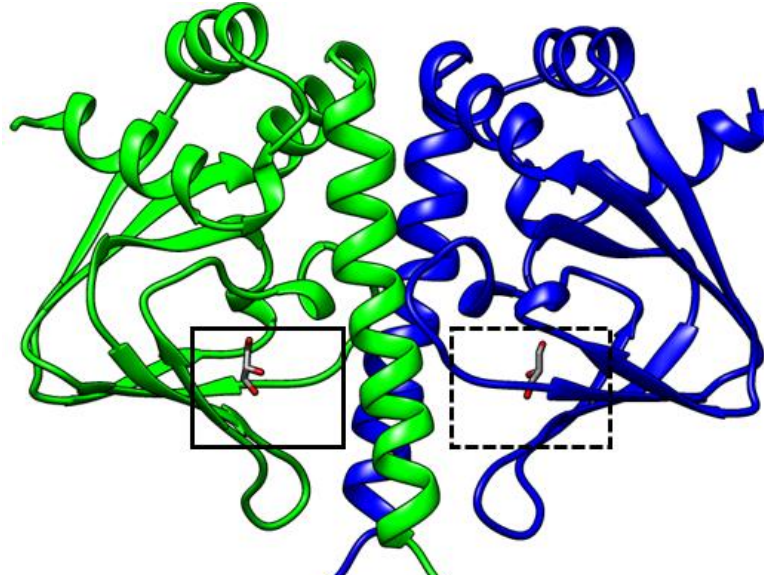
B.
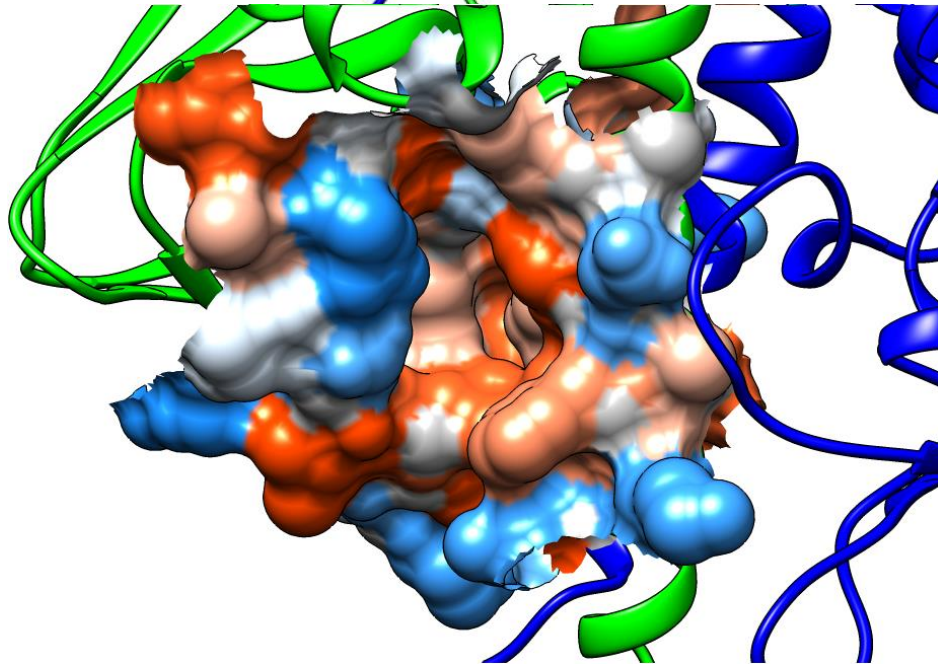
Figure 3.7 – Hydrophobic pocket of HcpR A. The location of the hydrophobic pockets

with respect to the full structure marked by a black box. The solid box indicates pocket

enlarged in B.; dotted box indicates the location of the pocket on the opposite side of

HcpR. **B.** The surface area of the pocket region of HcpR is denoted using Kyte-Doollitle

hydrophobicity scale where blue is more hydrophilic and red is more hydrophobic. In this

pocket is found an electron density consistent with glycerol.

Identifying residues involved in heme binding and coordination is paramount in understanding the mechanisms that govern their function and activation. Of interest were residues that could possibly be involved in heme binding and iron coordination in and around the hydrophobic pocket. Of the residues that are conserved in the N-terminal domain of the HcpR sub-group many are clustered around this pocket (Fig. 3.8). The side chain of methionine 68 is located prominently in the pocket and is conserved in all the HcpRs that were analyzed. There is also a region of very high sequence conservation that spans residues 84-94. The proline in this region (Pro89) forms a short helical region that inserts itself into the top of the hydrophobic pocket. While it does not feature any of the typical heme axial ligands (Cys, His), the high degree of conservation of this region points to it potentially playing an important role in the allosteric activation of HcpR. There are also a number residues located on the dimerization helix that are positioned in a favorable position. Met122 is conserved in all sequences analyzed and is located at the top of this pocket next to the extended loop region. Phe143 is also conserved across all sequences and is located near the front of the pocket. Met145 and His149 are not conserved in all sequences, only those most closely related to *P. gingivalis* however their positioning implicates them as potential axial ligands to the heme iron.

Met68, Met145, and His149 were of particular interest as methionine and histidine side chains are commonly implicated in heme iron coordination. All 3 residues are extended out into the pocket and are located on critical points of the structure that could influence activity: Met68 is located near the loop that is known as the flap, a region that is critical in the allosteric activation of FNR-CRP regulators; Met145 and His149 are located on points on the dimerization helix that are typically involved in

ligand binding in CRP like proteins and could influence the C-terminal domain

organization (Fig 3.9). Thus these 3 residues were chosen for mutational analysis in the

Δ*hcpR* knockout mutant. Of the 3 residues tested, only the double mutation of Met68

and Met145 inhibited growth of the bacteria grown in the presence of nitrite (Fig. 3A).

This is also seen in the regulation of *hcp,* with the M68A/M145A mutation resulting in a

complete loss in the ability of HcpR to upregulate *hcp in vivo* (Fig. 3B). However, the

single residue mutations of these residues resulted in no change in activity. This result

indicates that Met68/Met145 play an important role in activation of HcpR in response to

nitrosative stress but their function may be redundant between them.

```
P.endontalis            -------------------MTEGDFDLLLEAWQKSGLAGKMSTEEVAHLLRQCPCKKETL
PgHcpR                  -------------------MDPEFDLLLKAWKSSGLSVGMKDDELLALLESCSYRVERL
P.gulae                -------------------MNPEFDLLLKAWKGSGLAAGMKEDEVIALLESCSYRTERL
P.Chartae-1            MNPETVTYVTLMKLFWFLTGINKMDEKEINTLLQSDLFAGFTTQELTGLLDDLYYKINRY
P.Chartae-2            -----------------------MDEKEINTLLQSDLFAGFTTQELTGLLDDLYYKINRY
Macellibacteroides-Spp -----------------------MDEKEINTLLQSDLFAGFTTQELTGLLDNLYYKINRY
P.Macacae             --------------------------MIKQLTKSDLFQGYNCEQISGLLDKFKYRVKKL
                                          ::    *.*      . :::   **  .    :  :
                                              "Flap" Region      Extnended Loop

P.endontalis           KRGELYAIGGDKLRDLRIVGKGGIKAEMVGTSGKQLLMDTLTFGRIVAPALLFAEDNALP
PgHcpR                 KAEELYAIGGDKLQDLRIVGVGEIRAEMVGPSGKQILIDTLAVGRILAPALLFASENILP
P.gulae               KAEELYAIGGDKLQDLRIVGAGEIRAEMVGPSGKQILIDTLATGRILAPALLFASENILP
P.Chartae-1           NKDDILALSGDRCKDLMVVISGNLIARMVASSGKFVQIDKIGPGRVVAPAILFATHNVYP
P.Chartae-2           NKDDILALSGDRCKDLMVVISGNLIARMVASSGKFVQIDKIGPGRVVAPAILFATHNVYP
Macellibacteroides-Spp NKDDILALSGDRCKDLMVVISGNLIARMVASSGKFVQIDKIGPGRVVAPAILFATHNVYP
P.Macacae            KDKDIFALQGDLCREVNIILSGVLDARMTGPSGKEIQIDRLEAGRIIAPALIFATDNRFP
                      :   :: *: **   ::: ::   * : *.*.. *** : :* :  **::***::** .*   *
                                       M122   M68                  M145  H149

P.endontalis           VTLMANEESILFRMGKEDFRDLMHQSPQLMTNFIGIVSNISVFLMGKIYQLSLRSLQGKI
PgHcpR                VTLFANEDSVLFRIGKEEFKGMMHKYPTLMENFIGMISDISAFLMKKIHQLSLRSLQGKI
P.gulae              VTLLANEDSILFRIGKQEFKGTMHKYPALMENFIGMISDISAFLMKKIHQLSLRSLQGKI
P.Chartae-1          VNVLIEKEVVLFSVSRSTFLKAMQNNEKLLLNFIRSISDINRFLSEKIRFLSLKTLRGKI
P.Chartae-2          VNVLIEKEVVLFSVSRSTFLKAMQNNEKLLLNFIRSISDINRFLSEKIRFLSLKTLRGKI
Macellibacteroides-Spp VNVLIEKEVVLFSVSRSTFLKAMQSNEKLLLNFIRSISDINRFLSEKIRFLSLKTLRGKI
P.Macacae           VTVYAEGDTNILIFGREEFTHLMQQEEIILANFIRNISDINSFLSKKIKFLSLRTIKGKI
                     *.:  : :  :: ..:. *   *:.    :: ***  :*:*.  * .  ** ***::::***
                                          F143

P.endontalis          ADYLLQIYLKEGN---KRLQIDSSWKELADRFGVNRQSLARSLAQLEEEGLLRVEGKSIE
PgHcpR               GDYLFQLYTKDGS---NRIVVESSWKELSDRFGVNRQSLARSLSQLEEEGIIRVDGKSIE
P.gulae             GDYLLRFYTKDGS---SRIVVESSWKELADRFGVNRQSLARSLSQLEEEGIIRVDGKSIE
P.Chartae-1         AAYLLSASMAQDNT--LKVRIKESRQELSEKFGVSRQSLARSISELEDEGILTASARTIT
P.Chartae-2         AAYLLSASMAQDNT--LKVRIKESRQELSEKFGVSRQSLARSISELEDEGILTASARTIT
Macellibacteroides-Spp AAYLLSASMAQDNT--LKVRIKESRQELSEKFGVSRQSLARSISELEDEGILTASARTIT
P.Macacae          ADYLFTLSDQNANLMNYEIQIKEKWQTVADKFGINRQSLARGLAELEEEGYIEVQGKIIR
                     . **:      :  .    .: :... : ::::**:.******.:::**:** : ...: *

P.endontalis          ILQPHRMAGLE
PgHcpR              ILQPNRLSRLE
P.gulae            ILQPQRLSRLE
P.Chartae-1        ILDKNKLRNCE
P.Chartae-2        ILDKNKLRNCE
Macellibacteroides-Spp ILDKNKLRNCE
P.Macacae         IKNKPGLRLIE
                    * :   :   *
```

Figure 3.8 – Conserved residues of HcpRs of *P. gingivalis* and close relatives. An asterisk (*) denotes a residue that is fully conserved, a colon (:) indicates a strongly similar residues, and a period (.) indicates weakly similar residues.
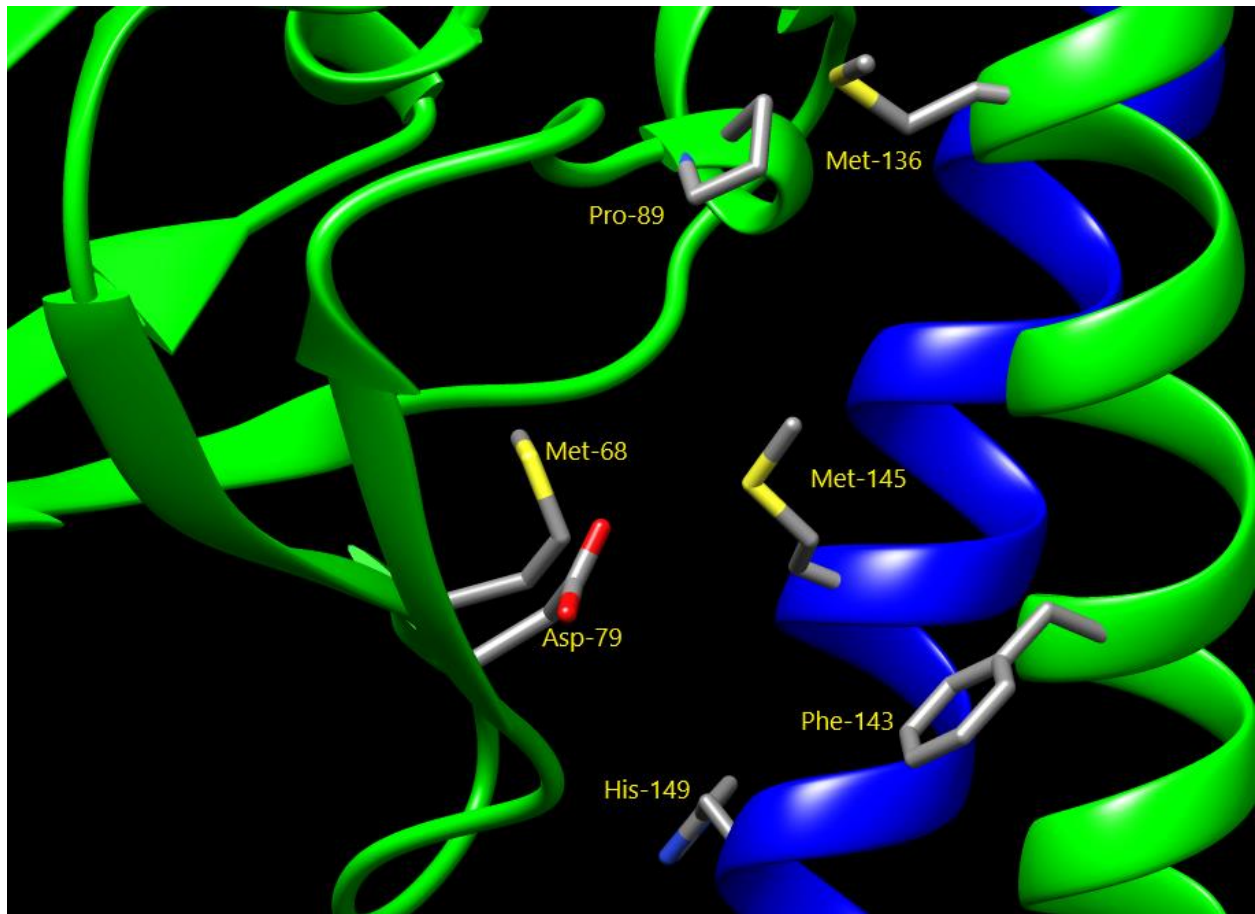
Figure 3.9 – Conserved residues in the hydrophobic pocket of HcpR. Location of conserved residues in the hydrophobic pocket. Met68, Met145 and His149 were all mutated to alanine for mutant studies.
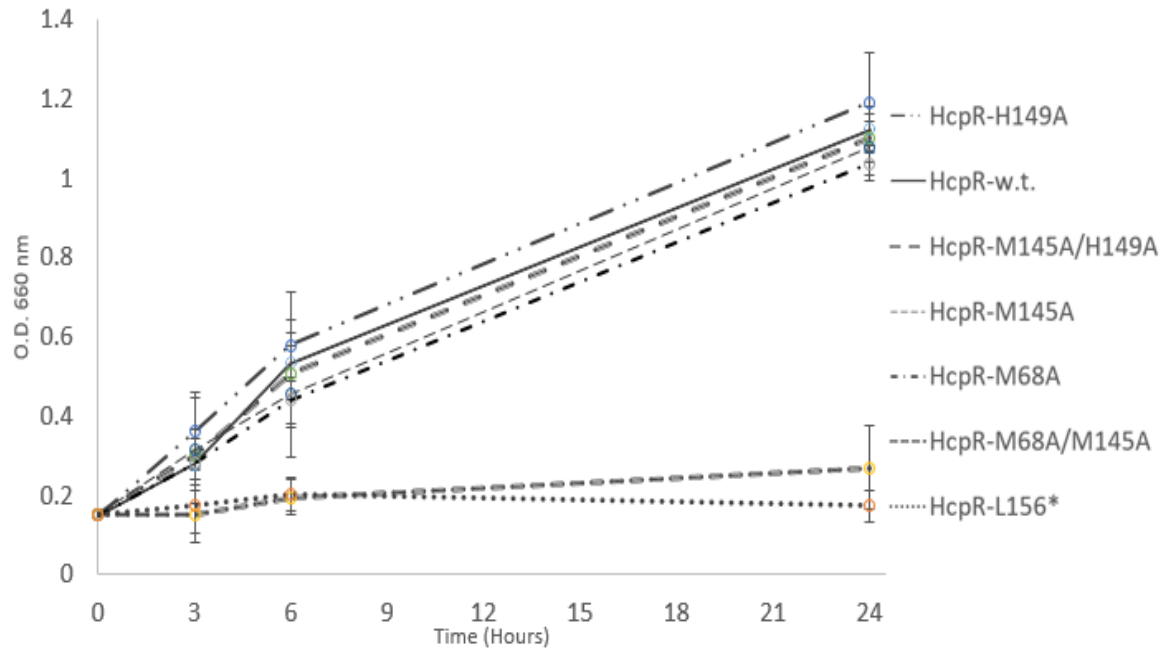
Figure 3.10 – Growth curve of V2807 complemented with HcpR mutants. Growth curve of the complemented ΔhcpR strains (V2807) grown with 2mM nitrite in mycoplasma media. Complementation with the wild type HcpR served as the positive control and complementation with the L156* HcpR served as the negative control.
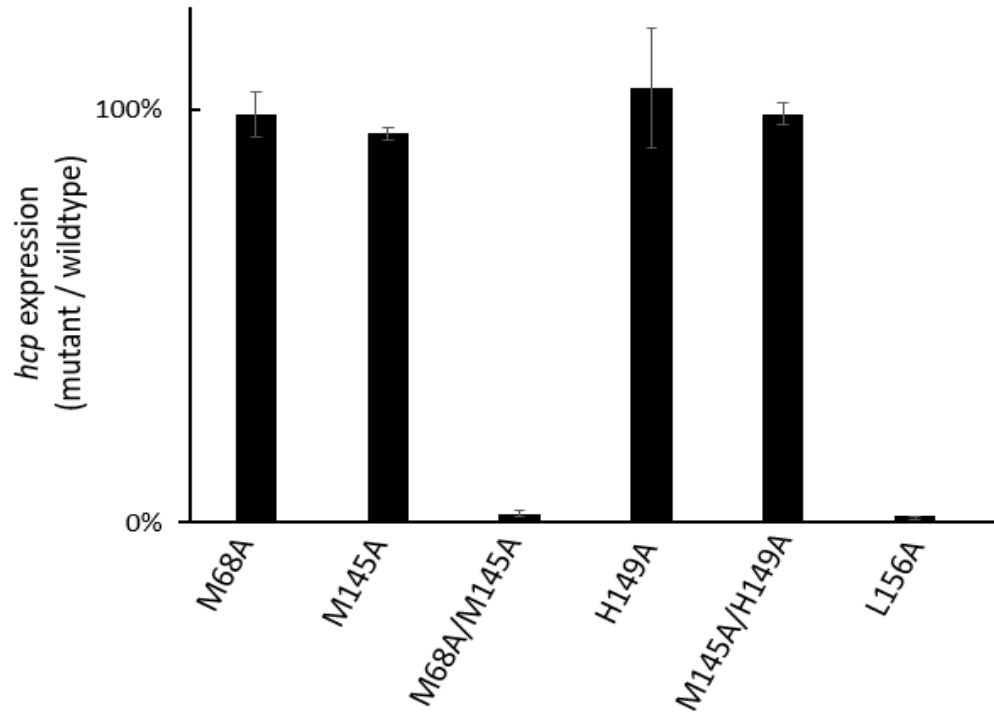
Figure 3.11 – qRT-PCR of V2807 complemented with HcpR mutants. Comparative gene expression of *hcp* in complemented strains in response to 2mM nitrite using qRT-PCR. All mutations are compared to wild-type HcpR transcript levels.

The best functionally and structurally characterized proteins bearing similarity to HcpR are DNR (from *P. aeruginosa*) and CooA (from *R. rubrum*). Bioinformatics studies revealed that HcpR shares 20% sequence identity to DNR, an FNR-CRP regulator found in *P. aeruginosa* that plays a role in regulation of nitrite respiration. HcpR shares 18.4% identity with CooA, an FNR-CRP regulator from *R. rubrum* that is important in the regulation of a CO oxidizing system (100). Despite a relatively low sequence identity between the 3 proteins there is a high similarity in the secondary and tertiary levels of protein folding (Fig. 3.12-14). The CooA and HcpR sensing domains superimpose with an RMSD of 0.958 Å and the HcpR and DNR sensing domains superimpose with an RMSD of 1.13 Å. The core β-barrel fold of the sensing domains, a key property of FNR-CRP family proteins, is maintained and is positioned alike in the structures. Likewise, all 3 of the proteins utilize the dimerization helix to stabilize the formation of a homodimer and it is positioned with the β-barrel analogously. Furthermore, the flap region of HcpR clearly aligns in the sequences and in the structural superposition of each protein.

In CooA the N-terminal proline residue (Pro2) of one subunit in the dimer directly acts as an axial ligand for the iron in the heme cofactor of the opposite subunit. Binding of CO to the heme iron displaces this proline leading to a substantial change in the structure. This displacement is the initial event that sends the allosteric signal through the protein thereby activating it. Although HcpR has a proline located at its N-terminus (Pro3), its position is a large distance away from a potential heme binding site. Thus coordination of the heme iron in HcpR occurs through residues that are not analogous to those in CooA.

Despite not having the structure of a heme bound form solved, DNR shares a slightly higher sequence similarity with HcpR than CooA. The opening of the hydrophobic pocket in DNR is in a similar position in the superposition of HcpR and DNR (Fig. 4C). Of the conserved residues found in the DNR subgroup, most are in contact with this cavity or are part of the cavity wall however these residues are not conserved in HcpR (70). This would imply that HcpR and DNR could bind to heme in a similar manner (the location of the hydrophobic pocket is similar) but the exact mechanisms and coordination may differ. His187, the crucial residue displaced in NO mediated activation of DNR, is not conserved in HcpR. The other axial ligand believed to be involved in coordination of heme in DNR, His139, is directly positioned over Met145 in the HcpR-DNR overlay. Similar to HcpR, a single mutation in this residue is not capable of full inactivation DNR, thus Met145 may serve an auxiliary role in heme binding and coordination in HcpR (101).
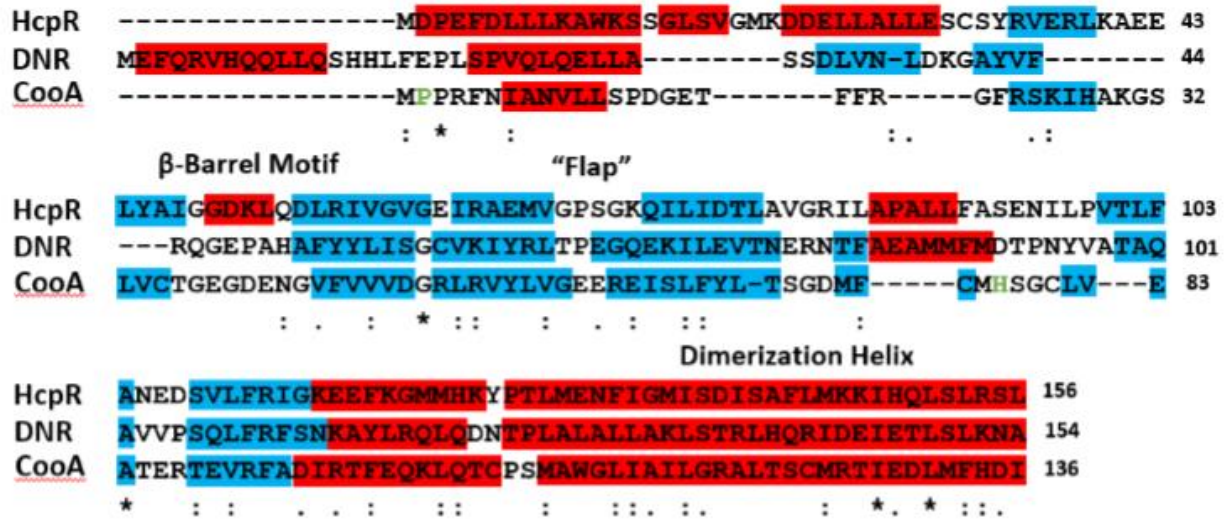
Figure 3.12 - Sequence alignment of HcpR, DNR, and CooA sensing domains.
Secondary structure features are shown in red (α-helices) and blue (β-sheets). An asterisk (*) denotes a residue that is fully conserved, a colon (:) indicates strongly similar residues, and a period (.) indicates weakly similar residues. Residues known to coordinate the heme iron in CooA are green. The sequence identity between HcpR and CooA is 18%; HcpR and DNR is 20%; DNR and CooA is 16%.
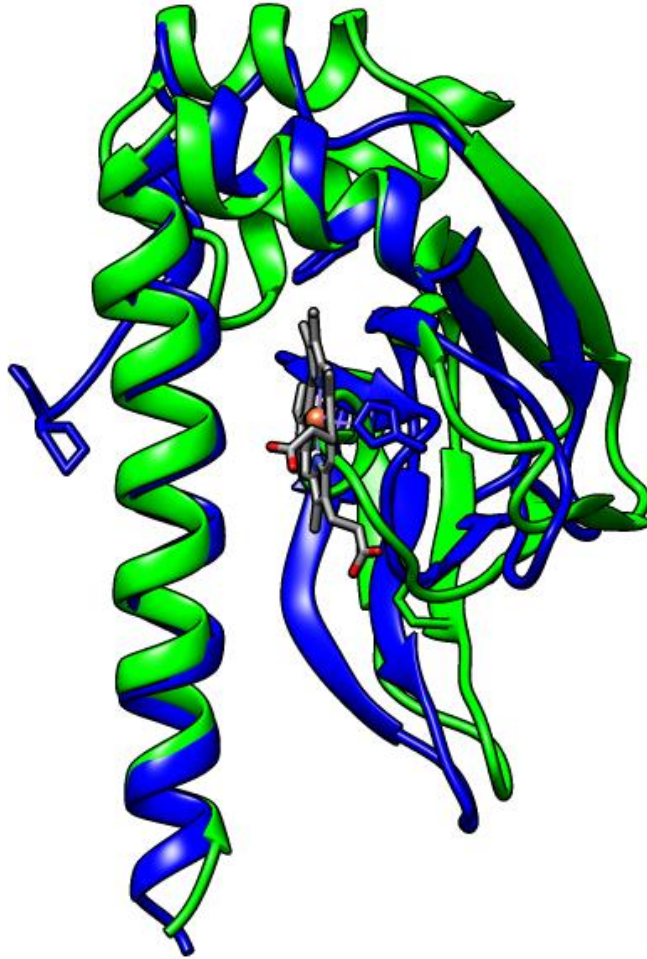
Figure 3.13 – Structural comparison of HcpR and CooA sensing domains
Superposition of HcpR (green) and CooA (blue) (PDB ID 4k8f) monomers of the N-terminal sensing domain showing the orientation of the dimerization helices and the heme binding domain. The RMSD of the alignment of the backbone atoms (minus the first 12 residues of the N-terminus) is 0.958Å.
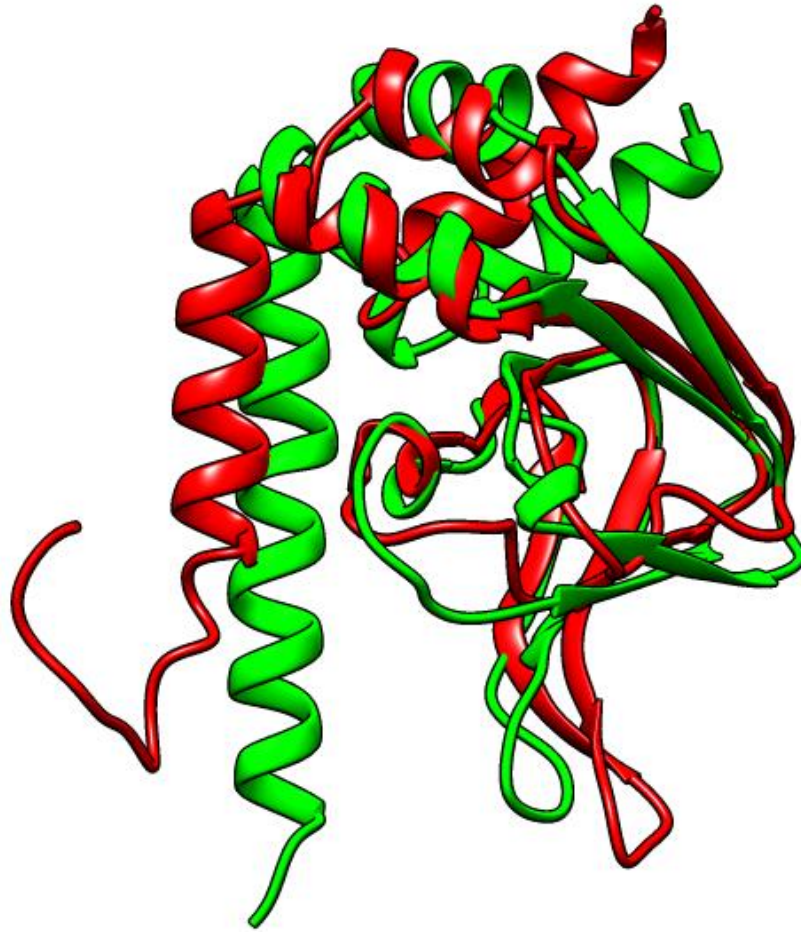
Figure 3.14 - Structural comparison of HcpR and DNR sensing domains

Superposition of the truncated DNR (red) (PDB ID 2z69) and HcpR (green) monomers

of the N- terminal sensing domain. The last 8 residues of the DNR dimerization helix are

unwound and lodged in the hydrophobic pocket of the opposite subunit of the dimer.

The RMSD between the two structures is 1.31 Å.

One of the properties that characterizes the FNR-CRP family of regulators is that they form homo-dimers. The crystal structure forms a homodimer, however we wanted to confirm the dimerization in solution of the full length protein. The sedimentation velocity experiments yield a sedimentation coefficient of 3.2S, corresponding to a molecular weight of ~48 kDa (Fig. 3.15). The *hcpR* gene encodes a protein with an estimated molecular weight of 24kDa, thus the observed 48kDa product in our sedimentation velocity experiments suggest that HcpR forms a dimer. Such data are in agreement with the results obtained from our structural analysis making it consistent with other members of the FNR-CRP family.
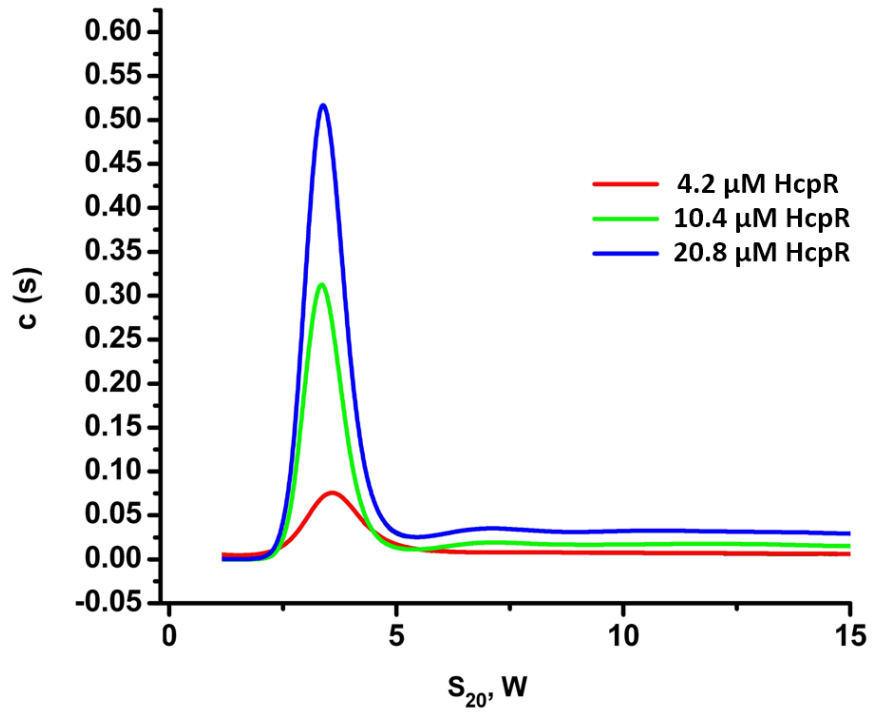
Figure 3.15. Sedimentation Velocity experiments of HcpR. Range of concentrations of full length rHcpR. The sedimentation coefficient of 3.2 Svedbergs indicate the HcpR forms a 48 kDa homodimer.

To gain an insight into the full length structure of HcpR, we performed small angle X-ray scattering (SAXS) to model the missing domain. The SAXS structural parameters are presented in Table 10. The SAXS data confirms the homodimerization of the full length protein, revealing an estimated molecular weight of 47 kDa via calculation of the Porod volume (Table 10). Using the DNA binding domain of DNR as template, a model of the full length HcpR was generated. This model was then fitted to the *ab initio* model generated and fitted to confirm the orientation of the 75 missing residues of the DNA binding domain. Rigid body modeling using SASREF against the solution scattering data revealed a slight change in the orientation of the two chains (Fig. 3.17-3.18) (80). To fit the solution scattering the two chains are slightly tilted into each other around the dimerization helix. This slight rotation creates the coiled-coil structure between the two dimerization helixes that is found in the full-length FNR-CRP proteins and increases the solvent excluded area between the two chains to 621.7 Å^2 (Fig. 3.18).
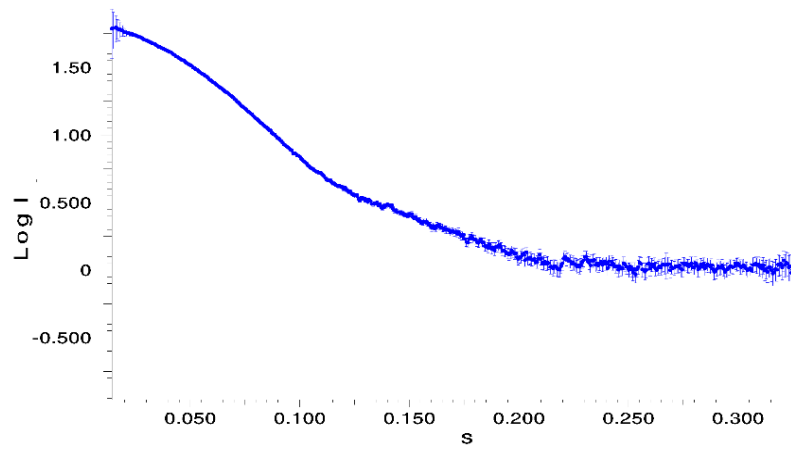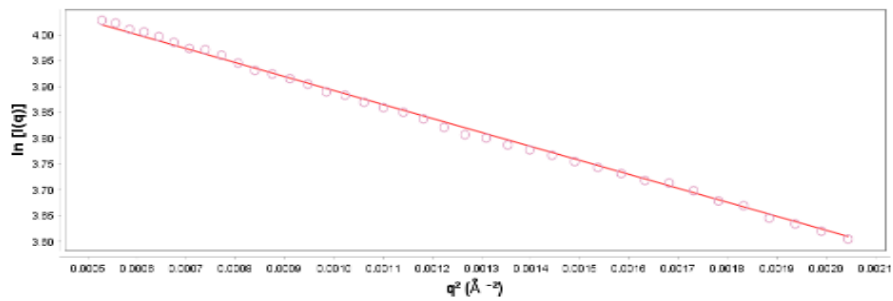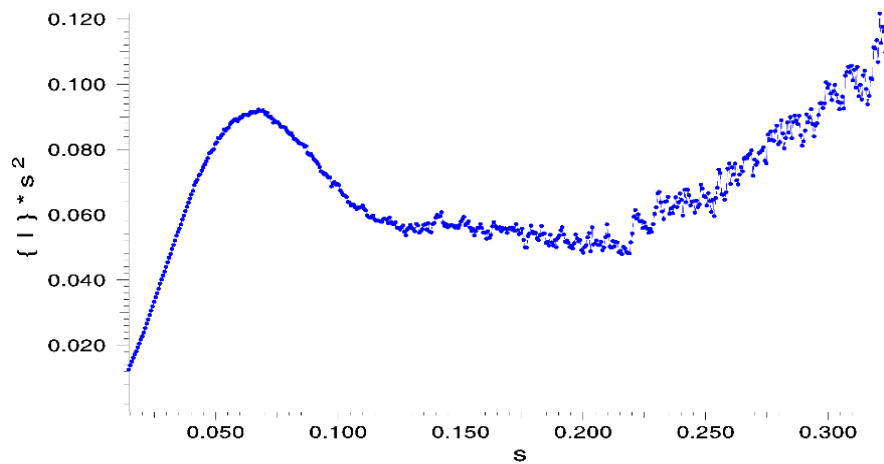
Figure 3.16 – SAXS scattering profile A. Scattering data shown in the log(I) vs. q graph. Error bars are shown on the graph for each data point. **B**. shows Guinier plot and the linear fit (solid line) of the Guinier region. The first 6 points were subtracted from the Guinier region. **C.** Kratky plot of the scattering data. This graph is characteristic of a partially disordered protein.

A.
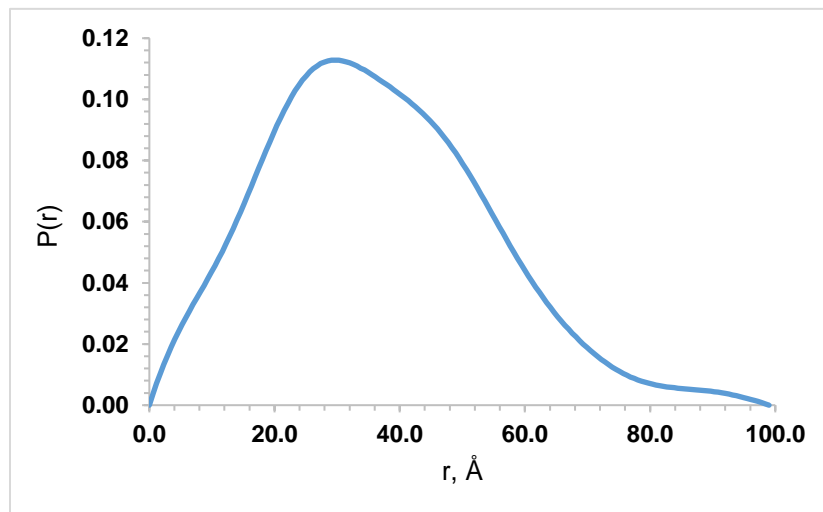
B.
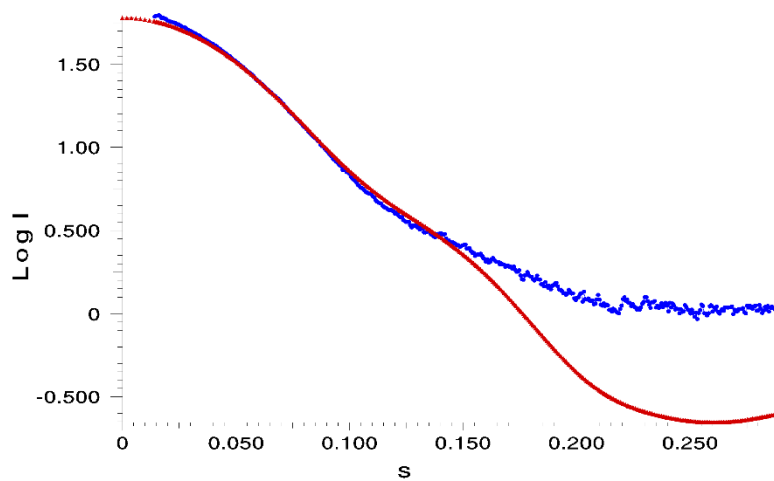
Figure 3.17 - Distance distribution graph and scattering profile of *ab initio* model A.

The distance distribution function (P(r) profile) of HcpR, indicates a max diameter of 96.2 Å. **B.** Log(I) scattering curves of HcpR and the theoretical scattering curve of the rigid body model. The Chi value between the two curves is 4.9.
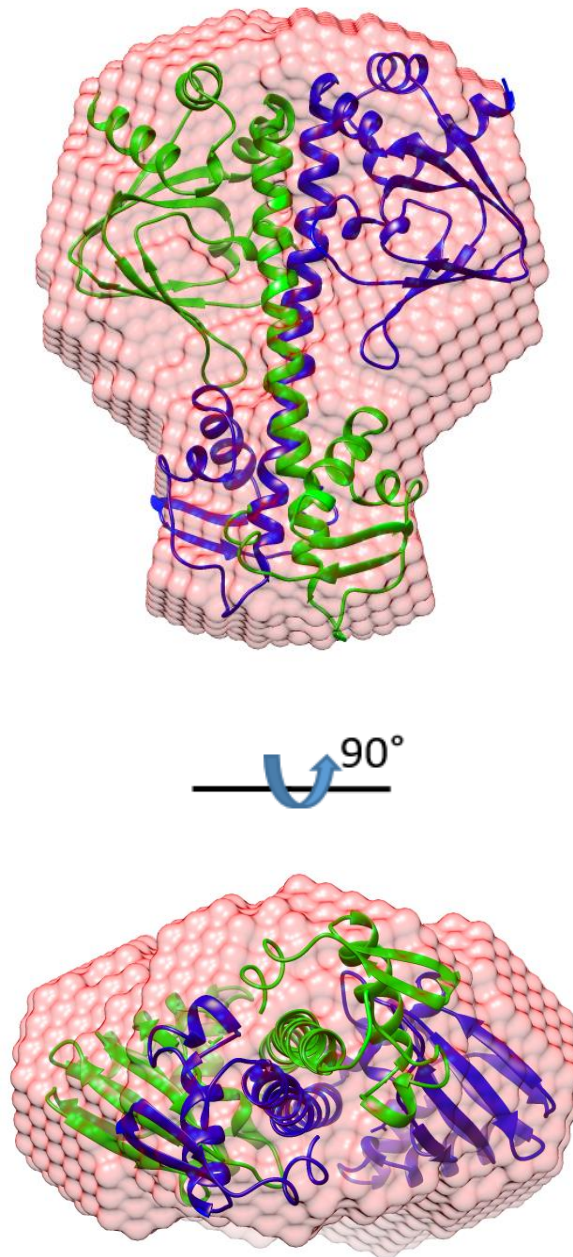
Figure 3.18 - *ab initio* model of HcpR. Rigid body modelling was performed using the chimeric HcpR against the solution scattering data of HcpR. The homo-dimeric model is superimposed onto the *ab initio* model (red) generated from the scattering curve

Table 10: Structural Parameters from SAXS experiments

I(0) (from P(r))	0.0637 ± 0.002
R_g (from P(r))	28.7 Å
I(0) (from Guinier)	0.064 ± 0.003
R_g (from Guinier)	28.3 Å
D_{max}	99 Å
M_r (Porod)	47 kDa
M_r (from dimer sequence)	48 kDa

The rigid body modeling also reveals a change in the orientation of the C-terminal DNA binding domains with respect to the N-terminal domains. To fit the solution scattering, the DNA binding domains of the chimeric model are rotated slightly with respect to the N-terminal domains. This may have effects on the ability of the flap region of the N-terminal to effect the C-terminal domain upon activation. Thus it would imply the binding of heme may cause a slight rotation of the N-terminal domain around the dimerization helices, repositioning the flaps. However, this model only fitted the experimental data at the low q regions and with an overall χ of 5.84 and an R_g of 26.85 (Figure 3.17). We use the Ensemble optimization method (EOM) to determine if a mixture of multiple conformers fitted the data better. In this method, a random pool of 100,000 conformers of HcpR were generated where the N-terminal sensing domain dimer was kept fixed and the DBD model was allowed to assume multiple conformations. The distribution of R_g was calculated from the initial pool and compared to 100 sub-ensembles. The best ensemble gave an average R_g of 28.62 and a χ of 0.722 and is represented by three main populations (Fig. 3.19). The conformations are among the possible that can be attained and should be interpreted as showing that the full length apo-HcpR has a significant degree of interdomain flexibility.
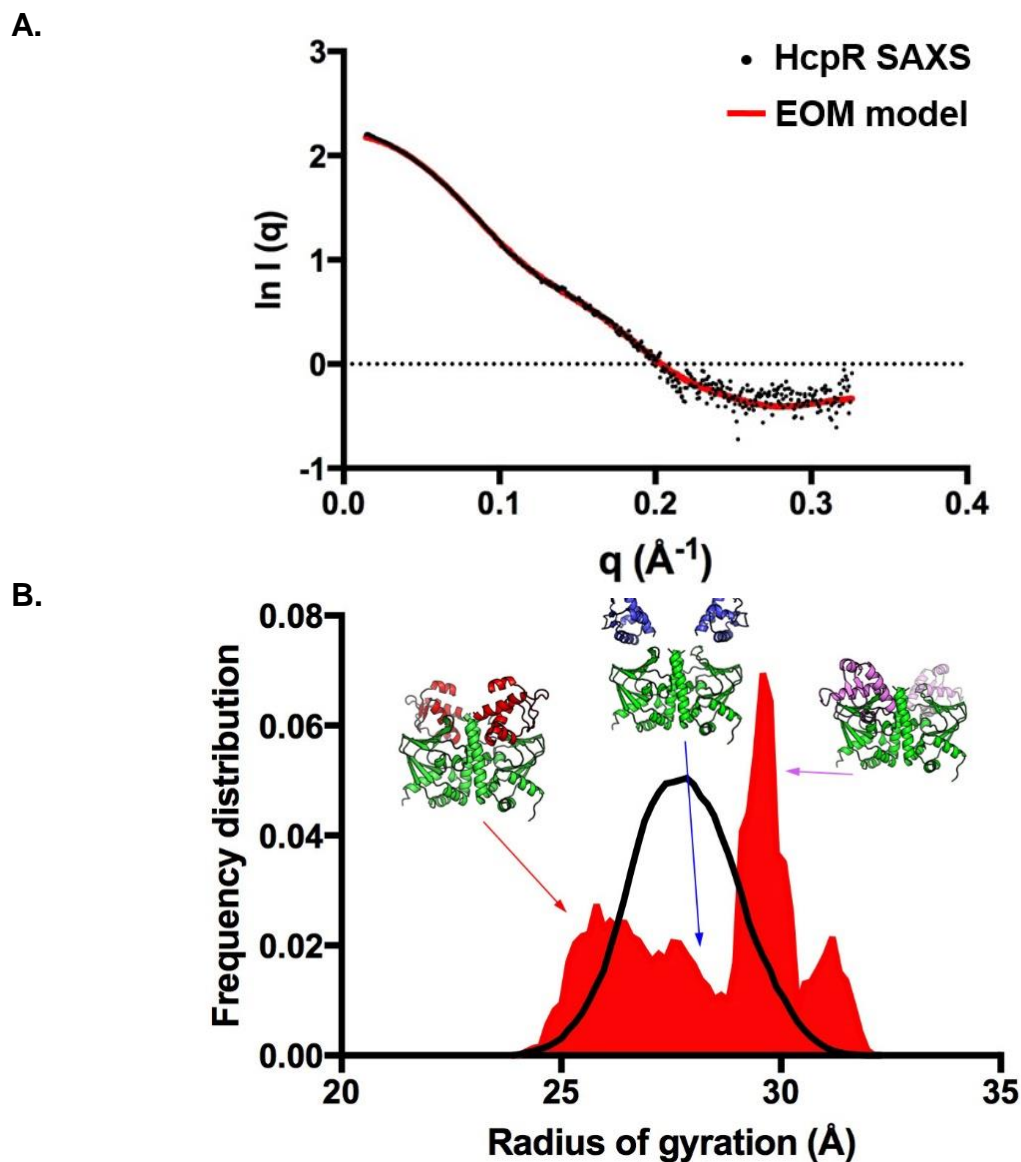
Figure 3.19. Flexibility of the Full Length HcpR. A. Scattering curves of the HcpR SAXS data overlaid with the experimental scattering curve of the EOM model. The curve has a Chi value of 0.722 The black dots represent the Full length HcpR SAXS scattering data and the red line indicates the best fit theoretical scattering curve of the EOM model. **B.** Distribution of the C-terminal DNA binding domain orientations. The orientation of the 3 main subpopulations is shown. The R_g of the best ensemble is 28.62.

To better understand the conformational changes involved in the activation of HcpR, the structure of the HcpR-SD was completed by modeling the missing DNA binding domain in the ON conformation using the structure of CRP as a template (PDB 1ciz). The model of the DNA binding domain forms a winged helix turn helix motif formed by 3 α-helical bundles and 3 β-strands in a α1-β1-α2-α3-β2-β3 arrangement where α3 is the DNA recognition helix (Fig. 3.20). When comparing the structure of our chimeric model developed from the rigid body modeling of the off form and the chimeric model of the on form there is a dramatic re-arrangement to switch to the ON form. As seen in the EOM modelling of the protein, the full length structure of HcpR appears to be very flexible in the area around Leu156. This region, known as the hinge in other FNR-CRP regulators, is important in the positioning of the DNA binding domain. In the modeled ON conformation, this region allows for significant rotation of the DNA binding domain around the N-terminal domain, positioning the DNA recognition helix in the correct orientation to make contact with the major grove of DNA. The model hints at the possibility of the DNA binding domain interacting with the heme directly. The loop region between α1 and β1 of the DNA binding domain extends up into the hydrophobic pocket, indicating the possibility for the residues to directly interact with the heme cofactor.
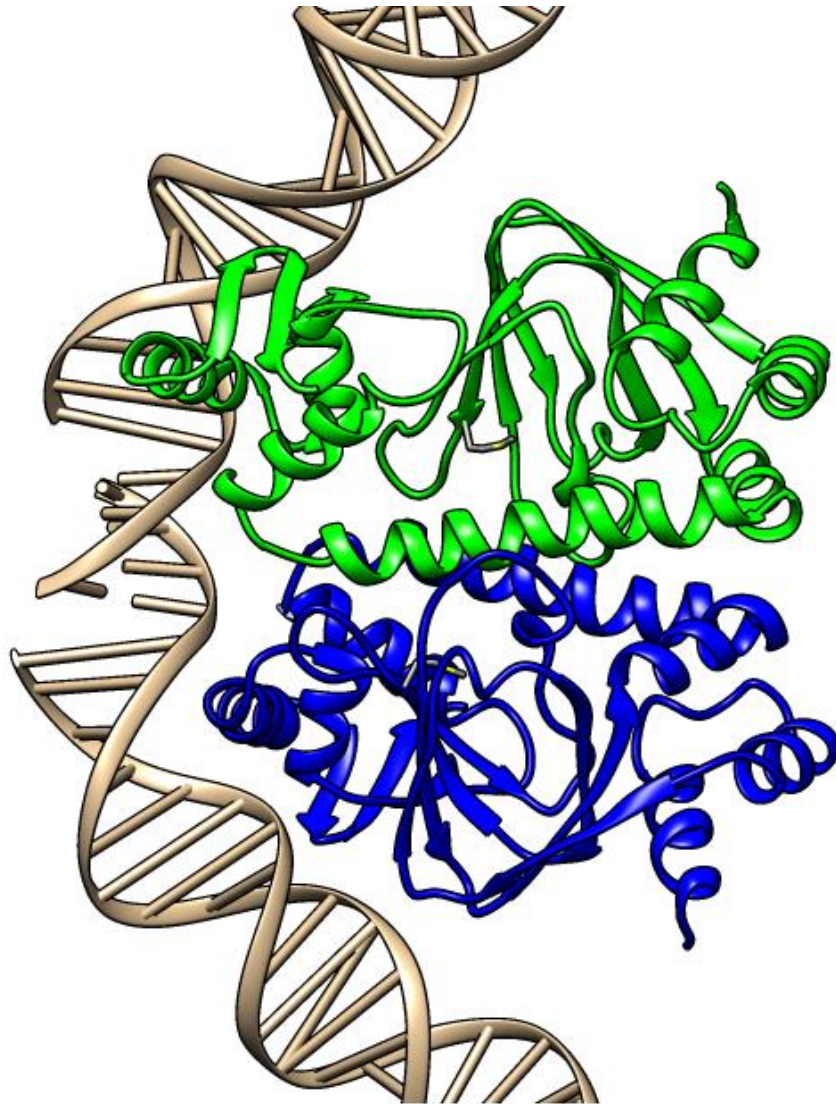
Figure 3.20 – Chimeric model of HcpR in the ON state. The C-terminal DNA binding

of HcpR was modeled using the crystal structure of CRP bound to DNA as a template.

The model shows the orientation of the DNA binding domain and the movement of the

domain around the "hinge" region.

Conclusion – Part 3

HcpR is a member of the FNR-CRP family of regulators: the N-terminal sensing domain consists of the secondary structural elements found in members of the family and the protein forms homo-dimers that are stabilized through a long helical region. HcpR has a hydrophobic pocket located between the dimerization helix and the β-barrel motif that is a potential heme binding site. Mutation of two methionine residues (Met68 and Met145) in this pocket abrogates activation of HcpR thus identifying the location of the binding site. The homodimerization is confirmed through sedimentation velocity experiments and SAXS experiments. Finally, Small Angle X-ray Scattering experiments of the full length HcpR reveal that the C-terminal DNA binding domain of HcpR has a high degree of interdomain flexibility.

IV.   Discussion

Periodontal disease is one of the most prevalent infectious diseases in the world and much effort has gone into understanding the complex relationship between the host immune response and the bacterial pathogens which are responsible for the dysregulation of the immune response. In recent years, much work has also gone into studying the inter-microbial interactions and the cooperativity of members of the oral microbiome in health and disease. In the complex environment of the periodontal pockets, *P. gingivalis* is able to thrive despite the high levels of reactive nitrogen species that are secreted by the host and by other bacteria, specifically the high levels of nitrite that can be found in the oral cavity. Understanding the ability of *P. gingivalis* to adapt and survive high levels of reactive nitrogen species has practical applications. Vegetables and fruits that are high in nitrates are recommended for daily consumption but they may also have added benefits to oral health. When these foods are eaten they drastically increase the levels of nitrite found in the oral cavity which can promote the growth of health promoting bacteria found in the oral cavity (10, 102). As shown in this work, *P. gingivalis* must have a robust response to these reactive nitrogen species and without an appropriate response it cannot survive. Thus, a nitrate rich diet not only promotes the growth of health associated bacteria but is also detrimental to the growth of the periodontal pathogen *P. gingivalis*.

With the exposure of *P. gingivalis* to nitrite or nitric oxide *hcp* is drastically up regulated. The *hcp* gene encodes for a putative NO reductase, although the gene product's exact function(s) in *P. gingivalis* are still under much scrutiny, with other studies claiming that it functions as a hydroxylamine reductase (52). In other obligate and

facultative anaerobes, Hcp has been shown to play an important role in NO and hydroxylamine reduction and detoxification however in the case of *P. gingivalis,* hydroxylamine does not stimulate up regulation of *hcp* (103, 104). Concentrations as low as 50nM of GSNO result in a 50 fold upregulation of *hcp* and concentrations as low as 200 µM of nitrite result in a 200 fold upregulation. These low thresholds indicate that HcpR is very sensitive to reactive nitrogen species in the form of NO and NO_2^- in the environment. The response time is also rapid. These fold changes are seen after a brief exposure of 15 minutes. The sensitivity of HcpR combined with the rapid response time allow *P. gingivalis* to respond to the rapid changes in reactive nitrogen species at concentrations that can occur in the oral cavity and in the pockets that characterize periodontal disease.

Despite the importance of the *hcp* gene in the response to reactive nitrogen species in obligate and facultative anaerobes, the mechanisms of gene regulation are only now being elucidated. The NsrR and FNR regulators have been shown to regulate *hcp* in *E. coli* and other related species (105). Furthermore, recent studies have also implicated the redox sensitive regulator OxyR in the regulation of *hcp* (106). However, the role that these regulators play in *hcp* expression is not consistent with those found in many Gram negative obligate anaerobes (specifically of the Bacteroidetes and δ-proteobacteria phylums and related species). In *P. gingivalis,* OxyR has no observable effect on *hcp* expression and regulation (54). Thus the study of HcpR will help to shed light on the regulation of *hcp* and the nitrosative stress response in many Gram negative obligate anaerobes.

With exposure to nitrite, the *hcp* gene is the most up regulated gene in the RNA-seq study and this up regulation is absent in the V2807 strain, confirming what is seen in the qRT-PCR studies. Furthermore, *hcp* is by far the most upregulated gene in the study at 144 fold; the next highest up-regulated gene is differentially regulated at 2.4 fold. Furthermore, there is no significant change in the down regulation of any genes, indicating the HcpR most likely plays a role as a transcriptional activator and does not act as a repressor. This is consistent with other members of the FNR-CRP family, who almost universally act as activators. There is no consistent difference in the transcriptome between the V2807 knock out strain and the wild type strain when comparing the profiles of both absent nitrite or plus nitrite. Furthermore, in the presence of nitrite, the overall transcription in the V2807 knockout strain appears to be lower than that of the wildtype, most likely due to the growth arrest brought on by the presence of nitrite.

Of note when comparing the transcriptional profiles of the V2807 knockout strain plus/minus nitrite, two of the most upregulated genes are both subunits of the cytochrome d ubiquinol oxidase, *cydA* and *cydB*. Under micro-aerophilic conditions, *P. gingivalis* has been shown to express and utilize the *cydAB* operon to consume oxygen and mediate oxygen based metabolism (107). Studies in the anaerobic bacteria *Moorella thermoacetica* reveal that cytochrome bd ubiquinol oxidase helps to protect against oxidative stress and contributes to oxygen tolerance (108). By decreasing the amount of reactive oxygen species it generates it avoids producing the very potent peroxynitrite anion.

The *hcp* knockout strain has a very similar phenotype to that of the *hcpR* knockout strain and does not grow in similar concentrations of nitrite. Furthermore, it was confirmed

that HcpR directly regulates the expression of *hcp* by binding directly to its promoter region. From the ChIP experiment, the *hcp* promoter was pulled down and enriched when compared to a negative control. Furthermore, complementing the *hcp* knockout strain with the Pg108 plasmid rescues the nitrite sensitive phenotype. Deleting the inverted repeat sequence in the *hcp* promoter results in a similar phenotype to the *hcp* knock out strain, indicating that HcpR regulates *hcp* expression via directly binding to the *hcp* promoter at an inverted repeat region upstream of transcription start site.

Here we report the structure of the sensing domain of HcpR (HcpR-SD). The structure verifies the inclusion of HcpR in the FNR-CRP family of regulators: the N-terminal domain forms the characteristic β-barrel structure and the homodimer oligomerization is confirmed through SAXS and sedimentation velocity experiments. The mechanism and exact location of heme binding is not immediately evident upon observation of the structure. There are a number of hydrophobic residues that line the space between the dimerization helix (α-7) and 2 of the β-sheets (β-3 and β-5) forming hydrophobic pocket. Of note, the hydrophobic pocket is in contact with the structural elements important in the allosteric activation of FNR-CRP regulators, the dimerization helix and the β-hairpin region known as the "flap" between β-sheets 5 and 6 (located along residues 68-77 in HcpR). Studies with other FNR-CRP regulators have shown that the flap plays an important role in transmitting the signal to the C-terminal helix-turn-helix DNA binding domain and has been shown to play a role in both the interdomain and intersubunit interaction necessary for transmission of a binding signal (109). The mutational studies do implicate this pocket, as simultaneously mutating both Met68 and Met145 produces an inert form of HcpR. However, single mutations of these two residues

reveal no changes in the activity. This is not completely unexpected, as the plasticity of heme binding receptors has been demonstrated in the past (100, 110-113). In many of these cases, the sensing domain is flexible and capable of axial ligand switching and re-arrangement, compensating for mutated residues.

FNR-CRP transcription factors are found in many species of anaerobic bacteria and have been proven to play a role in the regulation of oxidative and nitrosative stress responses (although they are not limited to these functions). In the presence of oxides and N-oxides, they promote the expression of genes such as *nir*, *nor*, and *nos* which are responsible for denitrification and nitrate/nitrite based respiration (71, 114). Thus understanding how HcpR agrees with and differs with other members of the family is important for elucidating the molecular mechanisms employed by HcpR.

Despite a relatively low sequence identity between HcpR, CooA, and DNR, the overall structure of the proteins is similar, with a central β-barrel that is highly conserved. The most significant change is the position of the N-terminal helix with respect to HcpR N-terminus. In CooA this portion of the N-terminal domain has been shown to be important in co-factor/ligand binding. The N-terminal proline residue directly acts as a ligand for the coordination of the iron in the heme cofactor to the opposite subunit. In HcpR, the conformation of the N-terminus makes this highly unlikely. Although HcpR has a proline located at its N-terminus (Pro3), its position is a large distance away from a potential heme binding site. Thus coordination of the heme iron in HcpR is likely to occur through different residues and in a potentially different manner. Another important CooA heme coordination residue, His77 located in the loop connecting β-5 and β-6, is absent in HcpR. As can be seen in the sequence overlays, the β5-β6 loop (residues 86-104) contains an

8 residue extension in HcpR and DNR that blocks the Heme binding site (Fig 3A). This region contains a hydrophilic loop region sandwiched in between two hydrophobic regions of core beta barrel fold and is orientated in the middle of the CooA binding site in the HcpR-CooA superposition. Thus to accommodate heme binding in a manner similar to CooA, this region would have to re-orientate itself to allow heme to occupy the site. Furthermore, the opening of the hydrophobic pocket in HcpR is oriented on the opposite face of the protein. In figure 3B, integration of heme into the CooA binding site occurs through the proximal face of the protein; in HcpR the hydrophobic pocket is oriented on the distal face of the protein. This would imply that binding of heme to HcpR would take place on the opposite face of the protein when compared to CooA.

Despite not having the structure of a heme bound form solved, the structure of DNR shares a slightly higher sequence similarity with HcpR and is believed to be a closer relative. The major structural differences occur due to the orientation of the DNR dimerization helix with respect to the sensing domain and not difference in overall fold. In the crystal structure of the truncated form of DNR, a portion of the dimerization helix is unwound and is lodged in the hydrophobic pocket that is composed of portions of the N-terminal domain and the dimerization helix. To accommodate the formation of this pocket the orientation of the dimerization helix is significantly different from that of HcpR (and other members of the FNR-CRP family) as can be most evidently seen in the overlay. Of note, the extended loop region in the proposed heme binding site is present in both DNR and HcpR. Furthermore, the opening of the hydrophobic pocket in DNR is in a similar position in the superposition. This would imply that HcpR and DNR could bind to heme in a similar manner (the location of the hydrophobic pocket is similar) however the

115

coordination and mechanisms of allosteric activation of the DNA binding and RNA polymerase recruitment may differ (the core residues of the hydrophobic pocket are not conserved).

In heme-based sensor proteins, the ability to change the coordination state of the heme-iron is utilized for signaling and allosteric activation. Thus understanding and identifying the residues involved in coordination is imperative to fully understanding the mechanisms of these proteins. It is not immediately clear which residues are involved in the coordination of heme iron in HcpR. The heme bound protein is stable and the spectral and resonance Raman data suggests that the ferrous form is primarily hexacoordinate. The primarily hexacoordinate nature of the heme bound form of HcpR transitions to a penta-coordinate system with the addition of NO to form the holo-protein. This is not uncommon, as a pentacoordinate system is observed in many heme binding proteins when NO is bound (as seen in DNR, CooA, and sGC). The innate affinity of NO for heme is much higher than that of CO or O_2 due in large part to its strong back-bonding with the iron. This increased affinity causes NO to exert a strong trans effect on Fe(II), resulting in a long and weak bond to an axial ligand (61, 62). This unique property of the NO-Fe(II) bond is used to the advantage of other heme based NO sensors. The primary molecular event correlated with sGC activation is the dissociation of the heme-proximal histidine bond upon NO binding to the distal face of the heme. This event (loss of proximal His coordination) triggers the structural allosteric changes within sGC that activate it (63, 64). A similar mechanism is also hypothesized to take place in DNR, where the dissociation of an axial histidine residue (His187) is the key regulatory step of the NO-mediated activation of DNR (110). In both cases, CO and O_2 do not apply a strong enough trans

effect on the iron to break the His-iron bond. This allows for the NO selective activation in both of these sensors. It is probable that HcpR follows a similar mechanism. Hcp is not upregulated in response to oxygen or oxidative stress and the Δhcp mutant of *P. gingivalis* is not sensitive to oxidative stress, thus HcpR is capable of selective activation in response to NO *in vivo* (52). Furthermore, the transient nature of the 6th axial ligand in the un-nitrosylated state implies that the 5th axial ligand may be the key regulator in the NO activation of HcpR.

Interestingly, the binding of Fe(III) heme to HcpR is possible and the addition of NO to this sample yields a spectrum that is similar to that of the Fe(II) hexa-coordinate system. Unlike CO and O_2, NO is capable of binding to Fe(III) and reducing it to Fe(II) heme (115). However, whether this subsequent hexa-coordinate system involves binding of NO or just binding to the protein axial ligands still needs to be studied.

In CRP, binding of cAMP leads to substantial structural change of the homodimer that is characteristic of FNR-CRP proteins (116). Likewise, in DNR, it is hypothesized the protein undergoes a similar large structural change after NO binding (46). It is believed that the sensor domain, dimerization helix, and DNA binding domain act as separate bodies, changing their orientation with respect to each other upon ligand binding. In the case of CRP, it is believed that cAMP binding in the space between the dimerization helix and the β-barrel of the N-terminal domain causes the N-terminal domain to move around the dimerization helices (99, 117). The movement of the N-terminal domain will influence the orientation of the C-terminal DNA binding domain through direct interaction with the "flap" region and the lower portion of the dimerization helix transitions from a disordered coil to an ordered helix (116). For this to occur, cAMP must make interactions with

residues located on the dimerization helix (99). On the basis of its overall structure and general folding with other FNR-CRP proteins, it could be assumed that NO binding to HcpR allosterically promotes adoption of similar structural changes to promote activation and DNA binding. For HcpR, binding of NO to the heme cofactor displaces 2 of the side chains coordinating the heme iron. It is possible that this displacement would then yield an allosteric transition. Although the identity of these residues are currently unknown, for activation to occur in the same manner as CRP and DNR, one of these residues is most likely located on the dimerization helix.

Understanding the complete structural basis for NO-induced allosteric activation in HcpR will most likely require the structure of the full-length and heme-bound forms of the protein. Our attempts at crystallizing the full-length HcpR have been unsuccessful thus far probably due to the dynamic character of the DNA binding domain as shown by the SAXS analysis. Our simplest working hypothesis of the mechanism is a two-state model, with an "on" and "off" state. Binding of NO to the protein-bound heme prompts an allosteric change to the on state of the protein via the dissociation of a key residue. The on state is capable of interacting with RNA polymerase and inducing transcription at a target promoter. While the on state of the protein may be dominated by a single conformer, the apo and off state is not. SAXS reveals that the DNA binding domain of apo-HcpR has a dynamic character. This would imply that the inactive, apo-form of the protein is an assemblage of different conformers which may be the source of its lower affinity for DNA. A possible mechanism of allosteric activation involves bound NO influencing the folding equilibrium of the DNA binding domain, causing one conformer with a high affinity for DNA to dominate. SAXS experiments using the heme bound and NO-bound form of the

protein would shed light on this potential mechanism, however our attempts at obtaining the solution scattering data of these forms of HcpR was unsuccessful due to aggregation and precipitation.

Based on the structural and biochemical data a putative mechanism of HcpR involves an "OFF" and "ON" state that involves allosteric activation by NO binding (Fig. 36) In the OFF state, HcpR is a 6-coordinate system with one of the bonds to the heme iron being a weak axial bond. In the presence of reactive nitrogen species, specifically NO, HcpR binds to the heme cofactor of HcpR. The binding of NO displaces the axial bonds to the heme. Displacement of these axial bonds ("specifically the "non weak" bond) is the molecular event that induces a perturbation that extends to the DNA binding domain. Gas binding stabilizes the DNA binding domain in the "ON" state allowing to bind to DNA and recruit RNA polymerase. Detoxification and removal of reactive nitrogen species leads to a decrease in intracellular NO. Loss of gas binding allows the axial bonds to reform switching the protein to the "OFF" state.
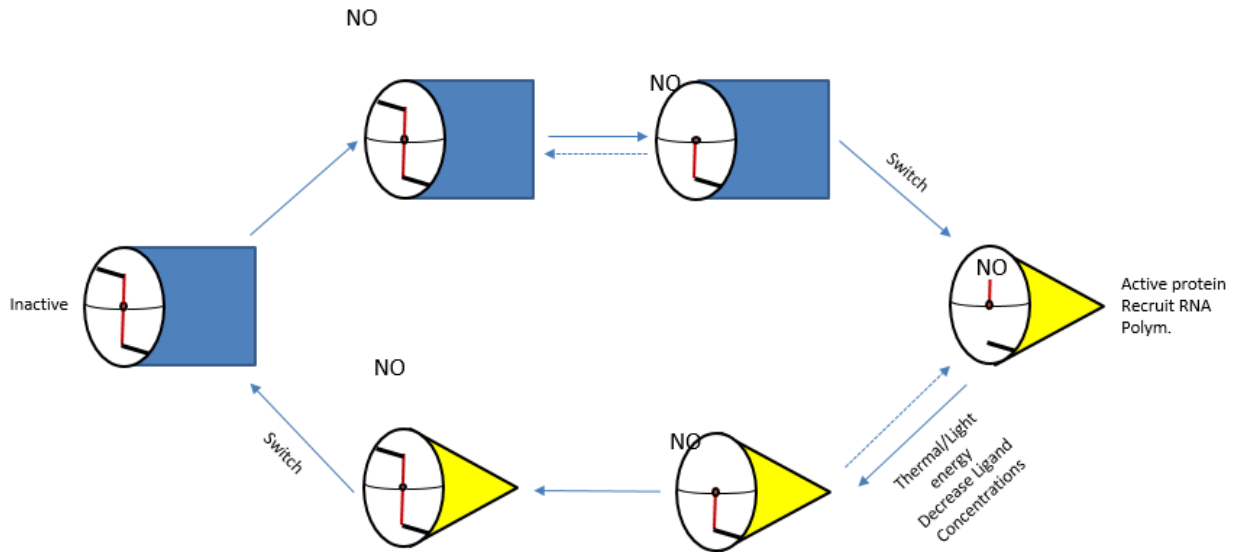
Figure 36 – Hypothetical model of HcpR activation. HcpR exists in a 6-coordinate

state in the un-gas bound state. Binding of nitric oxide displaces both axial ligands and

displacement of these axial bonds activates the protein. In the gas bound state HcpR is

a 5-coordinate system and is in the active form of the protein allowing it bind to DNA

and recruit RNA polymerase.

Conclusion

HcpR is a transcriptional regulator that is necessary for *P. gingivalis* survival in the presence of nitrite. Its functional purpose is to regulate the putative NO reductase Hcp*,* and it does this via sensing intra-cellular levels of NO and binding directly to the *hcp* promoter. Based on structural and biochemical data we show that HcpR is a member of the FNR-CRP family of regulators and demonstrate that the N-terminal sensing domain is capable of binding heme. We also have identified a hydrophobic pocket which may accommodate heme binding and have confirmed the functionality of this pocket through mutagenesis studies, implicating two methionine residues located in the pocket (Met68 and Met145) as important in the activation of the protein. Finally, the heme-bound form of the protein is primarily a hexa-coordinate system which changes to a penta-coordinate one after the addition of NO.

V. References

1. Dewhirst, F.E., Chen, T., Izard, J., Paster, B.J., Tanner, A.C., Yu, W.H., Lakshmanan, A., and Wade, W.G. (2010) The human oral microbiome. *J.Bacteriol.* **192,** 5002-5017

2. Human Microbiome Project Consortium (2012) Structure, function and diversity of the healthy human microbiome. *Nature.* **486,** 207-214

3. Segata, N., Boernigen, D., Tickle, T.L., Morgan, X.C., Garrett, W.S., and Huttenhower, C. (2013) Computational meta'omics for microbial community studies. *Mol Syst Biol.* **9,**

4. Mark Welch, J.L., Rossetti, B.J., Rieken, C.W., Dewhirst, F.E., and Borisy, G.G. (2016) Biogeography of a human oral microbiome at the micron scale. *Proc.Natl.Acad.Sci.U.S.A.* **113,** E791-800

5. Kreth, J., Zhang, Y., and Herzberg, M.C. (2008) Streptococcal antagonism in oral biofilms: *Streptococcus sanguinis* and *Streptococcus gordonii* interference with Streptococcus mutans. *J.Bacteriol.* **190,** 4632-4640

6. Hezel, M.P., and Weitzberg, E. (2015) The oral microbiome and nitric oxide homoeostasis. *Oral Dis.* **21,** 7-16

7. Gladwin, M.T., and Kim-Shapiro, D.B. (2008) The functional nitrite reductase activity of the heme-globins. *Blood.* **112,** 2636-2647

8. Sundqvist, M.L., Lundberg, J.O., and Weitzberg, E. (2016) Effects of antiseptic mouthwash on resting metabolic rate: A randomized, double-blind, crossover study. *Nitric Oxide.* **61,** 38-44

9. Velmurugan, S., Gan, J.M., Rathod, K.S., Khambata, R.S., Ghosh, S.M., Hartley, A., Van Eijl, S., Sagi-Kiss, V., Chowdhury, T.A., Curtis, M., Kuhnle, G.G., Wade, W.G., and Ahluwalia, A. (2016) Dietary nitrate improves vascular function in patients with hypercholesterolemia: a randomized, double-blind, placebo-controlled study. *Am.J.Clin.Nutr.* **103,** 25-38

10. Gross, E.L., Beall, C.J., Kutsch, S.R., Firestone, N.D., Leys, E.J., and Griffen, A.L. (2012) Beyond Streptococcus mutans: dental caries onset linked to multiple species by 16S rRNA community analysis. *PLoS One.* **7,** e47722

11. Marcenes, W., Kassebaum, N.J., Bernabe, E., Flaxman, A., Naghavi, M., Lopez, A., and Murray, C.J. (2013) Global burden of oral conditions in 1990-2010: a systematic analysis. *J.Dent.Res.* **92,** 592-597

12. Petersen, P.E., and Ogawa, H. (2012) The global burden of periodontal disease: towards integration with chronic disease prevention and control. *Periodontol.2000.* **60,** 15-39

13. Eke, P.I., Dye, B.A., Wei, L., Slade, G.D., Thornton-Evans, G.O., Borgnakke, W.S., Taylor, G.W., Page, R.C., Beck, J.D., and Genco, R.J. (2015) Update on Prevalence of Periodontitis in Adults in the United States: NHANES 2009 to 2012. *J.Periodontol.* **86,** 611-622

14. Jin, L.J., Lamster, I.B., Greenspan, J.S., Pitts, N.B., Scully, C., and Warnakulasuriya, S. (2016) Global burden of oral diseases: emerging concepts, management and interplay with systemic health. *Oral Dis.* **22,** 609-619

15. Savage, A., Eaton, K.A., Moles, D.R., and Needleman, I. (2009) A systematic review of definitions of periodontitis and methods that have been used to identify this disease. *J.Clin.Periodontol.* **36,** 458 467

16. Saglie, R., Newman, M.G., Carranza, F.A.,Jr, and Pattison, G.L. (1982) Bacterial invasion of gingiva in advanced periodontitis in humans. *J.Periodontol.* **53,** 217-222

17. Darveau, R.P. (2010) Periodontitis: a polymicrobial disruption of host homeostasis. *Nat.Rev.Microbiol.* **8,** 481-490

18. Hajishengallis, G., and Lamont, R.J. (2012) Beyond the red complex and into more complexity: the polymicrobial synergy and dysbiosis (PSD) model of periodontal disease etiology. *Mol.Oral Microbiol.* **27,** 409-419

19. Hajishengallis, G., Darveau, R.P., and Curtis, M.A. (2012) The keystone-pathogen hypothesis. *Nature Reviews Microbiology.* **10,** 717 725

20. Popadiak, K., Potempa, J., Riesbeck, K., and Blom, A.M. (2007) Biphasic effect of gingipains from *Porphyromonas gingivalis* on the human complement system. *J.Immunol.* **178,** 7242-7250

21. Stathopoulou, P.G., Benakanakere, M.R., Galicia, J.C., and Kinane, D.F. (2009) The host cytokine response to *Porphyromonas gingivalis* is modified by gingipains. *Oral Microbiol.Immunol.* **24,** 11-17

22. Olsen, I., Lambris, J.D., and Hajishengallis, G. (2017) *Porphyromonas gingivalis* disturbs host-commensal homeostasis by changing complement function. *J.Oral Microbiol.* **9,** 1340085

23. Olsen, I., and Hajishengallis, G. (2016) Major neutrophil functions subverted by *Porphyromonas gingivalis. J.Oral Microbiol.* **8,** 30936

24. Yilmaz, O., Watanabe, K., and Lamont, R.J. (2002) Involvement of integrins in fimbriae-mediated binding and invasion by *Porphyromonas gingivalis. Cell.Microbiol.* **4,** 305 314

25. Wang, M., Krauss, J.L., Domon, H., Hosur, K.B., Liang, S., Magotti, P., Triantafilou, M., Triantafilou, K., Lambris, J.D., and Hajishengallis, G. (2010) Microbial Hijacking of Complement-Toll-like Receptor Crosstalk*. Sci.Signal.* **3,** ra11

26. Hajishengallis, G., Liang, S., Payne, M.A., Hashim, A., Jotwani, R., Eskan, M.A., McIntosh, M.L., Alsam, A., Kirkwood, K.L., Lambris, J.D., Darveau, R.P., and Curtis, M.A. (2011) Low-Abundance Biofilm Species Orchestrates Inflammatory Periodontal Disease through the Commensal Microbiota and Complement*. Cell Host & Microbe.* **10,** 497 506

27. Lancaster, J.R.,Jr (1997) A tutorial on the diffusibility and reactivity of free nitric oxide*. Nitric Oxide.* **1,** 18-30

28. Kroncke, K.D., Fehsel, K., and Kolb-Bachofen, V. (1997) Nitric oxide: cytotoxicity versus cytoprotection--how, why, when, and where?*. Nitric Oxide.* **1,** 107-120

29. Stamler, J.S. (1994) Redox signaling: nitrosylation and related target interactions of nitric oxide*. Cell.* **78,** 931-936

30. Hill, B.G., Dranka, B.P., Bailey, S.M., Lancaster, J.R., and Darley-Usmar, V.M. (2010) What Part of NO Don't You Understand? Some Answers to the Cardinal Questions in Nitric Oxide Biology*. J.Biol.Chem.* **285,** 19699 19704

31. Gladwin, M.T., and Kim-Shapiro, D.B. (2008) The functional nitrite reductase activity of the heme-globins*. Blood.* **112,** 2636-2647

32. Lewis, J.P., Dawson, J.A., Hannis, J.C., Muddiman, D., and Macrina, F.L. (1999) Hemoglobinase activity of the lysine gingipain protease (Kgp) of *Porphyromonas gingivalis* W83*. J.Bacteriol.* **181,** 4905-4913

33. Alderton, W.K., Cooper, C.E., and Knowles, R.G. (2001) Nitric oxide synthases: structure, function and inhibition*. Biochem.J.* **357,** 593-615

34. Dudzinski, D.M., and Michel, T. (2007) Life history of eNOS: partners and pathways*. Cardiovasc.Res.* **75,** 247-260

35. Kone, B.C., Kuncewicz, T., Zhang, W., and Yu, Z.Y. (2003) Protein interactions with nitric oxide synthases: controlling the right time, the right place, and the right amount of nitric oxide*. Am.J.Physiol.Renal Physiol.* **285,** F178-90

36. Gyurko, R., Shoji, H., Battaglino, R.A., Boustany, G., Gibson, F.C.,3rd, Genco, C.A., Stashenko, P., and Van Dyke, T.E. (2005) Inducible nitric oxide synthase mediates bone development and *P. gingivalis*-induced alveolar bone loss. *Bone.* **36,** 472-479

37. Herrera, B.S., Martins-Porto, R., Maia-Dantas, A., Campi, P., Spolidorio, L.C., Costa, S.K., Van Dyke, T.E., Gyurko, R., and Muscara, M.N. (2011) iNOS-derived nitric oxide stimulates osteoclast activity and alveolar bone loss in ligature-induced periodontitis in rats. *J.Periodontol.* **82,** 1608-1615

38. Gyurko, R., Boustany, G., Huang, P.L., Kantarci, A., Van Dyke, T.E., Genco, C.A., and Gibson, F.C.,3rd (2003) Mice lacking inducible nitric oxide synthase demonstrate impaired killing of *Porphyromonas gingivalis. Infect.Immun.* **71,** 4917-4924

39. Latchman, D.S. (1997) Transcription factors: An overview. *Int.J.Biochem.Cell Biol.* **29,** 1305 1312

40. Ptashne, M., and Gann, A. (1997) Transcriptional activation by recruitment. *Nature.* **386,** 569 577

41. Huffman, J.L., and Brennan, R.G. (2002) Prokaryotic transcription regulators: more than just the helix-turn-helix motif. *Curr.Opin.Struct.Biol.* **12,** 98-106

42. Pabo, C.O., and Sauer, R.T. (1992) Transcription factors: structural families and principles of DNA recognition. *Annu.Rev.Biochem.* **61,** 1053-1095

43. Rivera-Gomez, N., Martinez-Nunez, M.A., Pastor, N., Rodriguez-Vazquez, K., and Perez-Rueda, E. (2017) Dissecting the protein architecture of DNA-binding transcription factors in bacteria and archaea. *Microbiology.* **163,** 1167-1178

44. Korner, H., Sofia, H.J., and Zumft, W.G. (2003) Phylogeny of the bacterial superfamily of Crp-Fnr transcription regulators: exploiting the metabolic spectrum by controlling alternative gene programs. *FEMS Microbiol.Rev.* **27,** 559-592

45. Schultz, S.C., Shields, G.C., and Steitz, T.A. (1991) Crystal structure of a CAP-DNA complex: the DNA is bent by 90 degrees. *Science.* **253,** 1001-1007

46. Giardina, G., Rinaldo, S., Castiglione, N., Caruso, M., and Cutruzzola, F. (2009) A dramatic conformational rearrangement is necessary for the activation of DNR from Pseudomonas aeruginosa. Crystal structure of wild-type DNR. *Proteins.* **77,** 174-180

47. Kuchinskas, M., Li, H., Conrad, M., Roberts, G., and Poulos, T.L. (2006) The role of the DNA-binding domains in CooA activation. *Biochemistry.* **45,** 7148-7153

48. Fang, F.C., Frawley, E.R., Tapscott, T., and Vazquez-Torres, A. (2016) Bacterial Stress Responses during Host Infection. *Cell.Host Microbe.* **20,** 133-143

49. Fang, F.C. (2004) Antimicrobial reactive oxygen and nitrogen species: concepts and controversies. *Nat.Rev.Microbiol.* **2,** 820-832

50. Pathania, R., Navani, N.K., Gardner, A.M., Gardner, P.R., and Dikshit, K.L. (2002) Nitric oxide scavenging and detoxification by the Mycobacterium tuberculosis haemoglobin, HbN in Escherichia coli. *Mol.Microbiol.* **45,** 1303 1314

51. Bryk, R., Griffin, P., and Nathan, C. (2000) Peroxynitrite reductase activity of bacterial peroxiredoxins. *Nature.* **407,** 211-215

52. Boutrin, M.C., Wang, C., Aruni, W., Li, X., and Fletcher, H.M. (2012) Nitric oxide stress resistance in *Porphyromonas gingivalis* is mediated by a putative hydroxylamine reductase. *J.Bacteriol.* **194,** 1582-1592

53. Poole, R.K. (2005) Nitric oxide and nitrosative stress tolerance in bacteria. *Biochem.Soc.Trans.* **33,** 176-180

54. Lewis, J.P., Yanamandra, S.S., and Anaya-Bergman, C. (2012) HcpR of *Porphyromonas gingivalis* is required for growth under nitrosative stress and survival within host cells. *Infect.Immun.* **80,** 3319-3331

55. Richardson, A.R., Dunman, P.M., and Fang, F.C. (2006) The nitrosative stress response of *Staphylococcus aureus* is required for resistance to innate immunity. *Mol.Microbiol.* **61,** 927-939

56. Seth, D., Hausladen, A., Wang, Y.J., and Stamler, J.S. (2012) Endogenous protein S-Nitrosylation in E. coli: regulation by OxyR. *Science.* **336,** 470-473

57. Miller, D.P., Hutcherson, J.A., Wang, Y., Nowakowska, Z.M., Potempa, J., Yoder-Himes, D.R., Scott, D.A., Whiteley, M., and Lamont, R.J. (2017) Genes Contributing to *Porphyromonas gingivalis* Fitness in Abscess and Epithelial Cell Colonization Environments. *Front.Cell.Infect.Microbiol.* **7,** 378

58. Shimizu, T., Huang, D., Yan, F., Stranava, M., Bartosova, M., Fojtikova, V., and Martinkova, M. (2015) Gaseous O2, NO, and CO in signal transduction: structure and function relationships of heme-based gas sensors and heme-redox sensors. *Chem.Rev.* **115,** 6491-6533

59. Tsai, A.L., Berka, V., Martin, E., and Olson, J.S. (2012) A "Sliding Scale Rule" for Selectivity between NO, CO and O(2) by Heme Protein Sensors(). *Biochemistry.* **51,** 172-186

60. Jain, R., and Chan, M.K. (2003) Mechanisms of ligand discrimination by heme proteins. *J.Biol.Inorg.Chem.* **8,** 1-11

61. Scheidt, W.R., Barabanschikov, A., Pavlik, J.W., Silvernail, N.J., and Sage, J.T. (2010) Electronic structure and dynamics of nitrosyl porphyrins. *Inorg.Chem.* **49,** 6240-6252

62. Spiro, T.G., Soldatova, A.V., and Balakrishnan, G. (2013) CO, NO and O as Vibrational Probes of Heme Protein Interactions. *Coord.Chem.Rev.* **257,** 511-527

63. Yoo, B.K., Lamarre, I., Martin, J.L., Rappaport, F., and Negrerie, M. (2015) Motion of proximal histidine and structural allosteric transition in soluble guanylate cyclase. *Proc.Natl.Acad.Sci.U.S.A.* **112,** E1697-704

64. Stone, J.R., and Marletta, M.A. (1994) Soluble guanylate cyclase from bovine lung: activation with nitric oxide and carbon monoxide and spectral characterization of the ferrous and ferric states. *Biochemistry.* **33,** 5636-5640

65. Liebl, U., Lambry, J., and Vos, M.H. (2013) Primary processes in heme-based sensor proteins. *Biochimica et Biophysica Acta (BBA) - Proteins and Proteomics.* **1834,** 1684 1692

66. Kiley, P.J., and Beinert, H. (2003) The role of Fe-S proteins in sensing and regulation in bacteria. *Curr.Opin.Microbiol.* **6,** 181-185

67. Cadby, I.T., Ibrahim, S.A., Faulkner, M., Lee, D.J., Browning, D., Busby, S.J., Lovering, A.L., Stapleton, M.R., Green, J., and Cole, J.A. (2016) Regulation, sensory domains and roles of two *Desulfovibrio desulfuricans* ATCC27774 Crp family transcription factors, HcpR1 and HcpR2, in response to nitrosative stress. *Mol.Microbiol.* **102,** 1120-1137

68. Lobato, L., Bouzhir-Sima, L., Yamashita, T., Wilson, M.T., Vos, M.H., and Liebl, U. (2014) Dynamics of the heme-binding bacterial gas-sensing dissimilative nitrate respiration regulator (DNR) and activation barriers for ligand binding and escape. *J.Biol.Chem.* **289,** 26514-26524

69. Reynolds, M.F., Parks, R.B., Burstyn, J.N., Shelver, D., Thorsteinsson, M.V., Kerby, R.L., Roberts, G.P., Vogel, K.M., and Spiro, T.G. (2000) Electronic absorption, EPR, and resonance raman spectroscopy of CooA, a CO-sensing transcription activator from *R. rubrum*, reveals a five-coordinate NO-heme. *Biochemistry.* **39,** 388-396

70. Giardina, G., Rinaldo, S., Johnson, K.A., Di Matteo, A., Brunori, M., and Cutruzzola, F. (2008) NO sensing in Pseudomonas aeruginosa: structure of the transcriptional regulator DNR. *J.Mol.Biol.* **378,** 1002-1015

71. Arai, H., Igarashi, Y., and Kodama, T. (1995) Expression of the nir and nor genes for denitrification of Pseudomonas aeruginosa requires a novel CRP/FNR-related transcriptional regulator, DNR, in addition to ANR. *FEBS Lett.* **371,** 73 76

72. Vogel, K.M., Spiro, T.G., Shelver, D., Thorsteinsson, M.V., and Roberts, G.P. (1999) Resonance Raman evidence for a novel charge relay activation mechanism of the CO-dependent heme protein transcription factor CooA. *Biochemistry.* **38,** 2679-2687

73. Yoshimoto, H., Takahasi, Y., Kato, D., and Umemoto, T. (1997) Construction of a plasmid vector for transformation of *Porphyromonas gingivalis. FEMS Microbiol.Lett.* **152,** 175-181

74. Heras, B., and Martin, J.L. (2005) Post-crystallization treatments for improving diffraction quality of protein crystals. *Acta Crystallogr.D Biol.Crystallogr.* **61,** 1173-1180

75. Winn, M.D., Ballard, C.C., Cowtan, K.D., Dodson, E.J., Emsley, P., Evans, P.R., Keegan, R.M., Krissinel, E.B., Leslie, A.G., McCoy, A., McNicholas, S.J., Murshudov, G.N., Pannu, N.S., Potterton, E.A., Powell, H.R., Read, R.J., Vagin, A., and Wilson, K.S. (2011) Overview of the CCP4 suite and current developments. *Acta Crystallogr.D Biol.Crystallogr.* **67,** 235-242

76. Adams, P.D., Afonine, P.V., Bunkoczi, G., Chen, V.B., Davis, I.W., Echols, N., Headd, J.J., Hung, L.W., Kapral, G.J., Grosse-Kunstleve, R.W., McCoy, A.J., Moriarty, N.W., Oeffner, R., Read, R.J., Richardson, D.C., Richardson, J.S., Terwilliger, T.C., and Zwart, P.H. (2010) PHENIX: a comprehensive Python-based system for macromolecular structure solution. *Acta Crystallogr.D Biol.Crystallogr.* **66,** 213-221

77. Emsley, P., Lohkamp, B., Scott, W.G., and Cowtan, K. (2010) Features and development of Coot. *Acta Crystallogr.D Biol.Crystallogr.* **66,** 486-501

78. Petoukhov, M.V., Franke, D., Shkumatov, A.V., Tria, G., Kikhney, A.G., Gajda, M., Gorba, C., Mertens, H.D., Konarev, P.V., and Svergun, D.I. (2012) New developments in the ATSAS program package for small-angle scattering data analysis. *J.Appl.Crystallogr.* **45,** 342-350

79. Franke, D., and Svergun, D.I. (2009) DAMMIF, a program for rapidab-initioshape determination in small-angle scattering. *Journal of Applied Crystallography.* **42,** 342 346

80. Petoukhov, M.V., and Svergun, D.I. Global Rigid Body Modeling of Macromolecular Complexes against Small-Angle Scattering Data. *Biophys.J.* **89,** 1237-1250

81. Kozin, M.B., and Svergun, D.I. (2001) Automated matching of high- and low-resolution structural models. *Journal of Applied Crystallography.* **34,** 33-41

82. Tria, G., Mertens, H.D.T., Kachala, M., and Svergun, D.I. (2015) Advanced ensemble modelling of flexible macromolecules using X-ray solution scattering. *IUCrJ.* **2,** 207-217

83. Pettersen, E.F., Goddard, T.D., Huang, C.C., Couch, G.S., Greenblatt, D.M., Meng, E.C., and Ferrin, T.E. (2004) UCSF Chimera--a visualization system for exploratory research and analysis. *J.Comput.Chem.* **25,** 1605-1612

84. Jones, P., Binns, D., Chang, H.Y., Fraser, M., Li, W., McAnulla, C., McWilliam, H., Maslen, J., Mitchell, A., Nuka, G., Pesseat, S., Quinn, A.F., Sangrador-Vegas, A., Scheremetjew, M., Yong, S.Y., Lopez, R., and Hunter, S. (2014) InterProScan 5: genome-scale protein function classification. *Bioinformatics.*

85. Dundas, J., Ouyang, Z., Tseng, J., Binkowski, A., Turpaz, Y., and Liang, J. (2006) CASTp: computed atlas of surface topography of proteins with structural and topographical mapping of functionally annotated residues. *Nucleic Acids Res.* **34,** W116-8

86. Sievers, F., Wilm, A., Dineen, D., Gibson, T.J., Karplus, K., Li, W., Lopez, R., McWilliam, H., Remmert, M., Soding, J., Thompson, J.D., and Higgins, D.G. (2011) Fast, scalable generation of high-quality protein multiple sequence alignments using Clustal Omega. *Mol.Syst.Biol.* **7,** 539

87. Webb, B., and Sali, A. (2016) Comparative Protein Structure Modeling Using MODELLER. *Curr.Protoc.Protein Sci.* **86,** 2.9.1-2.9.37

88. Townsend, Philip D. AND Jungwirth, Britta AND Pojer, Florence AND BuÃŸmann, Michael AND Money, Victoria A. AND Cole, Stewart T. AND PÃ¼hler, Alfred AND Tauch, Andreas AND Bott, Michael AND Cann, Martin J. AND Pohl,Ehmke (2014) The Crystal Structures of Apo and cAMP-Bound GlxR from Corynebacterium glutamicum Reveal Structural and Dynamic Changes upon cAMP Binding in CRP/FNR Family Transcription Factors. *PLOS ONE.* **9,** 1-21

89. Kelley, L.A., and Sternberg, M.J.E. (2009) Protein structure prediction on the Web: a case study using the Phyre server. *Nature Protocols.* **4,** 363 371

90. Wolfe, M.T., Heo, J., Garavelli, J.S., and Ludden, P.W. (2002) Hydroxylamine reductase activity of the hybrid cluster protein from *Escherichia coli. J.Bacteriol.* **184,** 5898-5902

91. Arp, D.J., Sayavedra-Soto, L.A., and Hommes, N.G. (2002) Molecular biology and biochemistry of ammonia oxidation by Nitrosomonas europaea. *Arch.Microbiol.* **178,** 250-255

92. Wang, J., Vine, C.E., Balasiny, B.K., Rizk, J., Bradley, C.L., Tinajero-Trejo, M., Poole, R.K., Bergaust, L.L., Bakken, L.R., and Cole, J.A. (2016) The roles of the hybrid cluster protein, Hcp and its reductase, Hcr, in high affinity nitric oxide reduction that protects anaerobic cultures of Escherichia coli against nitrosative stress. *Mol.Microbiol.* **100,** 877-892

93. Saveson, C.J., and Lovett, S.T. (1999) Tandem repeat recombination induced by replication fork defects in *Escherichia coli* requires a novel factor, RadC. *Genetics.* **152,** 5-13

94. Deinum, G., Stone, J.R., Babcock, G.T., and Marletta, M.A. (1996) Binding of nitric oxide and carbon monoxide to soluble guanylate cyclase as observed with Resonance raman spectroscopy. *Biochemistry.* **35,** 1540-1547

95. Spiro, T.G., and Strekas, T.C. (1974) Resonance Raman spectra of heme proteins. Effects of oxidation and spin state. *J.Am.Chem.Soc.* **96,** 338 345

96. Andrew, C.R., Green, E.L., Lawson, D.M., and Eady, R.R. (2001) Resonance Raman Studies of Cytochrome c Support the Binding of NO and CO to Opposite Sides of the Heme: Implications for Ligand Discrimination in Heme-Based Sensorsâ€ . *Biochemistry (N.Y.).* **40,** 4115-4122

97. Karow, D.S., Pan, D., Tran, R., Pellicena, P., Presley, A., Mathies, R.A., and Marletta, M.A. (2004) Spectroscopic characterization of the soluble guanylate cyclase-like heme domains from *Vibrio cholerae* and *Thermoanaerobacter tengcongensis.* *Biochemistry.* **43,** 10203-10211

98. Rodionov, D.A., Dubchak, I., Arkin, A., Alm, E., and Gelfand, M.S. (2004) Reconstruction of regulatory and metabolic pathways in metal-reducing delta-proteobacteria. *Genome Biol.* **5,** R90

99. Passner, J.M., Schultz, S.C., and Steitz, T.A. (2000) Modeling the cAMP-induced allosteric transition using the crystal structure of CAP-cAMP at 2.1 A resolution. *J.Mol.Biol.* **304,** 847-859

100. Roberts, G.P., Kerby, R.L., Youn, H., and Conrad, M. (2005) CooA, a paradigm for gas sensing regulatory proteins. *J.Inorg.Biochem.* **99,** 280-292

101. Rinaldo, S., Castiglione, N., Giardina, G., Caruso, M., Arcovito, A., Longa, S.d., D'Angelo, P., and Cutruzzolà, F. (2012) Unusual Heme Binding Properties of the Dissimilative Nitrate Respiration Regulator, a Bacterial Nitric Oxide Sensor. *Antioxidants & Redox Signaling.* **17,** 1178 1189

102. Velmurugan, S., Gan, J.M., Rathod, K.S., Khambata, R.S., Ghosh, S.M., Hartley, A., Van Eijl, S., Sagi-Kiss, V., Chowdhury, T.A., Curtis, M., Kuhnle, G.G., Wade, W.G., and Ahluwalia, A. (2016) Dietary nitrate improves vascular function in patients with hypercholesterolemia: a randomized, double-blind, placebo-controlled study. *Am.J.Clin.Nutr.* **103,** 25-38

103. Rodionov, D.A., Dubchak, I.L., Arkin, A.P., Alm, E.J., and Gelfand, M.S. (2005) Dissimilatory metabolism of nitrogen oxides in bacteria: comparative reconstruction of transcriptional networks. *PLoS Comput.Biol.* **1,** e55

104. Chismon, D.L., Browning, D.F., Farrant, G.K., and Busby, S.J.W. (2010) Unusual organization, complexity and redundancy at the *Escherichia coli* hcp-hcroperon promoter. *Biochem.J.* **430,** 61 68

105. Filenko, N., Spiro, S., Browning, D.F., Squire, D., Overton, T.W., Cole, J., and Constantinidou, C. (2007) The NsrR regulon of *Escherichia coli* K-12 includes genes encoding the hybrid cluster protein and the periplasmic, respiratory nitrite reductase. *J.Bacteriol.* **189,** 4410-4417

106. Seth, D., Hausladen, A., Wang, Y.J., and Stamler, J.S. (2012) Endogenous protein S-Nitrosylation in *E. coli*: regulation by OxyR. *Science.* **336,** 470-473

107. Lewis, J.P., Iyer, D., and Anaya-Bergman, C. (2009) Adaptation *of Porphyromonas gingivalis* to microaerophilic conditions involves increased consumption of formate and reduced utilization of lactate. *Microbiology.* **155,** 3758-3774

108. Das, A., Silaghi-Dumitrescu, R., Ljungdahl, L.G., and Kurtz, D.M.,Jr (2005) Cytochrome bd oxidase, oxidative stress, and dioxygen tolerance of the strictly anaerobic bacterium *Moorella thermoacetica. J.Bacteriol.* **187,** 2020-2029

109. Levy, C., Pike, K., Heyes, D.J., Joyce, M.G., Gabor, K., Smidt, H., van der Oost, J., and Leys, D. (2008) Molecular basis of halorespiration control by CprK, a CRP-FNR type transcriptional regulator. *Mol.Microbiol.* **70,** 151-167

110. Cutruzzola, F., Arcovito, A., Giardina, G., della Longa, S., D'Angelo, P., and Rinaldo, S. (2014) Distal-proximal crosstalk in the heme binding pocket of the NO sensor DNR. *Biometals.* **27,** 763-773

111. Farhana, A., Saini, V., Kumar, A., Lancaster, J.R.,Jr, and Steyn, A.J. (2012) Environmental heme-based sensor proteins: implications for understanding bacterial pathogenesis. *Antioxid.Redox Signal.* **17,** 1232-1245

112. Igarashi, J., Murase, M., Iizuka, A., Pichierri, F., Martinkova, M., and Shimizu, T. (2008) Elucidation of the heme binding site of heme-regulated eukaryotic initiation factor 2alpha kinase and the role of the regulatory motif in heme sensing by spectroscopic and catalytic studies of mutant proteins. *J.Biol.Chem.* **283,** 18782-18791

113. Cowley, A.B., Kennedy, M.L., Silchenko, S., Lukat-Rodgers, G.S., Rodgers, K.R., and Benson, D.R. (2006) Insight into heme protein redox potential control and functional aspects of six-coordinate ligand-sensing heme proteins from studies of synthetic heme peptides. *Inorg.Chem.* **45,** 9985-10001

114. Arai, H., Mizutani, M., and Igarashi, Y. (2003) Transcriptional regulation of the nos genes for nitrous oxide reductase in Pseudomonas aeruginosa. *Microbiology.* **149,** 29-36

115. Soldatova, A.V., Ibrahim, M., Olson, J.S., Czernuszewicz, R.S., and Spiro, T.G. (2010) New Light on NO Bonding in Fe(III) Heme Proteins from Resonance Raman Spectroscopy and DFT Modeling. *J.Am.Chem.Soc.* **132,** 4614 4625

116. Popovych, N., Tzeng, S.R., Tonelli, M., Ebright, R.H., and Kalodimos, C.G. (2009) Structural basis for cAMP-mediated allosteric control of the catabolite activator protein. *Proc.Natl.Acad.Sci.U.S.A.* **106,** 6927-6932

117. Tzeng, S.R., and Kalodimos, C.G. (2013) Allosteric inhibition through suppression of transient conformational states. *Nat.Chem.Biol.* **9,** 462-465
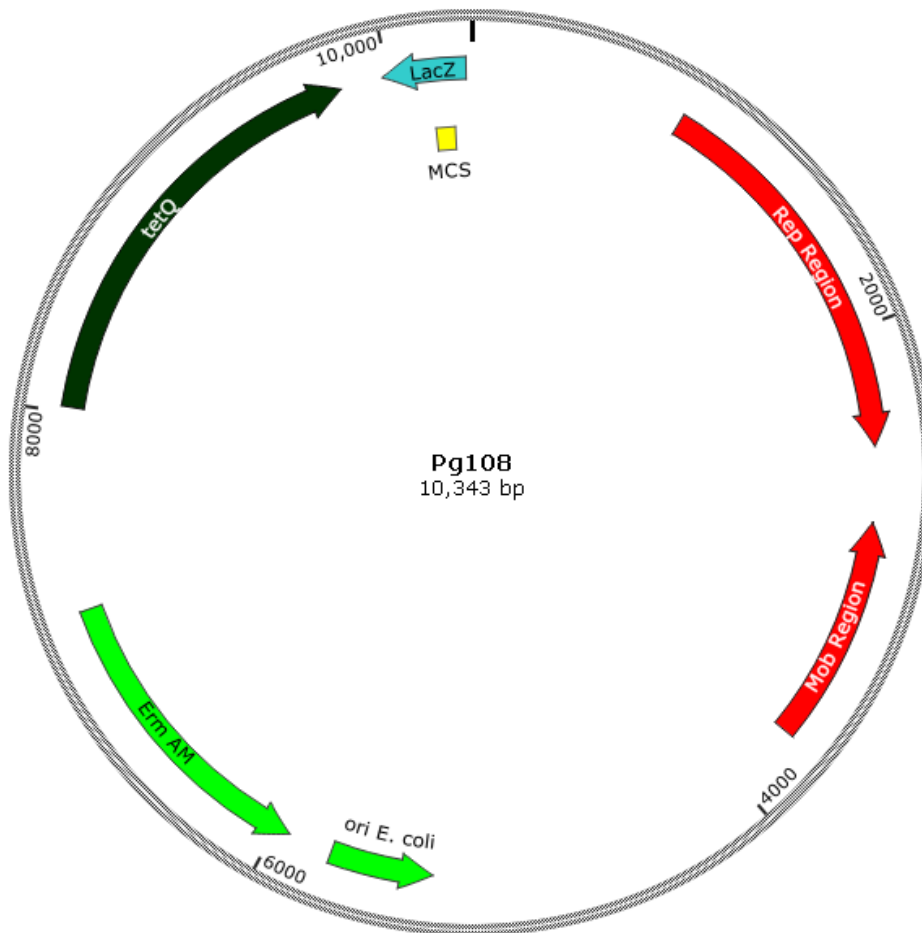
VI. Appendix

Figure A.1 - Pg108 Vector: full vector map

Pg0893 (*hcp*) knockout construct

```
TTGCTATCAATGCCAGGAAACAGCCGGCAATAAGGGATGTATCCTCAAAGGGGTATGCGG
TAAGGACTTTAGTACAGCTAATCTGATGGATTTGCTCGTCTTTAACCTCAAAGGTATTGC
CATCATAATGACTTCTATGAGGCGTGCCGGAGTGAAAGCCGATTACCGAAAGGCTGACAA
GGCGATCATGGAATCTCTATTTGCCACAATTACCAATGCCAACTTCGACTACTCTTCCAT
AGCCAAACGTGTAGAGAAACGTTCGCACTCAAAGCGGAATTGTACAGTTTGGCTTTTAC
GGTACCCCCGATAGCTTCCGCTATTGCTTTTTTGCTCATCGGTATTTGCAACATCATAGA
AATTGCATACCTTTGTTCCTCGGTTATATGTTTGCTCATCTGCAACTTTTTTTTCTTTGG
ACGGACAATTAAAGCAAAGATAGCAAACTTTATCCATTCAGAGTGAGAGAAAGGGGGACA
TTGTCTCTCTTTCCTCTCTGAAAAATAAATGTTTTTATTGCTTATTATCCGCACCCAAAA
AGTTGCATTTATAAGTTGAACTCAAGAAGTATTCACCTGTAAGAAGTTACTAATGACAAA
AAAGAAATTGCCCGTTCGTTTTACGGGTCAGCACTTTACTATTGATAAAGTGCTAATAAA
AGATGCAATAAGACAAGCAAATATAAGTAATCAGGATACGGTTTTAGATATTGGGGCAGG
CAAGGGGTTTCTTACTGTTCATTTATTAAAAATCGCCAACAATGTTGTTGCTATTGAAAA
CGACACAGCTTTGGTTGAACATTTACGAAAATTATTTTCTGATGCCCGAAATGTTCAAGT
```

133

```
TGTCGGTTGTGATTTTAGGAATTTTGCAGTTCCGAAATTTCCTTTCAAAGTGGTGTCAAA
TATTCCTTATGGCATTACTTCCGATATTTTCAAAATCCTGATGTTTGAGAGTCTTGGAAA
TTTTCTGGGAGGTTCCATTGTCCTTCAATTAGAACCTACACAAAAGTTATTTTCGAGGAA
GCTTTACAATCCATATACCGTTTTCTATCATACTTTTTTTTGATTTGAAACTTGTCTATGA
GGTAGGTCCTGAAAGTTTCTTGCCACCGCCAACTGTCAAATCAGCCCTGTTAAACATTAA
AAGAAAACACTTATTTTTTGATTTTAAGTTTAAAGCCAAATACTTAGCATTTATTTCCTG
TCTGTTAGAGAAACCTGATTTATCTGTAAAAACAGCTTTAAAGTCGATTTTCAGGAAAAG
TCAGGTCAGGTCAATTTCGGAAAAATTCGGTTTAAACCTTAATGCTCAAATTGTTTGTTT
GTCTCCAAGTCAATGGTTAAACTGTTTTTTGGAAATGCTGGAAGTTGTCCCTGAAAAATT
TCATCCTTCGTAGTTCAAAGTCGGGTGGTTGTCAAGATGATTTTTTTGGTTTGGTGTCGT
CTTTTTTTAAGCTGCCGCATAACGGCTGGCAAATTGGCGATGGAGCGGAAACGTAAAAGA
CGCGTTCTCGATGCCGGACAGTGTAATGACAGTTATTCGCTGGCGGTAATTGCCCTGAAG
CTGAAAGAAGTAATGGGATTGGATGACATCAACAAACTACCGATCGTCTACAACATTGCA
TGGTACGAACAGAAAGCTGTCATCGTCCTGCTCGCTCTACTCAGCCTCGGTGTCAAGAAC
ATCCATGTAGGCCCTACCCTACCTGCATTCCTATCACCGAATGTAGCGAAAGTGCTGATC
GAAAACTTCGGTATAGCAGGTATCGGTACGGTCGAAGAAGATATTCGGACGCTGATCGCA
```

hcpR-ermF promoter construct

```
CAATGCAGTAGTACGATACATGACGTACGTATTGCTCATCTGCAACTTTTTTTTCTTTGG
ACGGACAATTAAAGCAAAGATAGCAAACTTTATCCATTCAGAGTGAGAGAAAGGGGGACA
TTGTCTCTCTTTCCTCTCTGAAAAATAAATGTTTTTATTGCTTATTATCCGCACCCAAAA
AGTTGCATTTATAAGTTGAACTCAAGAAGTATTCACCTGTAAGAAGTTACTAATGGATCC
CGAATTCGATCTTCTTCTGAAAGCCTGGAAAAGCAGCGGACTCTCTGTCGGTATGAAAGA
CGATGAGCTCTTAGCCCTGCTTGAGAGTTGTTCATACAGAGTGGAACGGCTGAAAGCCGA
AGAGCTATATGCTATCGGTGGAGACAAGCTCCAAGACCTGCGAATCGTGGGTGTAGGTGA
GATTCGTGCTGAGATGGTGGGGCCTTCCGGCAAGCAGATTCTGATAGATACTTTGGCGGT
CGGACGCATCTTGGCTCCGGCCCTTCTTTTTGCTTCGGAGAATATTTTACCCGTTACCCT
GTTTGCTAATGAGGACAGTGTTCTTTTCCGCATCGGGAAAGAAGAGTTCAAAGGGATGAT
GCATAAGTATCCTACTCTGATGGAGAATTTCATAGGCATGATTTCCGATATCAGTGCTTT
CCTGATGAAGAAAATCCATCAGCTCAGCTTGCGAAGTTTGCAGGGCAAGATCGGAGACTA
CCTGTTTCAGCTTTATACGAAAGATGGCAGCAATCGGATTGTTGTCGAATCTTCATGGAA
AGAACTTTCCGATCGATTTGGCGTGAACAGGCAATCACTGGCACGCAGTCTCTCTCAGCT
TGAGGAAGAGGGTATCATCCGTGTGGATGGTAAAAGCATAGAAATACTCCAGCCCAACCG
ATTGTCGAGGCTGGAGTAAGTACAGATTATGACATGACGCGGTAACTATG
```

hcpR Flag construct

```
CAATGCAGTAGTACGATACATGACGTACGTATTGCTCATCTGCAACTTTTTTTTCTTTGG
ACGGACAATTAAAGCAAAGATAGCAAACTTTATCCATTCAGAGTGAGAGAAAGGGGGACA
TTGTCTCTCTTTCCTCTCTGAAAAATAAATGTTTTTATTGCTTATTATCCGCACCCAAAA
AGTTGCATTTATAAGTTGAACTCAAGAAGTATTCACCTGTAAGAAGTTACTAATGGATTA
TAAAGATCATGATGGTGACTACAAGGACCATGACATTGATTATAAAGATGATGATGATAA
AATGGATCCCGAATTCGATCTTCTTCTGAAAGCCTGGAAAAGCAGCGGACTCTCTGTCGG
TATGAAAGACGATGAGCTCTTAGCCCTGCTTGAGAGTTGTTCATACAGAGTGGAACGGCT
GAAAGCCGAAGAGCTATATGCTATCGGTGGAGACAAGCTCCAAGACCTGCGAATCGTGGG
TGTAGGTGAGATTCGTGCTGAGATGGTGGGGCCTTCCGGCAAGCAGATTCTGATAGATAC
TTTGGCGGTCGGACGCATCTTGGCTCCGGCCCTTCTTTTTGCTTCGGAGAATATTTTACC
CGTTACCCTGTTTGCTAATGAGGACAGTGTTCTTTTCCGCATCGGGAAAGAAGAGTTCAA
AGGGATGATGCATAAGTATCCTACTCTGATGGAGAATTTCATAGGCATGATTTCCGATAT
CAGTGCTTTCCTGATGAAGAAAATCCATCAGCTCAGCTTGCGAAGTTTGCAGGGCAAGAT
CGGAGACTACCTGTTTCAGCTTTATACGAAAGATGGCAGCAATCGGATTGTTGTCGAATC
TTCATGGAAAGAACTTTCCGATCGATTTGGCGTGAACAGGCAATCACTGGCACGCAGTCT
CTCTCAGCTTGAGGAAGAGGGTATCATCCGTGTGGATGGTAAAAGCATAGAAATACTCCA
GCCCAACCGATTGTCGAGGCTGGAGTAAGTACAGATTATGACATGACGCGGTAACTATG
```

X-ray Data collection and refinement statistics

Data collection statistics	HcpR Derivative	HcpR Native	HcpR Native
Radiation Source	Rigaku MM007	Rigaku MM007	SSRL
Space group	$P4_122$	$P4_122$	$C222_1$
Cell dimensions (Å)	a=b=145.30, c=77.93	a=b=144.97, c=77.97	a=133.47, b=138.85 c=44.55
Monomers/AU	2	2	2
Resolution (Å)	39.58–3.50 (3.63–3.50)	29.93–3.15 (3.26–3.15)	43.73-2.60 (2.70-2.60)
Measured reflections	91938	92849	93652
Unique reflections	10962 (1067)	14801 (1429)	13182 (1544)
Redundancy	8.4 (8.2)	6.2 (6.1)	7.3 (7.5)
I/σI	11.7 (5.2)	13.9 (4.2)	16.2 (5.5)
Completeness (%)	99.7 (100.0)	99.5 (99.3)	99.8 (99.4)
R_{merge} (%)[a]	13.5 (37.5)	7.7 (36.7)	6.6 (26.4)
Structure refinement			
Resolution limit (Å)		28.99–3.15 (3.39–3.15)	43.73-2.60 (2.70-2.60)
No. of reflections		14778 (756)	13165 (1294)
R_{work} (%)		19.6 (28.8)	23.50 (30.63)
R_{free} (%)[b]		23.9 (37.4)	30.47 (39.29)
R.m.s.d.standard geometry Bond lengths (Å)		0.010	0.009
Bond angles		1.25°	1.23°
Dihedral angles (%)			
Most favored regions		96.0	96.30
Allowed regions		3.33	3.70
Average B-factors (Å^2)			
All atoms		67.1	55.9
Protein alone		67.1	55.9
Water		60.0	53.50

[a]Rmerge = $\Sigma_{hkl}\Sigma_i/I_{hkli} - <I_{hkli}>/\Sigma_{hkl}\Sigma_i<I_{hkli}>$. [b]Rfree was calculated with 5% excluded reflection from the refinement

Vita

Benjamin Ross Belvin (Ross) was born on November 7th 1989 in Newport News, Virginia. He was raised in nearby Yorktown, Virginia, where he graduated from Grafton High School in 2008. He then made his way to Blacksburg, Virginia where he received a B. Sc. in 2012 with a focus on Biochemistry and Biology and a minor in Chemistry from Virginia Tech (Go Hokies!). After graduating from Virginia Tech, he made his way to Richmond where he joined the lab of Dr. Lewis at Virginia Commonwealth University and completed his M.S. in Biochemistry in 2014. After completing his M.S. he remained in the lab to complete his PhD in Biochemistry.